

**ELECTROCHEMICAL ACTUATION POTENTIAL OF DIAMINOPHENAZINE
LINKED PYRROLE DERIVATIVES**



A thesis submitted in fulfillment of the requirement for the Masters' Degree in the
Department of Chemistry, University of the Western Cape, South Africa.

Supervisor

Professor Priscilla GL. Baker

ABSTRACT

A novel monomer (Phenazine-2,3-diimino(pyrrole-2-yl)-PDP) derived from the condensation reaction between 2,3-diaminophenazine and a pyrrole derivative has been synthesized as a hinge molecule in the design of a zig-zag polymer with actuation possibility. The monomer was polymerized chemically and electrochemically to produce the new polymer material – polymerized Phenazine-2,3-diimino(pyrrole-2-yl) PPDP. Two very crucial properties of a good actuator material, relate specifically to its solubility testing and electrical conductivity. The hinged polymer material was studied intensively in terms of its spectroscopy; Fourier Transform Infrared - FTIR, ^1H NMR, thermal properties (Differential Scanning Calorimetry-DSC and Thermogravimetric Analysis-TGA) as well as voltammetry and conductivity. Conductivity was evaluated using three different approaches including; 4 probe measurements, plotting of I/V curves based on potentiostatic measurements and an electrochemical impedance experiment using a dielectric Solartron interface. Electrochemical kinetics of the polymer prepared as a thin film at glassy carbon electrode (GCE) was also done and it was clear that the thin film conductivity was vastly different from the compressed pellet conductivity (thick film). The zig-zag polymer was then further modified by homogeneous inclusion of gold nanoparticles to improve conductivity and solubility, in the thick film arrangement. Conductivity of the thin film was studied by electrochemical impedance spectroscopy with the relative charge transfer values being determined for unmodified and modified polymer systems. The solubility testing of the material plays an important role as it is required for a wide range of experimental applications. The zig-zag polymer showed great promise for applications; in dye sensitized solar cells and free standing interpenetrating polymer network (IPN), solubility testing and electrical conductivity would need to be improved in order to be used in these applications.

KEYWORDS

(Phenazine-2,3-diimino(pyrrole-2-yl)-PDP

Poly(Phenazine-2,3-diimino(pyrrole-2-yl)) PPDP

Zig-zag polymer

Conductivity

Thin films

Conducting polymer

Actuator

Electrochemical Impedance Spectroscopy

Solubility

Gold nanoparticles

Charge transfer resistance

Deformation

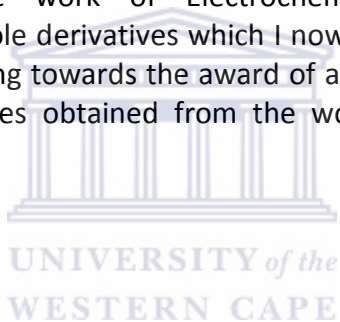
Expansion

Contraction



DECLARATION

I hereby declare that the work of Electrochemical actuation potential of diaminophenazine linked pyrrole derivatives which I now submit for the assessment on the programme of study leading towards the award of a master's degree is entirely my own work; quotes and phrases obtained from the work of others have been fully acknowledged and referenced.



Signed:

.....

MERYCK WARD

Date: December 2013

ACKNOWLEDGEMENTS

I would like to express my gratitude to the people who showed continuous support and encouragement, without these significant people this thesis would not be possible.

My supervisor Prof. Priscilla Baker for the opportunity to work in SensorLab research group, the guidance and support throughout my thesis has been greatly appreciated. Support, patience and understanding through my times of great procrastination and laziness, it was highly appreciated.

To all the colleagues who provided the insight and guidance, it was a pleasure and a privilege.

To my parents Helen and Leslie Ward, there are no words that can describe the love, support and encourage you provided me whenever I needed it. I just want to say thank you for everything.

My grandmother Elizabeth O'Shea for all her prayers for me and asking the Lord to guide me in the right direction and to the success of my career, thank you very much. Thank you Lord for giving me the ability and guidance to complete this work.

To the special person in my life, Aimee Nicole Valentine, thank you for all the support, guidance, patience and encouragement.

I appreciate everything that you do,
Very helpful and thoughtful too.
From the beginning, you've been there for me,
When I was down, you were strong like a tree.

You offer so much, a heart that is kind,
Thinking to help others, in your beautiful mind.
Your qualities combined, are extremely rare,
You wake up each morning, with a smile and care.

Everything you do, I respect and praise,
You're a wonderful person, you always amaze.
I Wish to say thank you, deep in my heart,
For so many lives, you're a big part.

by AnitaPoems

Contents

ABSTRACT	2
KEYWORDS	3
DECLARATION	4
ACKNOWLEDGEMENTS	5
LIST OF FIGURES	10
LIST OF TABLES	12
CHAPTER 1	13
Introduction.....	13
1.1 Pneumatic muscle actuators (PMA).....	13
1.2 Piezoelectric actuators.....	14
1.3 Electroactive polymer actuators (EAPs).....	15
1.4 Properties of EAP actuators.....	18
1.5 Conducting Polymers (CPs).....	19
1.6 Polypyrrole.....	20
1.7 Bilayer Actuators.....	24
1.8 Trilayer Actuators.....	26
1.9 Interpenetrating Polymer Networks (IPNs).....	28
MAIN AIMS AND OBJECTIVES	31
AIMS:.....	31
OBJECTIVES:.....	31
THESIS OUTLINE	32
CHAPTER 2	33

Design and synthesis of zig-zag polymers.....	33
2.1 Hinged molecular design	33
2.2 2,3-diaminophenazine (DAP)	37
2.3 Pyrrole-2-carboxaldehyde.....	37
CHAPTER 3	41
Materials and Methodology	41
3.1 Monomer synthesis - (Phenazine-2,3-diimino(pyrrole-2-yl)) – PDP	41
3.2 Materials	42
3.3 Solution Preparations	42
3.4 Solubility.....	44
3.5 Monomer Characterization	44
3.5.1 Fourier Transform Infrared (FTIR) Spectroscopy	44
3.5.2 Nuclear Magnetic Resonance (NMR) Spectroscopy	45
3.5.3 Differential Scanning Calorimetry (DSC).....	45
3.6 Polymerization	46
3.6.1 Chemical Polymerization.....	46
3.6.2 Electrochemical Polymerization	47
3.7 Gold (Au) Nanoparticles Synthesis	48
3.8 Polymer Characterization.....	49
3.8.1 Electrical Conductivity	49
Four Point Probe	49
Conductivity by Cyclic Voltammetry	50
Conductivity by Electrochemical Impedance Spectroscopy.....	51
3.8.2 Thermogravimetric Analysis (TGA).....	51
3.8.3 Voltammetric Techniques	52

Cyclic Voltammetry (CV).....	53
Square Wave Voltammetry.....	56
3.8.4 Spectroscopy.....	57
Electrochemical Impedance Spectroscopy (EIS).....	57
UV/Vis Spectroscopy.....	59
Fluorescence Spectroscopy.....	60
Scanning Electron Microscopy (SEM).....	60
CHAPTER 4:	62
Results and Discussion:	62
4.1 Monomer material formation.....	63
4.2 Starting Materials.....	64
4.2.1 2,3-diaminophenazine (DAP).....	64
4.2.2 Pyrrole-2-carboxaldehyde.....	67
4.3 Gold (Au) Nanoparticles.....	70
4.4 Characterization of PDP material	71
CHAPTER 5	73
PPDP POLYMERIZATION AND CHARACTERIZATION	73
5.1 Chemical Polymerization.....	73
5.2 Electrochemical Polymerization	76
5.3 Polymer Characterization.....	76
5.3.1 Electrochemical Behaviour of polymer material system.....	76
5.3.2 Electrochemical Impedance Spectroscopy	84

5.4	Electrical conductivity of Polymer	88
5.5	FTIR of Polymer	92
5.6	Solubility	93
5.7	Spectral properties (absorption – emission).....	93
5.8	Thermal Analysis	96
5.9	Surface Morphology	99
CHAPTER 6		102
Verification of the Monomer Composition.....		102
CHAPTER 7		108
Conclusion and Future work.....		108
7.1	Conclusion	108
7.2	Future Work.....	110
REFERENCES		112



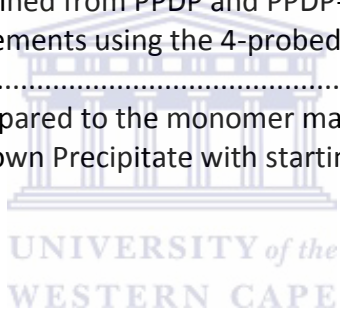
List of Figures

Figure 1. Bilayer actuator design	25
Figure 2. Trilayer actuator consisting of two conducting polymer layers on either side of a non-conductive tape.	26
Figure 3. Deformation of trilayer actuator.	27
Figure 4. Diagram of IPN setup	29
Figure 5. Zig-zag molecule containing calix[4]arene and quarterthiophene.....	33
Figure 6. Zig-zag molecule of [Zn(SPh) ₂ (BPyVB)] _n	34
Figure 7. Representation of the zig-zag organometallic framework.	35
Figure 8. Structure of TTFV-hinged molecular tweezers.	36
Figure 9. DAP is a solid chemical with a molecular formula of C ₁₂ H ₁₀ N ₄ and a molecular mass of 210 g/mol.	37
Figure 10. Pyrrole-2-carboxaldehyde has a molecular formula of C ₅ H ₅ NO with a molecular mass of 95.10 g/mol.	37
Figure 11. Proposed polymer formation	40
Figure 12. The Universal Probe containing the four probe needles used for conductivity measurements.	50
Figure 13. An electrochemical cell.	53
Figure 14. Cyclic voltammogram displaying a reversal technique of current versus potential.	54
Figure 15. A potential is scanned as a function of time a potential sweep is displayed. .	56
Figure 16. Complex EIS plot	58
Figure 17. On the left is the bode plot of Log Z vs. log ω and on the right bode plot of φ vs. log ω.	59
Figure 18. Incident beam used in SEM analysis	61
Figure 19. FTIR spectrum of 2,3-diaminophenazine.	64
Figure 20. UV/Vis analysis of 2,3-diaminophenazine.	65
Figure 21. 300 MHz 1H NMR spectrum of 2,3-diaminophenazine in DMSO-d ₆	66
Figure 22. Cyclic voltammogram of 2,3-diaminophenazine in 0.1 M HCl.	67
Figure 23. FTIR spectrum of pyrrole-2-carboxaldehyde.	68
Figure 24. 300 MHz 1H NMR spectrum of pyrrole-2-carboxaldehyde in DMSO-d ₆	69
Figure 25. Cyclic voltammetry of pyrrole-2-carboxaldehyde in 0.1 M HCl.....	69
Figure 26. UV/Vis of Au Nanoparticles	70
Figure 27. FTIR data of synthesized monomer, Phenazine-2,3-diimino(pyrrole-2-yl) PDP.	71
Figure 28. Zig-zag polymer material, poly(Phenazine-2,3-diimino(pyrrole-2-yl) PPDP....	75
Figure 29. CV of 2,3-diaminophenazine (a) and pyrrole-2-carboxaldehyde (b).	76
Figure 30. Electropolymerization to form the polymer PPDP (a) and PPDP-Au (b).	77

Figure 31. Characterization of PPDP (a) and PPDP-Au (b) in 0.1 M HCl solution at scan rates ranging between 100 – 250 mV/s.....	79
Figure 32. Randles-Sevcik for PPDP, plot of current vs square root of scan rate.....	81
Figure 33. Randles-Sevcik for PPDP-Au, plot of current vs square root of scan rate.	81
Figure 34. OSWV of PPDP (a) and PPDP-Au (b) both in 0.1 M HCl solution.	84
Figure 35. EIS spectra of PPDP (a) with +100 mV potential steps starting from -500 mV to 400 mV (vs Ag/AgCl) and PPDP-Au (b) with +100 mV potential steps starting from -400 mV to 400 mV (vs Ag/AgCl).....	85
Figure 36. Randles equivalent circuit of PPDP (a) and PPDP-Au (b).	85
Figure 37. FTIR of chemically (a) and electrochemically (b) polymerized polymer material.....	92
Figure 38. UV/Vis of 2,3-diaminophenazine (a), monomer material (a) and polymer (b).....	94
Figure 39. Photoluminescence of PPDP (polymer material) dissolved in THF.	96
Figure 40. TGA analysis of the 2,3-diaminophenazine, Polypyrrole and PPDP over a temperature ramp of 20 to 60 °C.	97
Figure 41. DSC analysis of PPDP, which displayed two endothermic transitions.....	98
Figure 42. SEM of Polypyrrole (a), Au nanoparticles (b), PPDP (c) and PPDP-Au modified system (d).....	99
Figure 43. Spherically shaped Au nanoparticles.....	100
Figure 44. Polymerization of the monomer of unfiltered and filtered solutions displayed the same voltammogram.....	102
Figure 45. Comparison of filtered and unfiltered solutions of PPDP.....	103
Figure 46. SWV of filtered and unfiltered PPDP at 200 mV/s.....	104
Figure 47. UV/Vis analysis of PPDP dissolved in THF (a), filtered yellow monomer solution (b) dissolved in a ratio of 1:1 of DMF and HCl.	105
Figure 48. FTIR analysis of the filtered solution.....	105
Figure 49. FTIR of unknown precipitate remaining after filtration.	106

LIST OF TABLES

Table 1. Properties of EAP actuators	16
Table 2. Comparative properties of EAPs, SMA and EAC	17
Table 3. Ionic and electronic electroactive polymer materials	18
Table 4. Advantages and disadvantages of the two basic EAP groups (Y. Bar-Cohen). ...	19
Table 5. Comparison between PPy actuators and Skeletal Muscles.	24
Table 6. Chemicals used for synthesis.	43
Table 7. Peak assignment for starting materials and monomer material.	72
Table 8. Current values obtained from the above cyclic voltammogram for both PPDP and PPDP-Au (figure 33).	79
Table 9. Peak separations obtained from the PPDP and PPDP-Au system	80
Table 10. Diffusion coefficient values of PPDP and PPDP-Au systems.	82
Table 11. Surface concentration of PPDP and PPDP-Au systems of the redox couple A-A' over various scan rates.	83
Table 12. Impedance data obtained from PPDP and PPDP-Au.	87
Table 13. Conductivity measurements using the 4-probed instrument	88
Table 14. FTIR of PPDP	93
Table 15. Filtered solution compared to the monomer material.....	106
Table 16. Comparison of Unknown Precipitate with starting materials.	107



CHAPTER 1

Introduction

The mechanism and principles for actuation of actuators in electronic, mechanical and electromechanical fields will be discussed. Simple examples of actuation from our everyday lives in living and mechanical systems include the way in which the human body converts energy obtained from metabolism of food, into motion. Mechanically this process is observed in automobiles where combustion of fuel results in the propulsion of the vehicle.

Actuators are types of physical objects which have the ability to control or move a mechanism or system; it also has the ability to convert electrical energy produced into mechanical motion. Exposed to external stimulus these actuators produce linear or rotary motion, with simple actuators having the ability to open and close valves. Development of new actuators suitable for robotic actuation has recently been studied, for applications such as pneumatic muscle actuators, piezoelectric actuators and electroactive polymers.

1.1 Pneumatic muscle actuators (PMA)

Pneumatic actuators have the ability to convert pneumatic power into motion, the system consists of a chamber in which compressed air, gas or a mixture is contained. According to T. Vo-Minh et al, 2010, an actuator consisting of a fibre-reinforced bladder (inner rubber tube), was able to function in an air enclosure by means of connecting flanges at both ends. A single outlet/inlet port existed through which compressed air passed in or out of the actuator. Geometrical arrangement of the fibre in the helical winding caused longitudinal contraction with an increase in pulling force. Lateral expansion occurred when air pressure in the chamber increased; this mechanical

property was useful for actuation purposes. In another example of these types of materials, pneumatic muscle actuators were observed to generate pulling forces during contractions. These muscle like actuators displayed unique lightweight, simple maintenance and yielding force to weight ratio characteristics (K. Wickramatunge et al, 2010). The main challenges associated with these actuators were the nonlinearity of the system and the nonlinearity of the actuator dynamics (T. Vo-Minh et al, 2010 and A. Hilderbrandt et al, 2005). The two main components of the system were the pneumatic muscle actuator and the control valve. Control valves were used to control the flow rate of compressed air which is required for perfect performance (B. Tondu et al, 2000).

1.2 Piezoelectric actuators

The piezoelectric effect was first discovered in the 1880's by P. Curie and J. Curie. Certain crystals which were subjected to mechanical strain became electrically polarized, with polarization being proportional to the strain. Deformation occurred in these materials when exposed to an electric field. Piezoelectric actuators convert electrical signals into controlled physical displacement. Movement of these actuators is used to adjust machine tools, lenses, mirrors and other equipment. These actuators display properties of high speed operation and compact size which are essential in many precision actuators and sensors. The main advantages of these actuators are; large forces, high displacement accuracy, high positioning resolution, fast response, cost effectiveness and they have the ability to generate frequencies greater than 20 kHz (J. Guo et al, 2013). The one major disadvantage of the piezoelectric actuator is the requirement of high voltages for deformation (M. Karpelson et al, 2012). According to J. Guo et al, 2013, the piezoelectric actuators can be used for a variety of application including; nanoscale positioning resolution, ultra-precision machine tools, nanofabrication's and various nanotech microscopes. Piezoelectric diaphragm actuators

used as globe control valves displayed a working temperature range between -13 to 90 °C, maximum operating pressure of 4.5 bar, linearity < 3% and hysteresis < 3%. Multi-layer piezoelectric actuators used for vibrational control in nanotechnology produced modified specifications of high operating temperatures up to 200 °C and operating voltage of -20 to 120 V (developed by the company PICMA).

1.3 Electroactive polymer actuators (EAPs)

Polymers which change shape and size when exposed to electrical stimulus are called electroactive polymers. According to L. Ceseracciu et al, 2011, the electroactive expansion and contraction of the actuator material occurred due to the change in carbon-carbon bond length which was induced by charge injections. These materials include piezoelectric, electrostrictive, ionic, conducting polymers etc. They displayed large displacements and quick responses when exposed to external stimuli such as an electrical field. Electroactive polymer materials converted the electrical or chemical energy produced into mechanical energy through electrical responses of the materials. There are a variety of electroactive polymers with different controllable properties which produce permanent or reversible responses. The basis on which these actuators exist is highly dependent on the initial stretching ability of the material (K. Kim et al. 2007). Application of electrical stimulus to the EAPs will allow for elongation or contraction, with the conversion of electrical energy into mechanical energy (R. Palakodeh et al, 2006). The main properties of EAP actuators include strain, stress, amount of work density, electromechanical coupling and relative speed cycles (Table 1).

Table 1. Properties of EAP actuators

Type	Maximum strain %	Maximum stress MPa	Work Density $\text{kJ}\cdot\text{m}^{-3}$	Electro-mechanical coupling	Comment	Relative speed (cycle)
Natural Muscle	>40	0.35	40	0.40	High cycle life	Slow-Fast
Dielectric elastomer	20-380	7.2	10-3400	0.15-0.90	Low current	Fast
Relaxor Ferro-electric Polymer	<7	45	1000	0.40	Low current	Fast
Electrostrictive Graft Polymer	2	43	0.25	low	Low current	Fast
Liquid Crystal Elastomers	10	-	20	0.75	Photo-activation	Slow
Conducting polymer	2	34	100	<0.05	Stiff (1GPa)	Fast
Carbon Nanotubes	0.2	1	-	low	Big temp range	Fast
Ionic Polymer Metal Composites	2	30	-	low	Kits available	Fast

Conducting polymers play an important role in EAP actuators, the main operation of these actuators is based on volume expansion/contraction generated by ion movement. Large displacements resulting from the ion movement have led to the development of these EAPs. EAPs can be classed into two categories i.e. ionic and electronic driven polymers. These EAPs experience actuation strains of more than 10 % and may be formed into many different shapes for the use in actuators or sensors. The design of these EAPs allow for operations with similarities to biological muscle movement. According to Y. Bar-Cohen, 2004, the new emerging actuation material such as EAPs displayed deformations which electroactive ceramics and shape memory alloys could not match. Shape memory alloys are novel materials with shape retention capabilities when heated. This material has low yield strength and can easily undergo shape

changes, but heat above the transformation temperature will yield the original shape of the material. Any resistance to this shape change could generate extremely large forces which could be used in the mechanism for remote actuation. The most common shape memory alloy is nickel titanium called Nitinol. Nitinol displayed actuation properties including energy conversion efficiency (5 %), work output (~1 J/g) and transformation temperatures between ± 100 °C. Flexinol NiTi alloy SMA wires, manufactured by DYNALLOY, Inc, with a diameter of ~0.38 mm displayed a pull force of ~2000 g (~19.5 N) with obtained stress values of 170 N/mm² (force per cross-sectional area). Electroactive ceramics (piezoelectric and electrostrictive) are widely used in various applications due to properties such as small size, precision positioning, high energy density and quick frequency response. Applications of these materials include motors, translators and manipulators in devices such as ultrasonic motors and inchworms.

Table 2. Comparative properties of EAPs, SMA and EAC

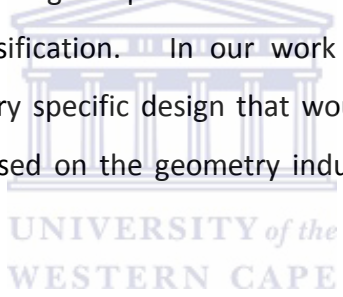
Property	Electroactive polymers (EAP)	Shape Memory Alloys (SMA)	Electroactive Ceramics (EAC)
Actuation displacement	>10 %	<8 % short fatigue life	0.1 – 0.3 %
Force(MPa)	0.1 – 3	About 700	30 – 40
Reaction Speed	µsec to sec	sec to min	µsec to sec
Density	1 – 2.5 g/cc	5 – 6 g/cc	6 – 8 g/cc
Drive Voltage	4 – 7 V	NA	50 -800 V
Power consumption	m-watts	Watts	Watts
Fracture toughness	Resilient, elastic	Elastic	Fragile

From the comparative data it was evident that EAPs have superior ability for actuation displacement, low drive voltage and good mechanical strength.

Table 3. Ionic and electronic electroactive polymer materials

Ionic EAP	Electronic EAP
Carbon Nanotubes (CNT)	Dielectric elastomer EAP
Conductive Polymers (CP)	Electrostrictive Graft Elastomers
ElectroRheological Fluids (ERF)	Electrostrictive Paper
Ionic Polymer Gels (IPG)	Electro-Viscoelastic Elastomers
Ionic Polymer Metallic Composite (IPMC)	Ferroelectric Polymers
-	Liquid Crystal Elastomers (LCE)

From the examples extracted from literature, the most promising material to pursue in the design of a fast response, large displacement the actuator material was selected from the electronic EAP classification. In our work we pursued the design of a conductive polymer with a very specific design that would facilitate the displacement requirement for actuation, based on the geometry induced during crosslinking in the polymerization step.



1.4 Properties of EAP actuators

N. Terasawa et al, 2013 showed that the ionic liquids used in EAP actuator designs have low volatility, high conductivity and wide potential windows, which are essential for quick response actuators and high electrochemical stability components. The advantages and disadvantages of the two EAP categories presented in table 4, these are important to consider in the selection of actuators.

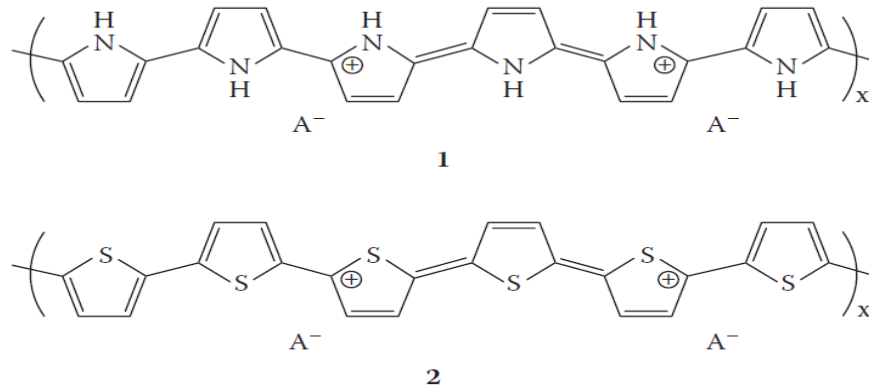
Table 4. Advantages and disadvantages of the two basic EAP groups (Y. Bar-Cohen).

EAP type	Advantages	Disadvantages
Electronic	<ul style="list-style-type: none"> • Exhibit rapid response (milliseconds) • Can hold strain under dc activation • Induces relatively large actuation forces • Exhibits high mechanical energy density • Can operate for a long time in room conditions 	<ul style="list-style-type: none"> • Requires high voltages (~100 MV/meter). Recent development allowed for (~20 MV/meter) in the Ferroelectric EAP • Independent of the voltage polarity, it produces mostly monopolar actuation due to associated electrostriction effect.
Ionic	<ul style="list-style-type: none"> • Natural bi-directional actuation that depends on the voltage polarity. • Requires low voltage • Some ionic EAP like conductive polymers have a unique capability of bi-stability 	<ul style="list-style-type: none"> • Requires using an electrolyte • Require encapsulation or protective layer in order to operate in open air conditions • Low electromechanical coupling efficiency • Except for CPs and NTs, ionic EAPs do not hold strain under dc voltage • Slow response (fraction of a second) • Bending EAPs induce a relatively low actuation force • Electrolysis occurs in aqueous systems at >1.23 V



1.5 Conducting Polymers (CPs)

CPs are continuously being used in the development of intelligent material systems and structures, with applications of these materials including; robotics (A. Khaldi et al, 2011), prosthetics (E. Biddiss et al, 2008) and drug delivery systems (H. Xu et al, 2006, Y. Bar-Cohen, 2004)). Prosthetic materials have the ability to operate biological muscles with high fracture toughness, large actuation strain and inherent vibration damping. Microvalves could be used in drug delivery systems in the pharmaceutical industry. There is a wide variety of CPs but the most commonly used include polypyrrole, polyaniline and polythiophene, (G. Wallace et.al, 2009).



Scheme 1. Repetitive units of CPs which include polypyrrole (1) and polythiophene (2), with the incorporation of the (A⁻) counterion onto the polymer backbone.

These polymers consist of repeating structural units which are created through a process called polymerization. These commonly used conducting polymers undergo dimensional changes upon doping and dedoping. This mechanical property allows for it to be used as an electrochemically driven mechanical actuator.

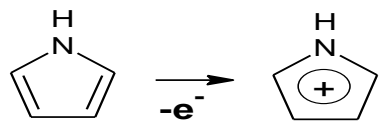
1.6 Polypyrrole

Polypyrrole is a well-known conducting polymer material with properties such as relatively high conductivity, easy synthesis and high stability (Y. Tang et al, 2013, R. Ansari, 2006 and K. Maksymiuk, 2006). Polypyrrole is a good electrical conductor (both in oxidative and reductive states) due to its π -conjugated electrons along the backbone in a polymer network system. This conjugated polymer also displays high thermal stability, large electrochemical activity at a higher pH, aqueous stability and stability under environmental conditions. Polypyrrole systems have additional advantages of large dimensional changes, high stress generation and high work capacity per cycle. Upon chemical and electrochemical polymerization, polypyrrole comprises of polymer chains stabilized by their respective counterions for maintaining charge neutrality. Material composition and electrochemical properties change under electrochemical

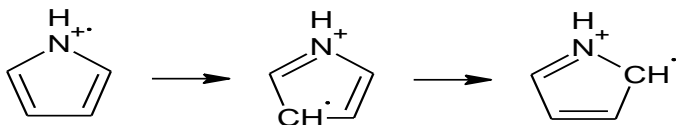
reactions. P-doping during the polymer oxidation process involved the extraction of a number of consecutive electrons from the polymer chains creating positive charges along the chains. According to T. Vernitskaya et al, 1997, the oxidation process of pyrrole to polypyrrole is irreversible, even with extensive research into the mechanism of the reaction; the problem has not yet been solved. They also looked at the electrochemical synthesis mechanism to determine if this process could be reversible, two synthesis schemes were reviewed.



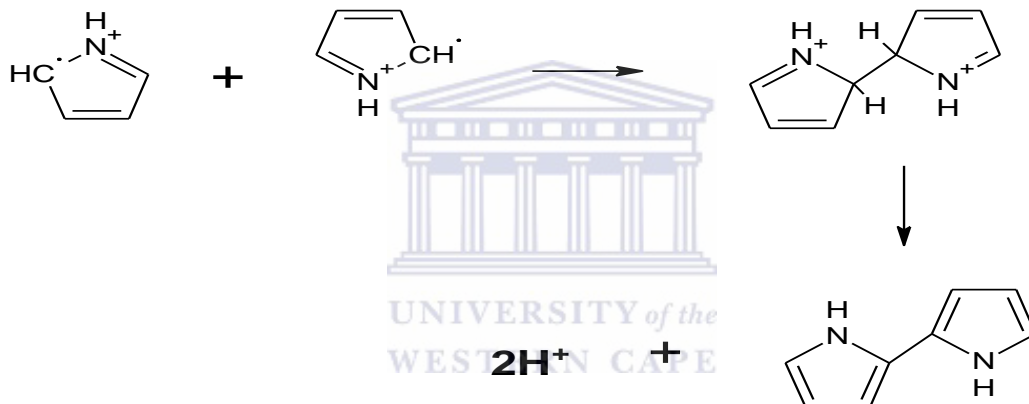
Monomer Oxidation



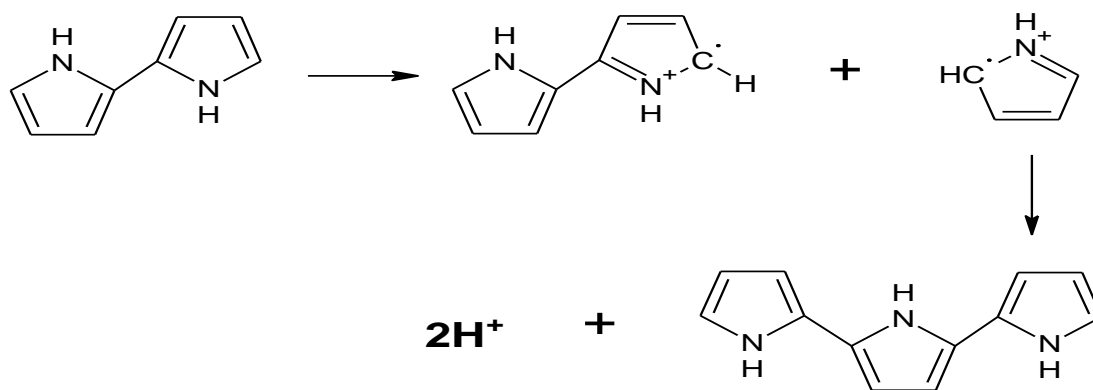
Resonance forms



Resonance forms



Chain Growth

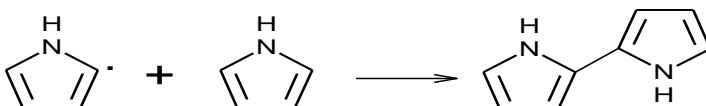


Scheme 2. Oxidative coupling of pyrrole molecules.

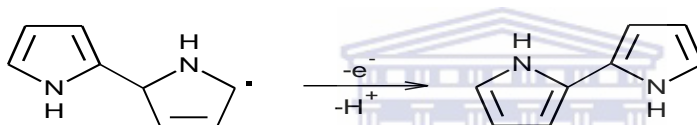
Monomer Oxidation



Radical Growth



Repeat Oxidation and Loss of Proton



Further Oxidation and chain growth

Scheme 3. Alternative polymerization mechanism of pyrrole (T. Vernitskaya et al, 1997).

These mechanisms explained by T. Vernitskaya et al, 1997, confirmed the inability of the mechanism to proceed in the reverse direction (polypyrrole to pyrrole). Polypyrrole actuators in the form of PPy/Adhesive tape according to Y. Nishioka, 2011, were placed in electrolyte solutions with a counter electrode. When negative charges were applied to the actuator, ions in the actuator were repelled and the actuator shrunk. Positive charges applied, caused an expansion of the actuator as positive ions were absorbed into the actuator. Table 5 below is a representation of the comparison of polypyrrole actuators with that of biological muscles (J. Madden et al, 2004).

Table 5. Comparison between PPy actuators and Skeletal Muscles.

	PPy Actuators	Skeletal Muscles
Operating Stress (MPa)	Under 10	0.1
Strain (%)	Up to 40	20
Durability	Up to 10^6	10^9
Work Density (kJ/m^3)	Up to 140	8

1.7 Bilayer Actuators

Bilayer actuators were the first type of conducting polymer actuators to be discovered in 1992. The initial use of bilayers was for the determination of volume changes and identification of the volume change mechanism. Bilayers provided a way to study conjugated polymers such as polypyrrole, polyaniline and polythiophene etc. The actuator comprised of a tape adhered to a film of conducting polymer electrogenerated onto a metallic electrode. The bending of the bilayer actuator is as a result of electrochemical reactions caused by the swelling or shrinking of the bilayer. The metallic counter electrode is used, by allowing current to flow through the bilayer system. A big part of the consumed electrical energy is lost in order to produce electrochemical reactions at the counter electrode (e.g. solvent dissociation, requires a high overpotential).

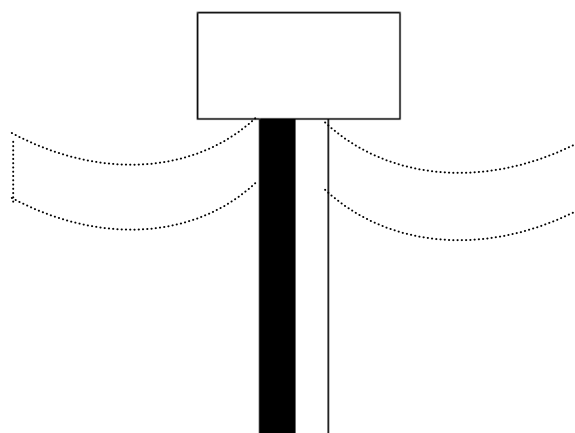


Figure 1. Bilayer actuator design

Applying potentials to the bilayer actuator will result in deformation, dependent upon the applied potential. The bilayer actuator will deform until the potential is changed resulting in the actuator moving in the opposite direction (figure 1). E. Jager et al, 2001, studied the electrochemistry of the polymer which was deposited onto a substrate. Electrochemical oxidation and reduction caused volume changes resulting in the deformation of the active layer. Ionic movement to and from the polymer was the process which was responsible for the deformation. Responses of these actuators when dc and ac voltages were applied have been studied by D. Sutar et al, 2007. The bilayer created was PPy-DBS/Au film which was made possible by electrochemically polymerizing the polymer onto gold coated polystyrene. Actuator abilities were demonstrated using this bilayer formation in aqueous media. The bilayers produced by U. Zainudeen et al, 2008, contained PEDOT(DBS)/PPy(DBS), this was produced by electropolymerization of the PEDOT onto the PPy film (previously prepared). They discovered that the inclusion of PEDOT (DBS) produced significant improvements in strain and force differences between redox states at faster scan rates. I. Lin et al, 2011, studied the characterization of alumina-coated/uncoated Au/SiN_x bilayer cantilevers, by

thermal cycling and isothermal holding tests. These bilayer cantilevers were used for the determination of the performance and reliability requirements of micro-electromechanical systems.

1.8 Trilayer Actuators

Trilayer actuators consist of three layers, with the middle layer being a porous material used for electrolyte storage. On either side of the porous layer are the conducting polymer layers. In aqueous media, the flow of current is applied across both conducting polymer films. This flow of current induces movement of the trilayer film, which results due to the volume change in the two conducting polymer films. The potential applied to the trilayer film, causes oxidation of the CP film at the anode (ions inserted into the CP film from electrolyte solution, ions maintain electroneutrality and cause swelling) and reduction of the CP film at the cathode (ions are expelled and the film shrinks).

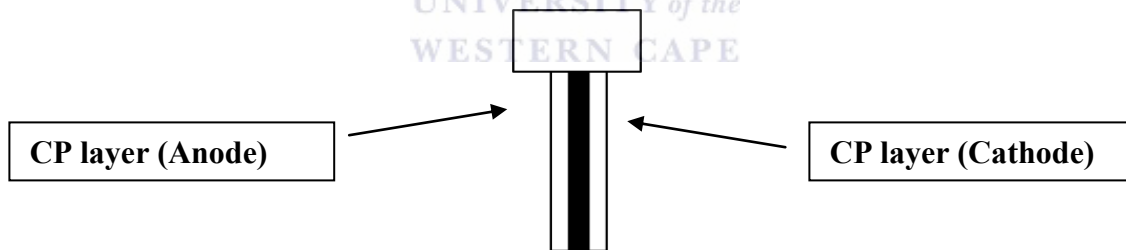


Figure 2. Trilayer actuator consisting of two conducting polymer layers on either side of a non-conductive tape.

Conducting polymers prefer being in the neutral form, as mass diffusion occurs when the polymer is in the oxidized state. Larger ions force the smaller more mobile ions to migrate into the polymer to maintain a neutral charge, resulting in an increase in the volume of the polymer. E. Jager et al, 2013, have developed new methods for micro-fabrication and patterning using photolithography to produce thin film trilayer

actuators. The degree of deformation of the trilayer actuators was dependent upon the thickness of the actuators.

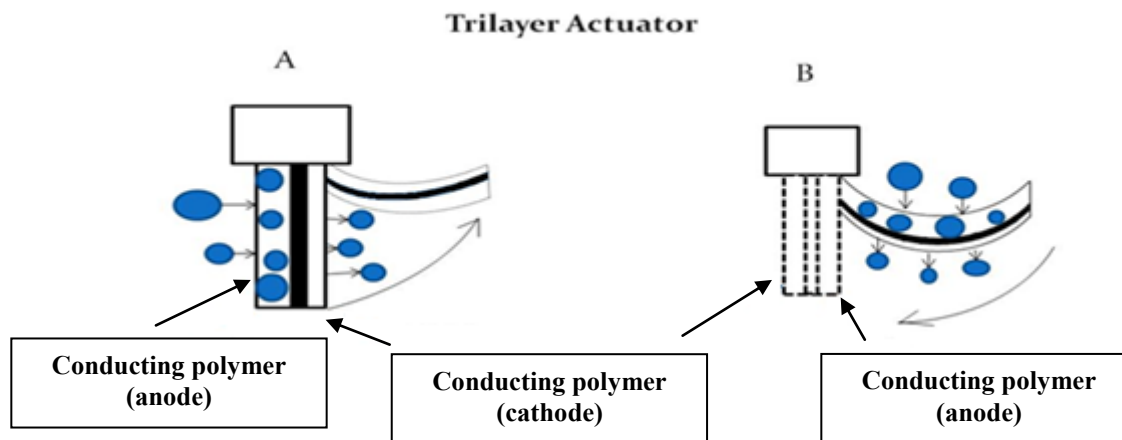


Figure 3. Deformation of trilayer actuator.

The trilayer actuator in figure 3 comprised of two conducting polymer (CP) layers, either side of a non-conductive adhesive tape. Potentials applied to the anode CP layer caused oxidation to occur which allowed ions to move from the solution into the CP film. Reduction occurred at the cathode film, causing reduction and shrinking in the film as ions are expelled. The trilayer PPy/PVDF/PPy was used to combine important EAP properties including diffuse impedance, double layer capacitance, conducting polymer resistance and charge transfer resistance (C. Nguyen et al, 2012). They discovered that the strain-to-charge density ratio was dependent upon applied voltage. Experimental data obtained was effective to accurately predict current responses and tip curvature. According to G. Han et al, 2004, the trilayer sandwich of PPy/Au/PPy was electrochemically synthesized by the oxidation of pyrrole in aqueous solutions and then sputtering the solution onto a thin gold film. The polypyrrole layers were doped using different dopants e.g. dodecylbenzene sulfonate (DBS) for one layer and the other layer with benzenesulfonate (BS). According to the experimental data obtained, the bending responses of the trilayer exceeded that of the bilayer actuator. This improvement was associated with the gold nano layer (highly conductive layer).

The one major disadvantage of these trilayer and bilayer actuators is the delamination process. Delamination results in the separation of layers due to continuous stress upon applied potential, this only allows for low amounts of deformation cycles. A new approach to actuator design based on interpenetrating polymer network (IPN) matrix actuator designs were created in order to overcome the delamination process that occurred. Incorporation of a graded interlayer reduced the stress intensity of the system which increased the resistivity of the layers to experience functional failure (cracking and debonding). The interface associated with the gradient of IPNs was beneficial in preventing crack formation and delamination (Y. Xuan et al, 2012).

1.9 Interpenetrating Polymer Networks (IPNs)

IPNs comprise of a combination of at least two polymers which display different characteristics. An absence of covalent bonds during this preparation is made possible when one polymer network is synthesized or crosslinked independently in the presence of the other (V. Bhardwaj et al, 2012). The IPN consists of two conducting polymer layers embedded towards the outside of a solid polymer electrolyte (SPE) matrix, which host the ions for deformation. The rate of deformation directly influenced the size of the IPN matrix; smaller IPN matrices yielded much higher frequencies. The development of the IPN by using two cross-linked polymers; Polyethylene Oxide (PEO) which ensured ionic conductivity and Polybutadiene (PB), allowed for adjustments to the required mechanical properties. According to C. Plesse et al, 2012, chemical polymerization of 3,4-ethylenedioxythiophene (EDOT) lead to the formation of a PEDOT gradient, whose concentration decreased from the outside towards the centre of the IPN matrix. Incorporation of the EDOT into the SPE allowed for deformation upon stimulus with various potentials. These IPN matrices were designed to operate in air,

with the SPE providing the ions for deformation. The major factor influencing the rate at which the IPN bends is the relative size of the IPN matrix, thus different IPN systems were explored. Initial IPN matrices developed were of a thickness of 250 μm which produced 3.5×10^6 cycles at a maximum frequency of 10 Hz. The IPN thickness was not suitable for the photolithography technique. The technique therefore required new host matrices with better mechanical properties and lower thickness. The photolithography technique is used for patterning parts of a thin film or substrate. The use of a different elastomeric partner with the IPN matrix was explored, using polytetrahydrofurane (PTHF). IPN matrices with very small thickness (ranging from 12 μm - 17 μm) were used for micro-sized actuators which could reach a frequency range of 30 to 200 Hz. These micro-actuators were developed by using photolithography and plasma dry etching process (A. Khaldi et al, 2011).

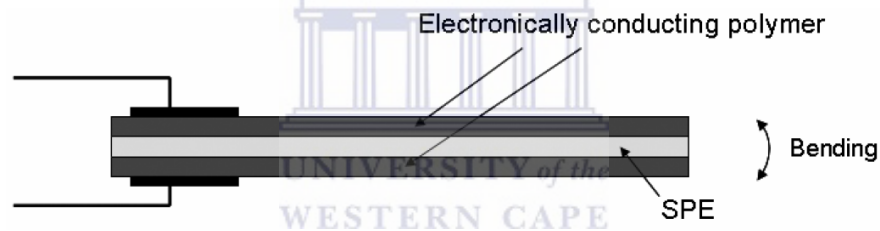


Figure 4. Diagram of IPN setup

The representation in figure 4 displayed the conducting IPN where electronic conducting polymers were selectively embedded towards the outside faces of the SPE IPN matrix. Deformation of the IPN matrix was dependent upon the frequency and voltage applied to the system. Moving rate of deformation increased as the film thickness decreased (D. Brandell et al, 2008).

Actuators have been used in a wide variety of applications with electroactive polymer actuators displaying the best desired properties for actuation such as actuation displacement, fracture toughness, density and reaction speed. Electroactive polymer

materials displayed favourable properties with respect to displacement capacity which were comparative to human muscle movements. Electronic and ionic EAPs were found to have the desired displacement ability with ionic EAP having the added advantage of low operating voltages. The actuator material proposed in this research follows the design of ionic EAPs produced by polymerization of a pyrrole derivative as the monomer with a very rigid geometry. It is envisaged the controlled geometry, together with the achievable displacement along the polypyrrole backbone, will greatly enhance the displacement potential of an actuator based on the novel polymer compound.



MAIN AIMS AND OBJECTIVES

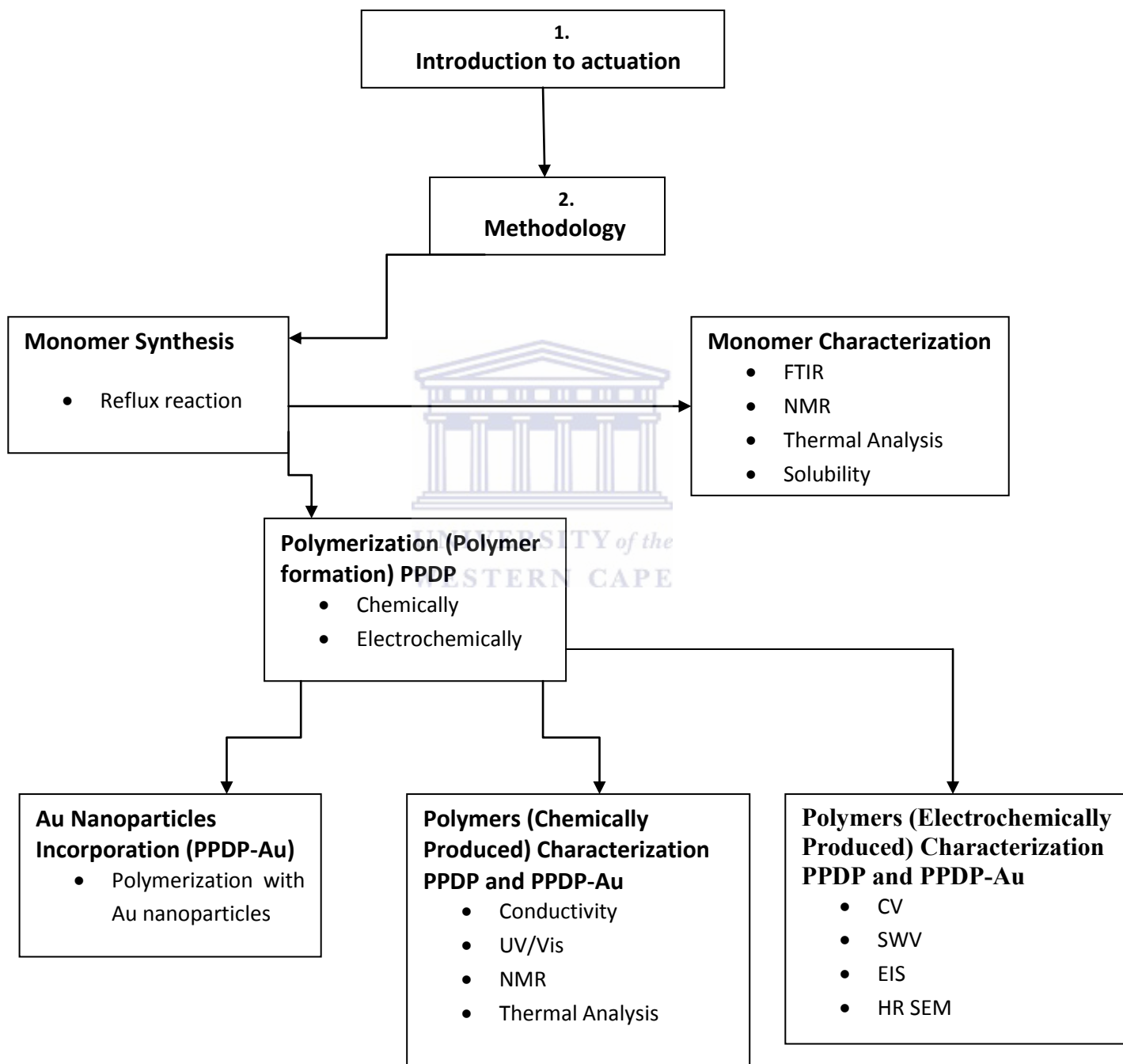
AIMS:

- Synthesis of a hinged molecule by Schiff-base formation;
- Polymerization of the pyrrole unit in the hinged molecule, to produce a repeating zig-zag polymer;
- Solubility testing of the chemically produced polymer;
- Actuation efficiency of the novel polymer synthesized by chemical and electrochemical methods.

OBJECTIVES:

- Material preparation
 - Phenazine-2,3-diimino(pyrrole-2-yl) – monomer
 - poly(Phenazine-2,3-diimino(pyrrole-2-yl)) – polymer
 - Polymer system modified with Gold Nanoparticles
- Determination of the chemistry for crosslinking to produce monomer material:
 - Spectroscopic and electrochemical evaluation of monomer synthesis
 - Solubility testing of the monomer in common organic solvents
 - Synthesis and characterization of gold nanoparticles incorporation
- Characterization of the monomer:
 - Spectroscopy to study the structural behaviour of the crosslinked product
- Electrochemical synthesis and characterization of the polymer and Au modified polymer system
- Chemical synthesis and characterization of the polymer and Au modified polymer system
- Comparison of conductivity of the polymer and Au modified polymer systems
- Evaluation of the solubility testing characteristics of the polymer products.

THESIS OUTLINE



CHAPTER 2

Design and synthesis of zig-zag polymers

Molecular design for improved actuation performance and starting materials (2,3-diaminophenazine and pyrrole-2-carboxaldehyde used for the novel zig-zag polymer preparation will be discussed.

2.1 Hinged molecular design

A hinged molecule such as calix[4]arene interconnected by rigid rods of quarterthiophene was among the first polymers designed to have the zig-zag shape in their geometry. Attraction between the quarterthiophene rods occurred when the material was in the oxidized state which in turn contracted the overall material. Oxidation of these rods caused π - π stacking to produce reversible molecular displacement during actuation. These hinged rigid structures which have great amount of internal volume were found to be capable of experiencing large volume changes upon application of potentials.

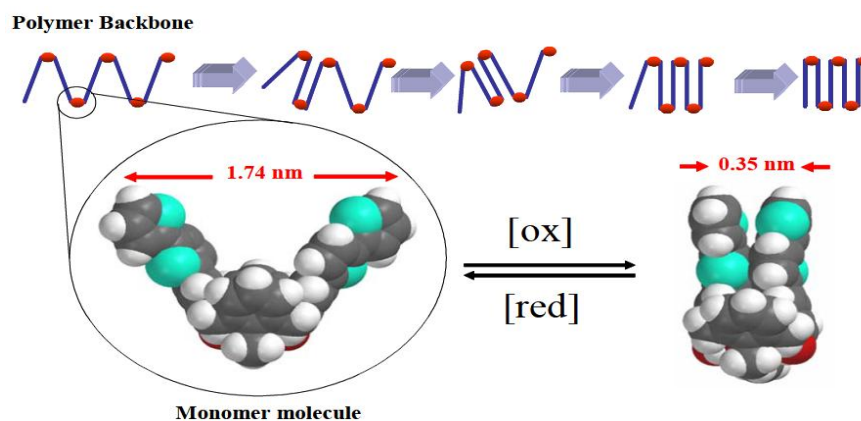


Figure 5. Zig-zag molecule containing calix[4]arene and quarterthiophene

Calix[4]arene hinge molecule was interconnected to quarterthiophene rigid rods which formed the polymer backbone (chain) represented in figure 5. When the zig-zag molecule was exposed to a potential the rods attracted one another (P. Anquetil et.al, 2002). Films using this setup displayed conductivities of 10^{-1} S/m, densities between 550 and 750 kg/m³ and tensile strengths of 20 MPa in the dried form and 1.3 MPa when soaked in acetonitrile. The system also displayed a reversible strain in the order of 20%.

Y. Lui et al, 2012, studied the behaviour of tetrahedral Zn center, with two coordination spots already taken up by SPh⁻ (phenyl sulfide) groups. The two remaining coordination sites were ready to be occupied by bifunctional ligands which resulted in the formation of helical or zig-zag chain-like structures. The zig-zag structure formed was [Zn(SPh)₂(BPyVB)]_n.

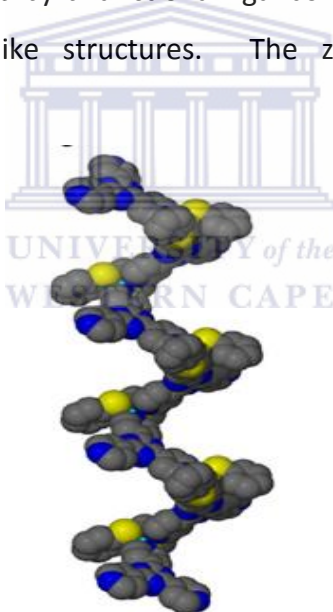


Figure 6. Zig-zag molecule of [Zn(SPh)₂(BPyVB)]_n.

The zig-zag polymer material represented in figure 6 was used as building blocks for the generation of helical and zig-zag polymer materials. The optical and thermal properties of the polymer were studied. The thermal analysis revealed a polymer material which

was thermally stable up to temperatures of 210 °C, with optical properties in terms of UV/Vis revealed onset absorption at 400 and 420 nm.

The design of coordination polymers (metal organic frameworks) often use metallic centres due to their magnetic, electrical and non-linear optical properties. P. Phuengphai et al, 2013, designed metal organic frameworks by using hydrogen bonds, π - π contacts and other weak and non-covalent interactions (also studied by D. Braga et al, 1995). The zig-zag polymer chain generated from the combination Zn(II)/dpe/acetate with secondary building units produced a tetrahedral geometry.

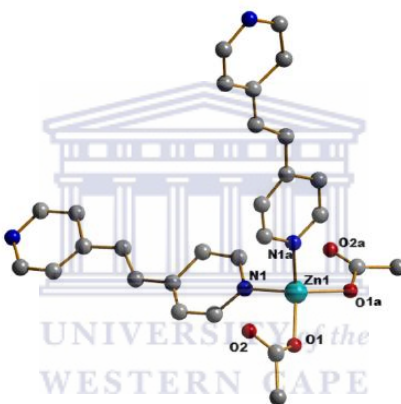


Figure 7. Representation of the zig-zag organometallic framework.

The formation of the metal organic framework resulted from the connection of mononuclear units through two dpe (1,2-bis(4-pyridyl)ethene) ligands to the other Zn(II) ions, resulting in the generation of infinite zig-zag chains. π - π Interactions occurred along the dpe units which are closely connected 2D layers. The organometallic framework in figure 7 displayed good heterogeneous properties, high size-selectivity towards compounds with benzaldehyde and high conversion of acetaldehyde to dichloromethane. Conversion values observed for this molecule were in the range of 57% to 74% when using tetrahydrofuran and dichloromethane respectively, whereas the conversion of the benzaldehyde was 14% when using dichloromethane.

Another design was explored by G. Chen et al, 2010, such as TTFV-hinged molecular tweezers. The exploration of the molecular tweezers displayed two functional π -conjugated groups which were connected to a central TTFV (tetrathiafulvalene) core made possible by covalent linkage. The formation of the tweezers produced a closely spaced hinged molecule, which could grip a guest molecule through non-covalent forces such as π -stacking or charge-transfer interactions. Oxidation of the tweezers caused the molecular hinge to rotate into a linear orientation and thus releasing the guest compound.

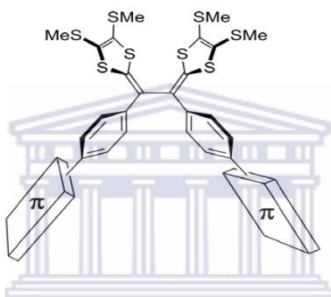


Figure 8. Structure of TTFV-hinged molecular tweezers.

Electrochemistry of the molecular hinge tweezers displayed a reversible redox couple in cyclic voltammetry which related to a two electron transfer process. The chemical reversibility of the material in figure 8 occurred due to the electron transfer process which was useful in the preparation of molecular switching devices.

In the current research we propose to exploit the zig-zag polymer conformation for actuation. The novel polymer formation will follow on the synthesis of a monomer based on 2,3-diaminophenazine and pyrrole-2-carboxaldehyde crosslinked in a classical Schiff base formation. Polymerization of the pyrrole moiety will produce the desired zig-zag polymer.

2.2 2,3-diaminophenazine (DAP)

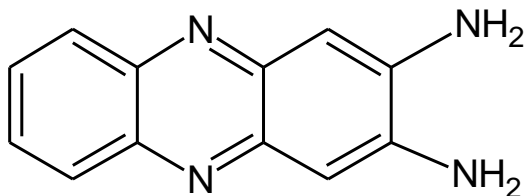


Figure 9. DAP is a solid chemical with a molecular formula of $C_{12}H_{10}N_4$ and a molecular mass of 210 g/mol.

The solid orange DAP (figure 9) obtained from Sigma-Aldrich was labeled as light sensitive and therefore stored in an amber glass bottle. An alternative means for obtaining this material would be to chemically reduce o-phenylenediamine by using horseradish peroxidase (P.J. Tarcha et al, 1987). DAP displays strong luminance in both polar organic solvents and aqueous buffer solutions. DAP can be used as a marker for the determination of fluorometric lacasse activity and in immunoassay determination of enzyme-catalyzed reactions (S. Sylvester et al, 2012).

2.3 Pyrrole-2-carboxaldehyde

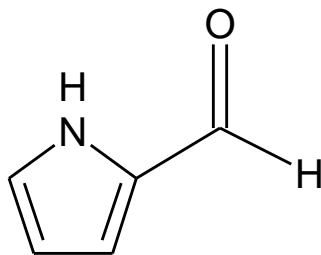
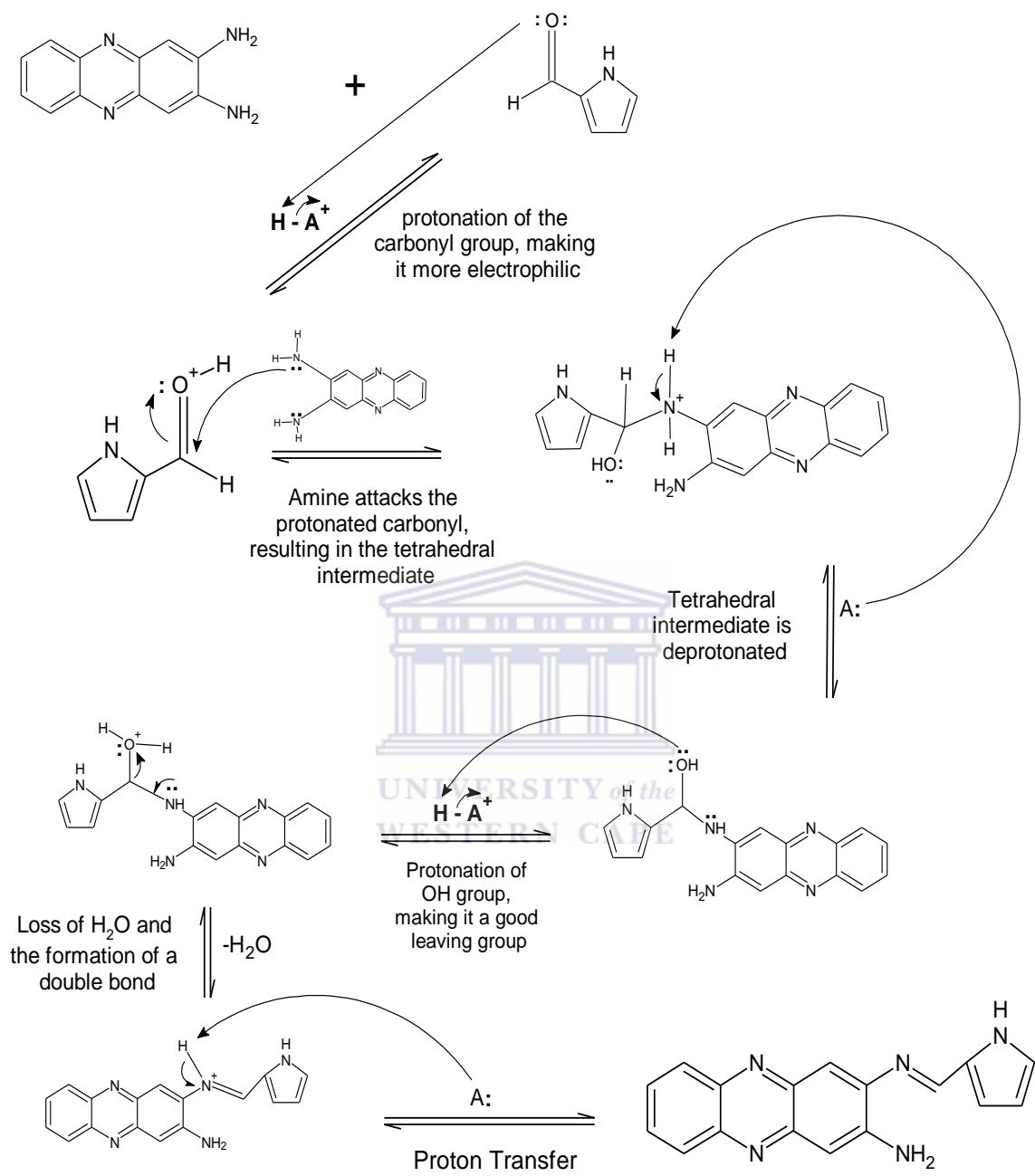


Figure 10. Pyrrole-2-carboxaldehyde has a molecular formula of C_5H_5NO with a molecular mass of 95.10 g/mol.

This slightly yellow crystalline material (figure 10) was obtained from Sigma Aldrich with relevant material safety data sheets (MSDS) and NMR documents. The chemical can be stored at room temperature for short periods of time, but to obtain maximum product performance the chemical should be stored -20°C for long term use. The chemical is soluble in both DMSO and methanol. This chemical is a derivative of pyrrole and was used in the synthesis of Schiff base compounds including; Co(III) complexes with unsymmetrical Schiff base ligands (S. Meghdadi et al, 2011) and 2-aminophenol-pyrrole-2-carboxaldehyde with metal complexes (B. Singh et al, 2010). A similar scheme was followed for the synthesis of the monomer in the present research (Scheme 4)





Scheme 4. Proposed mechanism for monomer formation.

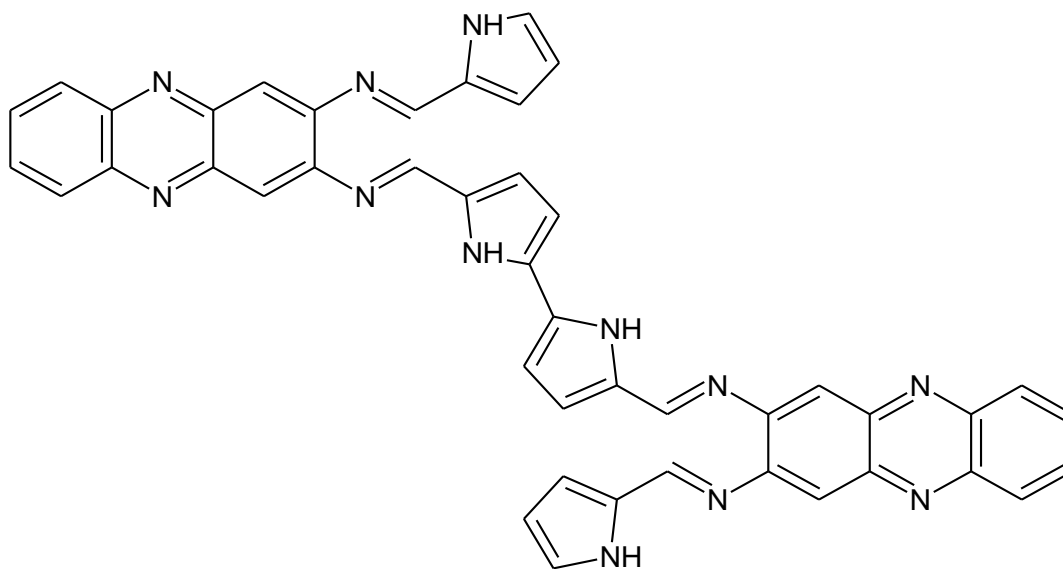


Figure 11. Proposed polymer formation

The zig-zag arrangement may be obtained by polymerization of the pyrrole moiety to produce the desired polymer. The crosslinking of the synthesized monomer will be pursued, through the pyrrole functionality by chemical and electrochemical synthesis produce a zig-zag polymer structure (figure 11).

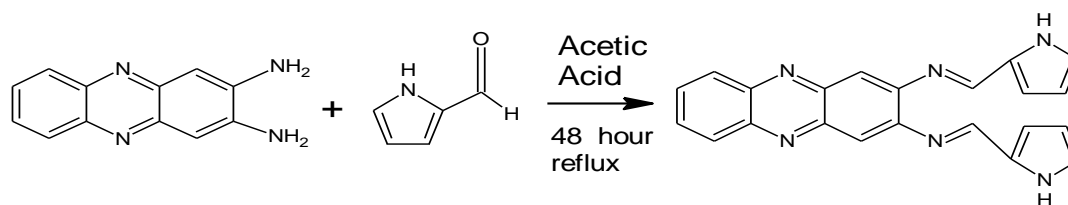
CHAPTER 3

Materials and Methodology

In this chapter all methodology required for material preparation and characterization will be discussed. Monomer synthesis, characterization and polymerization, chemically and electrochemically to obtain the polymer material, will be performed. Modification of the polymer system by gold (Au) nanoparticles and the respective characterization is presented.

3.1 Monomer synthesis - (Phenazine-2,3-diimino(pyrrole-2-yl)) – PDP

Monomer synthesis was prepared by dissolving 1 mmol of 2,3-diaminophenazine, 2.1 mmol of Pyrrole-2-carboxaldehyde (98 %) in 40 mL of Acetic Acid (99.7 %). A reflux reaction (48 hours) was set-up and heated at 130 °C, Acetic Acid (boiling point = 120 °C) was used as the solvent for refluxing. At completion of the synthesis, a precipitate resulted and was filtered and washed with methanol. The new monomer material (Phenazine-2,3-diimino(pyrrole-2-yl)) – PDP was then dried under vacuum at 70 °C, overnight. The sample was weighed and a yield of 60 % was obtained. The reflux setup consisted of a 100 mL round bottomed flask to which a reflux condenser was attached. The round bottom flask was placed in an oil bath (oil level should not be higher than the level of solution in the round bottom flask) and heated (hot plate with a temperature controller). The scheme below (Scheme 5) is carried out under carefully controlled pH (pH values below 6.0) conditions, with linkage of the two starting materials occurring at the position where the aldehyde group is lost.



Scheme 5. Schiff base formation of PDP.

The condensation reaction was used to produce the novel monomer material by the crosslinking of starting materials.

3.2 Materials

All reagents used for synthesis and characterization were analytical grade and were obtained from Sigma-Aldrich. Deionized water was obtained from the Millipore Synergy water system which is nuclease free (resistivity of 18 M Ω); this water was used in the preparation for all aqueous solutions. A list of chemicals used throughout the experimental procedures is provided (table 6).

3.3 Solution Preparations

Solutions were prepared using general analytical methods and formulas which were required for respective preparations.

For solutions which were prepared from solid materials, the following equation was used,

$$\text{Mass} = \frac{\text{Molecular Mass} \times \text{Concentration}(\text{desired}) \times \text{Volume}(\text{final})}{1000} \quad \text{eqn. 1}$$

For solutions whose concentration could be calculated the following was used;

$$C_i V_i = C_f V_f \quad \text{eqn. 2}$$

Where;

C_i = initial concentration

V_i = initial volume

C_f = final concentration

V_f = final volume

Solution 1: 0.1 M Hydrochloric acid solution was prepared by diluting 1.68 mL of 37 % HCl to 500 mL with water. The HCl was slowly added to the water already present in the beaker, solution was allowed to be stirred for a few minutes to thorough mixing.

Solution 2: 0.1 M Lithium Perchlorate solution was prepared by dissolving 5.3195 g of LiClO_4 in 500 mL of water.

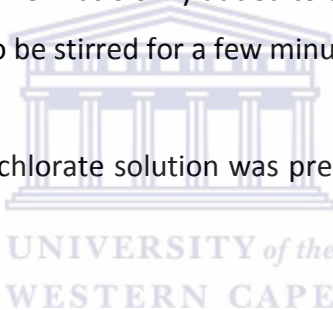


Table 6. Chemicals used for synthesis.

Chemical Name	Purity	Chemical Company
Pyrrole-2-carboxaldehyde	98 %	Sigma-Aldrich
2,3-diaminophenazine	90 %	Sigma-Aldrich
Acetic Acid	99.7 %	Sigma-Aldrich
Hydrochloric Acid (HCl)	37 %	Sigma-Aldrich
Dimethylformamide	99.8 %	Sigma-Aldrich
Anhydrous Iron(III) chloride	99.9 %	Sigma-Aldrich
Tetrahydrofuran (THF)	99.9 %	Sigma-Aldrich
Methanol (MeOH)	99.9 %	Sigma-Aldrich
Hydrazine	35 wt. % in H_2O	Sigma-Aldrich

Dimethylsulfoxide (DMSO)	99.9 %	Sigma-Aldrich
Polyvinylsulfonic Acid (PVSA)	25 wt. % in H ₂ O	Sigma-Aldrich
Pyrrole	98 %	Sigma-Aldrich
Lithium Perchlorate (LiClO ₄)	98 %	Sigma-Aldrich

3.4 Solubility

Solubility is the property of a material to dissolve in gaseous, solid and liquid solvent to create a solution of solute in solvent. When a solute is left in contact with a solvent, it dissolves until the solution is saturated. Various factors influence the solubility of materials which may include the chemical and physical properties of the material as well reaction conditions including; temperature, pH and pressure. The solubility testing of the monomer and polymer material was performed by dissolving 10 mg in 1 mL of various solvents including, Tetrahydrofuran (THF), Methanol (MeOH), Dichlorobenzene (DCB), Dimethylformamide (DMF), Dimethylsulfoxide (DMSO), Chloroform (CH₃Cl) and various other organic and inorganic solvents. The solubility testing of the monomer was performed as this is a requirement for a wide range of applications.

3.5 Monomer Characterization

3.5.1 Fourier Transform Infrared (FTIR) Spectroscopy

This technique was used for the identification and determination of the structure of materials, by obtaining an infrared spectrum of emission and absorption of solids, liquids and gases. This mathematical process (fourier transform) converts raw data obtained into actually spectra. Analysis of starting materials (2,3-diaminophenzaine and Pyrrole-2-carboxaldehyde) and monomer material were performed on solid samples and were run on a Perkin Elmer Spectrum 100 instrument. FTIR was done for the

confirmation of the functional groups present in the sample and to determine if the crosslinking of the starting materials had occurred.

3.5.2 Nuclear Magnetic Resonance (NMR) Spectroscopy

NMR studies the properties of molecules containing magnetic nuclei by applying a magnetic field and observing the frequency of the resonant electromagnetic field. The NMR technique is simple in concept but spectra can sometimes be highly complex, however data resulting from the spectra provides much information about the structural formation of materials. ¹H NMR was performed on starting materials by dissolving them in DMSO. The samples were performed on a Bruker 300 MHz instrument. The sample for NMR was prepared by dissolving 20 mg of the starting materials and dissolving them in 1 mL of DMSO-d₆. NMR was used to confirm the chemical structure of the starting materials.

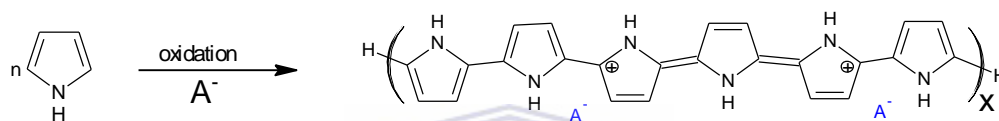
3.5.3 Differential Scanning Calorimetry (DSC)

DSC is a thermal analysis technique which looks at how heat capacity (C_p) is changed by temperature under controlled atmosphere. Materials are exposed to temperature ramps, which allow for heat capacities of materials to be tracked as heat flows. The sample under investigation and a reference sample were exposed to the same temperature ramp. DSC analysis was performed on the new monomer material by weighing out 4mg and exposing it to a controlled environment (air or inert gas including; nitrogen or helium) on a Thermal Analysis (TA) Q20 series system. The monomer material was exposed to a temperature ramp between -100 °C and 250 °C. DSC analysis of materials was done in order to confirm the thermal behaviour of the materials.

3.6 Polymerization

3.6.1 Chemical Polymerization

The dopant counter ions (A^-) were incorporated into the chain during polymerization. This influences the polymerization process as well as the properties of the polymer material. The most common and widely used oxidants are ammonium persulfate and Iron(III)Chloride, whilst hydrogen peroxide and various other trace metals (Ce^{4+} , Cu^{2+} , Cr^{6+}) have also been used.



Scheme 6. Pyrrole polymerization

Polymerization of pyrrole to form the complex, dynamic structure called polypyrrole which is used as the chain molecule, is represented in scheme 6. Usually upon polypyrrole formation the number of repetitive monomer units was between 3 and 4, the A^- is the counter ion incorporated during synthesis. Chemical polymerization of the monomer material to produce the polymer poly(Phenazine-2,3-diimino(pyrrole-2-yl))-PPDP was achieved through reaction of 0.5 mmol PDP and 5 mmol Anhydrous Iron(III)Chloride ($FeCl_3$). The $FeCl_3$ solution was added dropwise to the already stirred PDP solution (reaction between $FeCl_3$ and water was exothermic). The solution was allowed to stir for 24 hours before filtration and washing with methanol. Iron(III)chloride was used as an oxidant in the production of the conducting polymer by incorporating a positive charge onto the backbone of the polymer.

3.6.2 Electrochemical Polymerization

This polymerization occurred at the electrode surface in an electrochemical cell using a solvent with relevance for polymerization. The solvent should be as pure as possible as it plays an important role in the reaction mechanism. When the initial layer of the polymer was deposited onto the electrode surface it became a reactant which determined the rest of the polymerization process. The counter ion which was introduced into the system balanced the charge on the polymer backbone. Incorporation between the polypyrrole planes which favour α - α bonding was achieved. Potentials chosen for polymerization influenced the rate of oxidation and therefore polymerization. If the rate of polymerization is too slow, oxidation of the monomer will occur without deposition, which results in polymer chain (backbone) not reaching its preferred chain length. All polymerization and characterization of polymeric systems were performed on screen printed carbon electrodes (SPCE). The formation of the polymer material at the electrode surface was done using a technique called cyclic voltammetry. The monomer material was polymerized in an electrochemical window between -400 mV and +700 mV at a scan rate of 50 mV/s using a BAS 100W Electrochemical Analyzer. PDP was dissolved in 2 mL of dimethylformamide (DMF) and then diluted to 4 mL with 0.1 M hydrochloric acid (HCl). This polymerization cycle was repeated 25 times to allow for growth at the the electrode surface, with polyvinylsulfonic acid (PVSA) used as a surfactant. The modified polymer system was produced by using the same parameters used for electrochemical polymerization of the monomer, but an extra addition of 600 μ L of the Au nanoparticles was added to the polymerization solution. Polymerization of PDAP occurred in 0.1M HCl solution between a potential window of -800 mV and 400 mV at a scan rate of 10 mV/s. The polymerization solution was purged with Argon gas and light was prevented from entering the electrochemical cell. Distillation of pyrrole was performed before polymerization occurred. Polymerization occurred in 0.1 M LiClO₄ at a scan rate of 50

mV/s between a potential window of -400 mV and 700 mV. The polymerization solution was purged with argon gas and a blanket of argon was kept above the solution. The polymer was prepared as a thin film by polymerization on screen print carbon electrodes which was used for diffusion and morphology analysis. Chemical and electrochemical polymerization of the novel monomer materials was performed to produce the zig-zag polymer material.

3.7 Gold (Au) Nanoparticles Synthesis

Gold nanoparticles (AuNPs) were synthesized through the reduction of 1.0 mM HAuCl₄ using sodium citrate as the reducing agent. 20 mL of 1.0 mM HAuCl₄ solution was added to a 50 mL Erlenmeyer flask on a stirring hot plate, the solution was then stirred and allowed to reach boiling temperature. To this boiling solution, 2 mL of 1 % solution of sodium citrate, (C₆H₅O₇Na₃) was added. Gold nanoparticles gradually formed as the citrate reduced Au³⁺ to Au⁰, with solution changing to a deep red colour upon constant heating. The deep red Au nanoparticles solution was characterized in terms of UV/Vis spectroscopy, with the solution requiring dilution as the original solution was too concentrated for the instrument. A new solution was prepared by diluting 1 mL to 10 mL with water. The spectral property of the Au nanoparticles was read on a UV/Vis instrument using VisionPro software. Incorporation of the gold nanoparticles into the PPDP system was performed during both chemical and electrochemical polymerization process.

Gold nanoparticles display exceptional properties including; optical, electronic and molecular recognition properties which allow for these nanoparticles to be used in a wide variety of applications. Incorporation of these gold nanoparticles into the polymer system was essential for the improvement in conductivity. The gold nanoparticles (600 µL) were introduced into the polymer system by the addition of the nanoparticles during

the electropolymerization process. Synthesis of the Au nanoparticles was performed for the incorporation into the polymer material to improve the conductivity. According to D. Li et al, 2009 sulfur-terminated polymers can directly bond to the surface of gold nanoparticles through sulfur gold interactions to form perfect cores of the polymer/gold nanocomposites. V. Chechik et al, 1999 studied the formation of stable monolayers on planar Au substrates when using thiolated dendrimers. Therefore Au nanoparticle modification of the polymer was selected as the initial means of not only improving conductivity, but also to prepare the polymer material for potential modification in biosensing applications.

3.8 Polymer Characterization

3.8.1 Electrical Conductivity

Electrical conductivity may be defined as the materials ability to conduct electrical current, denoted by the symbol σ (sigma) with units of Siemens per meter. Samples of PPDP, PPy and PPDP-Au were evaluated for conductivity. Thick films were prepared by compressing the polymer material into a pellet. Polymer was compressed at 2 tons of pressure resulting in the formation of a polymer pellet which was then used for conductivity measurements. The properties of the pellet were determined beforehand namely pellet thickness, diameter and surface area. These properties were essential in the calculation for the determination of conductivity.

Four Point Probe

The Universal Probe combined with the RM3000 Test Unit is a unique system which measures the diffuse layer resistivity (where the layer is of the opposite conductivity type to the substrate, or the substrate is an insulator). Upon measurement all four probes are in contact with the polymer pellet.

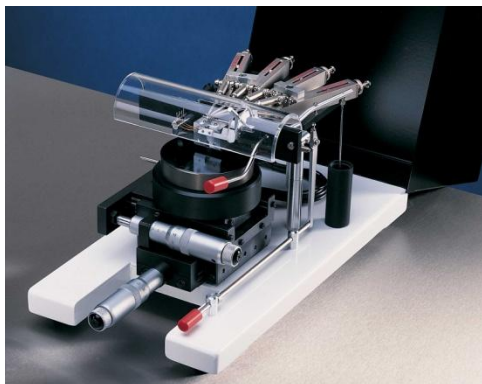


Figure 12. The Universal Probe containing the four probe needles used for conductivity measurements.

Conductivity by Cyclic Voltammetry

Conductivity measurements were performed on a Biologic potentiostat by performing a cyclic voltammogram of current (I) versus potential (V). This was made possible as the pellet was placed in a special cell designed for the purpose of conductivity measurements, at a scan rate of 20 mV/s between a potential window of ± 1 V. The resistance from the data obtained was used to determine the conductivity of the polymer material. The following equation was used to calculate the conductivity (M. Hashim, et al., 2012);

$$\sigma = \frac{1}{R} + \frac{\ell}{s} \quad \text{eqn. 3}$$

Where;

σ = conductivity

R = resistance

ℓ = pellet thickness

s = surface of the pellet

Conductivity by Electrochemical Impedance Spectroscopy

The Solartron 1296A Dielectric Interface system was used for conductivity measurements, which provided fast, accurate repeatable impedance measurements. The measurement was performed over a range of frequencies 100 kHz to 0.01 Hz, the impedance is related to the conductivity and capacitance of the material. The resistivity of the material was determined and two methods were used for the calculation of conductivity, with eqn. 3 being the first and the other;

$$\sigma_{AC} = 2\pi \times f \times Cd/A \times \tan \delta \quad \text{eqn. 4}$$

with $\epsilon_r = Cd/\epsilon_0 A$

and $\epsilon_r \epsilon_0 = Cd/A$

Where;

f = frequency

d = thickness

C = capacitance

A = area of the cell

$\tan \delta = \epsilon_i/\epsilon_r$ with; ϵ_i = imaginary permittivity; ϵ_r = real permittivity;

ϵ_0 = absolute dielectric constant



Conductivity of the materials was a necessity as it is one the main requirements for actuation materials.

3.8.2 Thermogravimetric Analysis (TGA)

TGA is a technique which measures the mass change of materials as a function of temperature or time under a controlled atmosphere. As the temperature of the system is increased, the materials under investigation will decompose. Materials were weighed

(10 mg) for analysis on a TA Q50 system with a temperature ramp between 20 °C and 600 °C, system was under controlled environment (same as DSC analysis). TGA analysis of starting materials, PPDP and PPy were performed. This technique was used to determine the thermal stability of the materials under the influence of a temperature ramp.

3.8.3 Voltammetric Techniques

This includes the study of chemical reactions which take place in solution at the interface of an electron conductor (the electrode) and an ionic conductor (electrolyte). Analysis of these electron movements can be obtained by means of Cyclic Voltammetry (CV), Square Wave Voltammetry (SWV) which are techniques used to determine the redox potentials of as well as formal potentials, conductivities and diffusion coefficients of polymeric systems. These two techniques used are the most popular for electrochemical analysis. Other quantities such as electron transfer rates and redox potentials can also be obtained using electroanalytical methods. Voltammetric techniques are defined by the application of applied potentials to an electrode which is monitored by the current flowing through the electrochemical cell.



Figure 13. An electrochemical cell.

An electrochemical cell usually consists of a three electrode setup including; a working electrode (WE - electron transfer facilitator), a reference electrode (standard indicator of the potential of WE). In order to maintain constant potential while current is being applied (balance redox events) to the system, a counter/auxiliary electrode (AE) is employed to balance the current experienced by the WE. The electrolyte solution was stirred to create uniformity; solution was purged with Argon gas – remove to main text.

Cyclic Voltammetry (CV)

CV is one most commonly used electrochemical technique which consists of plotting current which flows as a function of potential, for the study of both inorganic and organic compounds. Instruments using this technique provided information vital for the understanding of chemical reactions coupled with the charge transfer steps. The

instrument used for this technique was the PalmSens electrochemical sensor interface system with PSTrace software. Under controlled conditions the amount of current obtained can be related to the concentration of species (good for quantitative analysis). CV is a reversal scan technique which involves the application of a potential gradient in both forward and backward directions. Current flow that occurs is due to the oxidation/reduction process which results in ion flow. Peak positions allow for the determination of redox potentials and peak areas allow for the quantification of charge during the redox process.

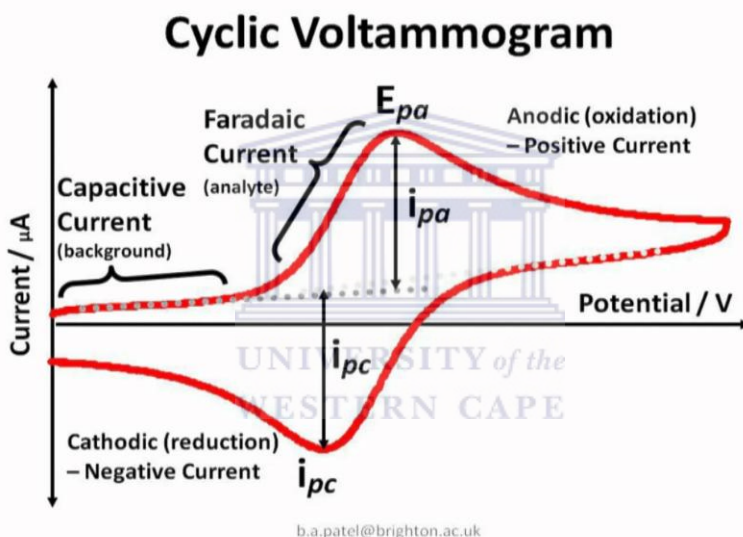


Figure 14. Cyclic voltammogram displaying a reversal technique of current versus potential.

In potentiodynamic electrochemical measurement the working electrode potential was ramped linearly with time. Initial potential (V_1) was the starting point at which the voltammogram began and was ramped until the vertex potential (set potential or V_2) was reached. Once the vertex potential had been reached the ramp was then reversed. Moving towards positive potentials the anodic peak current (i_{pa}) values as well as the potential (E_{pa}) value similarly when the ramp was reversed the cathodic peak current

(i_{pa}) was obtained as well as the potential (E_{pa}). In CV the initial current obtained was the capacitive current which was due to the double charge layer being formed at the surface of the electrode. The peak values (oxidation or reduction peaks) of the analyte which was due to the faradaic current. CV systems may be reversible, irreversible or quasi-reversible.

In reversible CV systems the mean surface concentrations (C_O and C_R) should show superimposed forward and reverse traces of current versus potential. Kinetic reversibility is shown by a peak separation near

$$\Delta E_p = \frac{60}{n} \text{ mV} \quad \text{eqn.5}$$

$$\text{with } \frac{I_{pa}}{I_{pc}} = 1 \text{ at } 298 \text{ K.}$$

Considering the Nernstian system $O + ne \leftrightarrow R$, for irreversible systems where adsorbed O is reduced in a totally irreversible one-step, one electron reaction. Irreversibility results due to the slow electron movement or chemical reactions occurring at the electrode surface. Irreversible systems display no return peak or a $\Delta E_p > 200 \text{ mV}$.

Quasi-reversible systems display behaviour which lies in between reversible and irreversible systems. Characterization of PPDP and the modified PPDP-Au system on screen printed carbon electrodes were performed in 0.1 M HCl (Solution 1). These polymer systems were characterized between a potential of $\pm 1 \text{ V}$ over a range of scan rates from 100 – 250 mV/s. Upon completion of the characterization techniques the polymeric systems were then quantitatively assessed in terms of diffusion coefficients and formal potentials.

Square Wave Voltammetry

This technique displays great sensitivity as well as efficient rejection of background, scan rate being directly proportional to the frequency. Larger amplitudes yield larger response signals but faradaic peaks broaden and the potential resolution becomes lost. The inventors of this sensitive technique was Ramaley and Krause but the technique had been extensively been developed by Osteryoungs and their coworkers. Square wave voltammetry is usually carried out on a stationary electrode (WE), where waveform and measurements occurred.

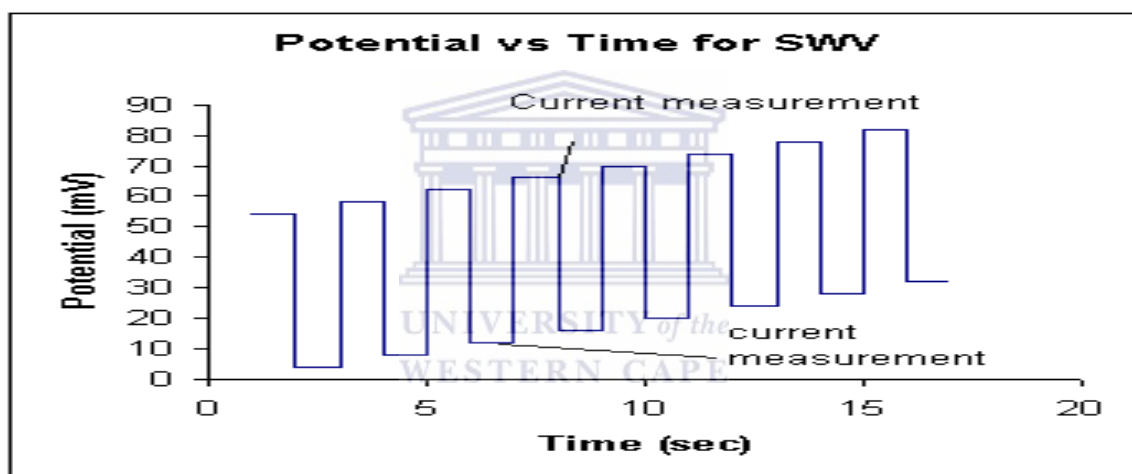


Figure 15. A potential is scanned as a function of time a potential sweep is displayed.

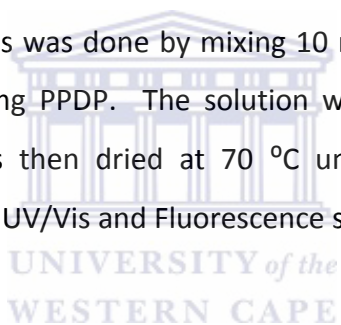
Oxidation and reduction species are displayed as a peak when a square wave is superimposed onto the potential sweep. Minimizing of the current signal from capacitive charge current can be achieved by measuring the current of each potential charge before the next step. Each electrochemically synthesized polymer system was characterized in 0.1 M HCl solution, with oxidation and reduction scans performed individually. Upon determination of the voltammograms obtained from the respective CV's, the square scanning potential window was adjusted. Various frequencies were used as a function of the steps, the steps remained constant while frequency changed to

display scan rates of 100 mV/s, 200 mV/s and 300 mV/s. Initially a reduction potential scan was performed and then the potential was reversed to determine the oxidation behaviour.

The voltammetric techniques were used to determine the redox behaviours of the material as well as; diffusion coefficients, formal potentials, peak separations, electron transfer and surface concentrations of the materials.

3.8.4 Spectroscopy

The polymer material was dedoped before performing spectral analysis with hydrazine (35 % wt solution in H₂O). This was done by mixing 10 mL of Hydrazine with 30 mL of H₂O and approximately 100 mg PPDP. The solution was then filtered to obtain the dedoped polymer, which was then dried at 70 °C under vacuum, overnight. The dedoped product was used for UV/Vis and Fluorescence spectroscopy.



Electrochemical Impedance Spectroscopy (EIS)

In electrochemical impedance spectroscopy a cell or electrode impedance is plotted as a function of frequency. The theory of this technique is based on the equivalent resistance and capacitance values for the systems resistance to the flow of electrical current. EIS is capable of high precision and is commonly used for the evaluation of heterogeneous charge-transfer parameters as well as double-layer structures. EIS is usually measured by applying a potential to an electrochemical cell and then measuring the current through the cell. An impedance plot displays the dependence of impedance on the frequency in a complex plane. This represents the dependence of imaginary on real impedance, which can be analyzed by equivalent electrical circuit fitting for the given electrode system and process. The resistance (R) of the system can be displayed

in the following equation (Ohm's Law), which display the ratio between voltage (V) and current (I);

$$R = \frac{V}{I} \quad \text{eqn. 6}$$

Resistance of the system is independent of the applied frequency, but the AC current and voltage through the resistor are in phase with one another.

The Nyquist plot of impedance is usually in the form of a semi-circle part as well as a linear part. The semi-circle at higher frequencies is associated with electron transfer processes; whereas the linear lower frequencies behavior is typical of diffusion processes.

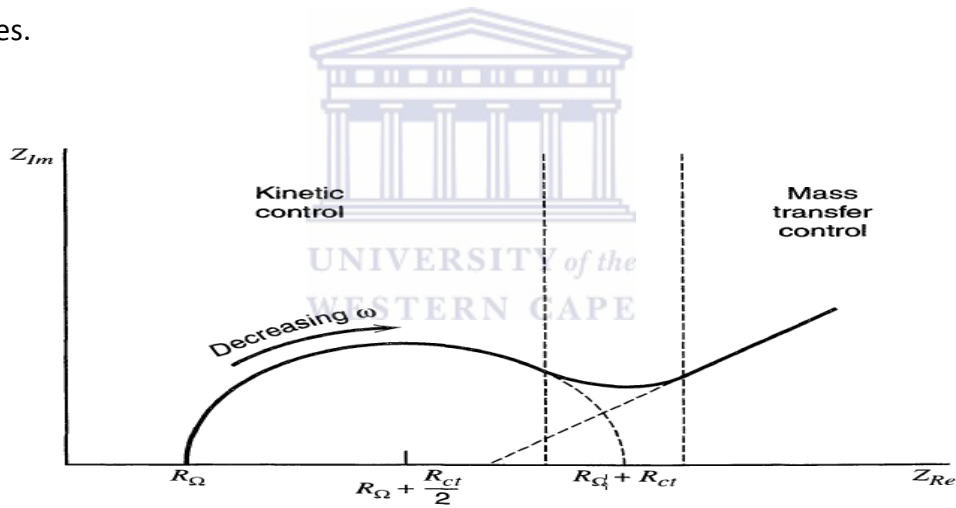


Figure 16. Complex EIS plot

In a typical impedance plot for an electrochemical system, regions of mass-transfer and kinetic control are displayed at low or high frequencies (figure 16). The determining factor of the system is the charge transfer resistance, R_{ct} . An alternative method for displaying impedance data is the bode plot in which the logarithm of the magnitude $|Z|$

and the phase angle (ϕ) are presented as a function of the frequency of rotation (ω) (figure 17).

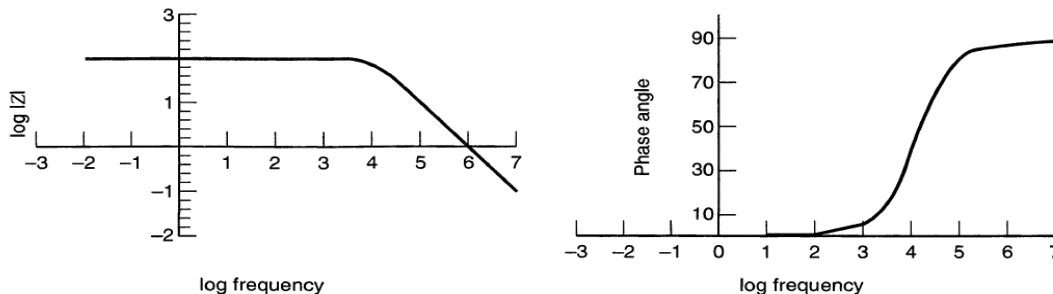


Figure 17. On the left is the bode plot of $\text{Log } |Z|$ vs. $\log \omega$ and on the right bode plot of ϕ vs. $\log \omega$.

This 3-electrode system was used to study the electrochemical impedance of the electrochemical systems, using the predetermined potential window from CV. The starting potential applied was -500 mV with subsequent potential steps (10 steps at +100 mV increments) until the final potential was reached (+500 mV). The frequency range used was from 10 Hz to 100 kHz. The electrochemical impedance spectroscopy was used to determine the charge transfer resistance values which were associated with the conductivity of the different prepared materials.

UV/Vis Spectroscopy

Many molecules absorb ultraviolet or visible light. Ultraviolet (UV), visible (Vis) and near infrared (NIR) are used for adsorption spectroscopy or reflectance spectroscopy in the UV region. Transition metal ions, highly conjugated organic compounds and biological macromolecules can all be quantitatively determined when using UV/Vis. This technique measures transitions from the ground state to the excited state.

UV/Vis analysis was performed by preparing a 1mg/ml solution of the PPDP material dissolved in tetrahydrofuran (THF). The analysis was performed on a UV/Vis system between 200 and 900 nm. The solution needed to be diluted as the adsorption of the

material was above 1. UV/Vis analysis was also performed on 2,3-diaminophenazine as well as filtered monomer solution (solution used for electropolymerization) which was yellow in colour. The UV/Vis instrument used for analysis was a Nicolet Evolution 100 using VisionPro software. This technique was used to determine the amount of light absorbed by the polymer material as well as to determine energy bands of the material.

Fluorescence Spectroscopy

This technique deals with electronic and vibrational states. Initially a species is first excited by absorbing a photon (quantum of light) from the ground state to the excited electronic state. The loss of vibrational energy which allows the photon to reach the lowest vibrational state occurs as a result of the collision with other molecules. Fluorescence spectroscopy measures the transitions from the excited state to the ground state. Excitation and emission wavelengths of the material were determined by initially completing the UV/Vis analysis of the material. The analysis was performed using a Nicolet Evolution 100 instrument with VisionPro software. Fluorescence spectroscopy was used to determine the fluorescent ability of the material for the potential application in dye sensitized solar cells.

Scanning Electron Microscopy (SEM)

This technique uses electrons to form images; it also has large field depths which allows for more of the sample to be focused on at one time. It has a very high resolution which allows for sample magnification at the nanometer scale. Electrons which interact with sample atoms produce backscattered electrons which are captured as the analytical signal.

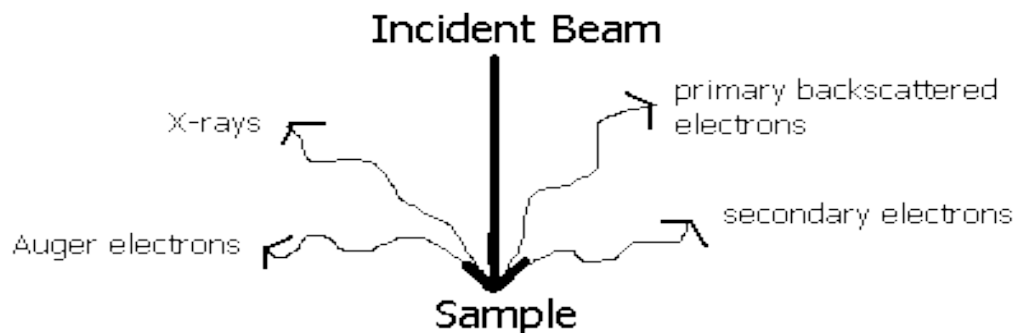


Figure 18. Incident beam used in SEM analysis

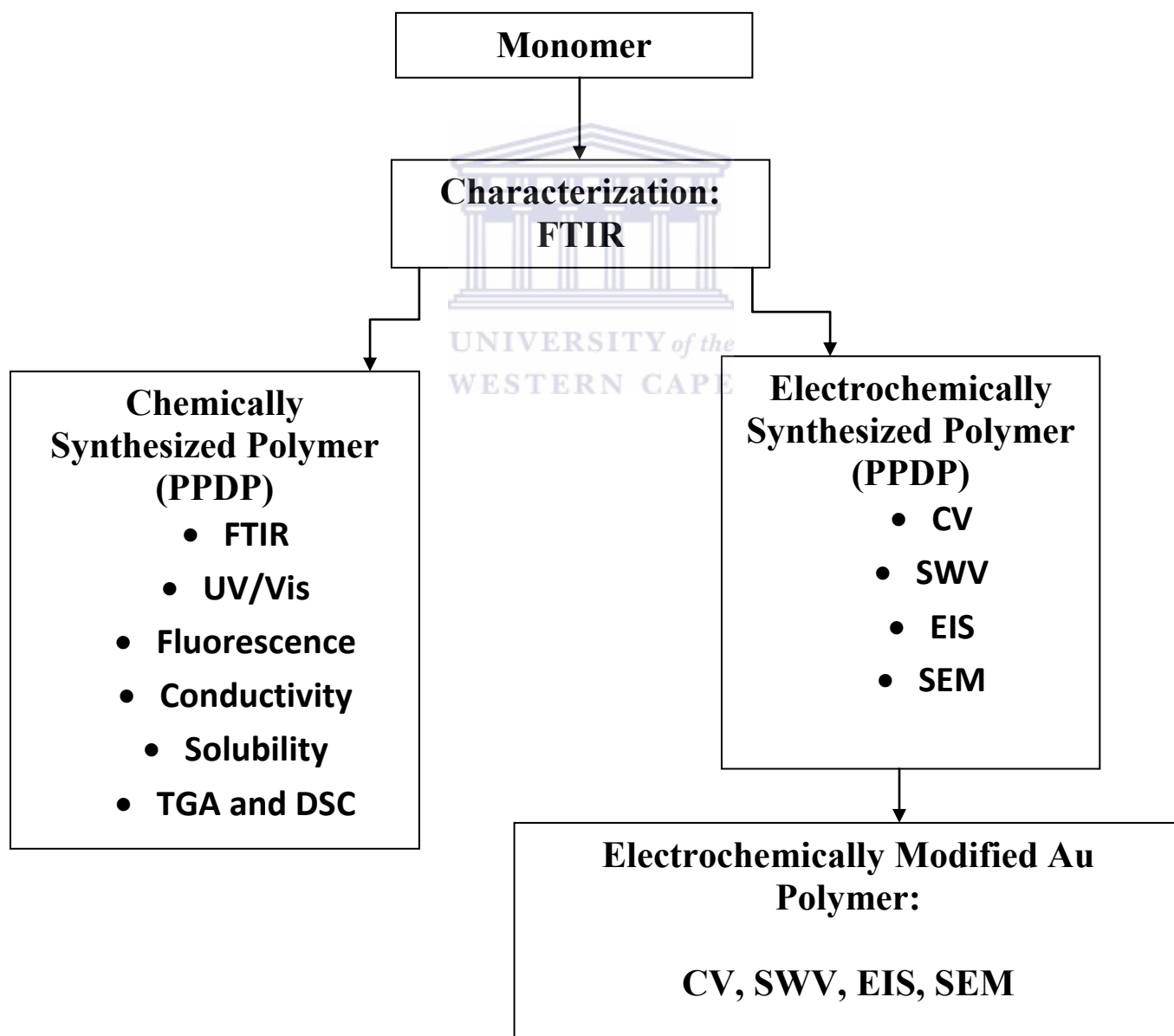
The incident beam travels through the electromagnetic field and lenses from the instrument and the beam is focused onto the sample. When the beam hits the sample, electrons and x-rays are ejected from the sample, collection of these scattered electrons is performed by a detector. SEM analysis will be used to study the morphology of the novel zig-zag polymer and the Au nanoparticles modified polymer system.

The monomer proposed in this work is completely novel and has not been used in actuation evaluation before. The two important parameters for efficient actuation in EAP are conductivity and solubility. Conducting polymers are notoriously insoluble in common organic solvents and the solubility testing of the new EAP, will be evaluated using a variety of organic solvents.

CHAPTER 4:

Results and Discussion:

The characterization of starting materials, monomer and polymer for conformation of the desired product and its properties by spectroscopy, morphology and electrochemistry, will be presented.



4.1 Monomer material formation

The synthesized monomer material, phenazine-2,3-diimino(pyrrole-2-yl) will be abbreviated PDP, for convenience. The monomer was synthesized by condensation reaction of 2,3-diaminophenazine and pyrrole-2-carboxaldehyde in the presence of acetic acid (Scheme 5). The formation of Schiff base was catalyzed by dilute acid. Ideally the Schiff base formation takes place smoothly between pH 3-5. Since dehydration is acid-catalyzed, it seems clear that an increase in acidity should result in an increase in the rate of dehydration and thus in the rate of reaction. The amine is nucleophilic owing to the unshared pair of electrons on nitrogen. As the acidity of reaction medium increased, the amine was protonated and became non nucleophilic. Addition to the carbonyl group no longer took place. The reaction was a balance between two steps which depended upon the pH in opposite ways. Therefore, the reaction required a careful control of pH. The solution had to be acidic enough to protonate some carbonyl groups, but not so acidic that all of the amino groups were protonated. At higher acid concentration, all the amine molecules were in the non-reactive protonated form. At the other extreme of low acid concentration, none of the carbonyl compound was in the reactive protonated form. In between these two extremes was the optimum pH (pH 3-5) at which the rate of reaction was the greatest. At this pH, some of amines were protonated, but some were free. The disappearance of the C=O in the PDP monomer material, indicated that the linkage between the 2,3-diaminophenazine and pyrrole-2-carboxaldehyde occurred at the position where C=O bond was cleaved. This was evident in the reaction mechanism (Scheme 4) of the monomer. The resulting monomer material was obtained in 60 % yield.

4.2 Starting Materials

4.2.1 2,3-diaminophenazine (DAP)

The DAP starting material was characterized in terms of spectroscopy and electrochemical behaviour. FTIR data of the solid chemical displayed transmittance bands in the IR spectra which related to the DAP material, the three bands present at 3429 cm^{-1} , 3301 cm^{-1} and 3167 cm^{-1} are characteristic of the IR bands associated with primary amines. Two of these bands are assigned to the -NH_2 vibrational frequencies. The stretching vibration of the C=N band was observed at a wavenumber of 1641 cm^{-1} . The C=C vibrational band present at 1487 cm^{-1} which are associated with the resonance of big π bonds (K. Thomas et al, 2001 and J. Kui et al, 1998). The stretching vibration at 1222 cm^{-1} was associated with that of an aliphatic amine.

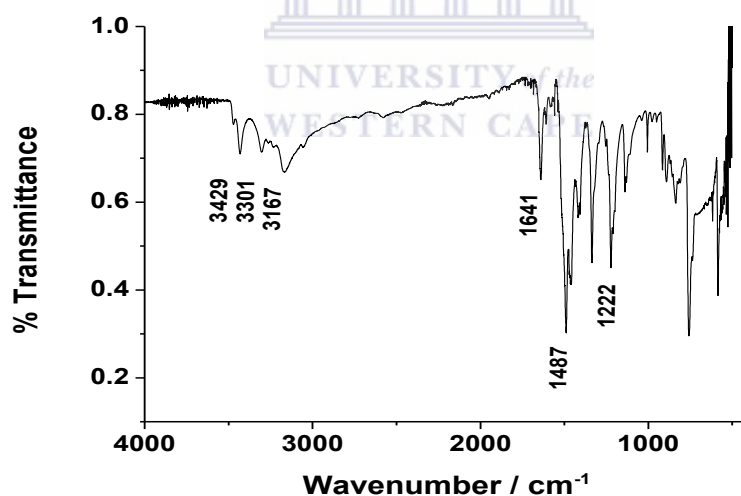


Figure 19. FTIR spectrum of 2,3-diaminophenazine.

The DAP was dissolved in a 1:1 ratio of DMF: 0.1 M HCl solution, this was then characterized by UV/Vis analysis. The spectrum obtained displayed two characteristics absorption bands, the band at 260 nm was assigned to the benzene $\pi \rightarrow \pi^*$ electronic

transition and the other peak at 440 nm, assigned to the $n \rightarrow \pi^*$ electronic transition (P. Zhou et al, 2011 and J. Kui et al, 1998).

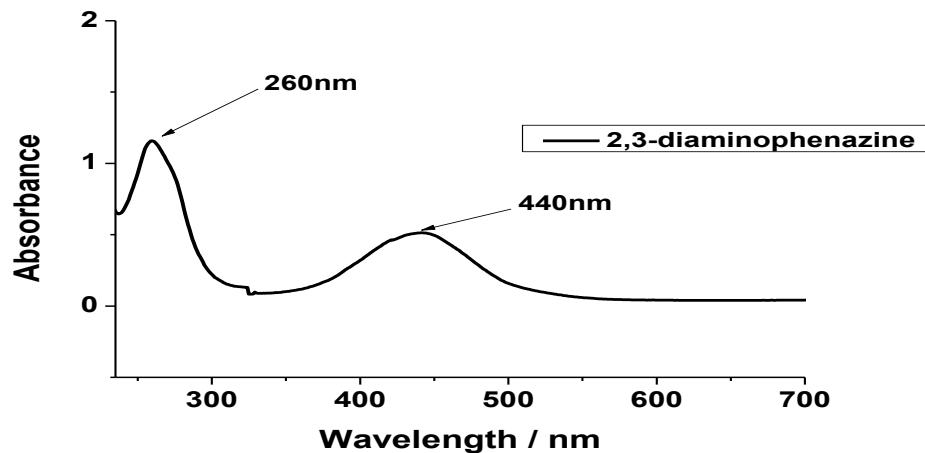


Figure 20. UV/Vis analysis of 2,3-diaminophenazine.

The ^1H NMR displayed four peaks with chemical shifts positioned at 7.93 ppm (4), 7.56 ppm (3), 6.97 ppm (2) and 6.31 ppm (1). Multiplets chemical shift which were in the aromatic region (between 6-8.5 ppm) were due to position 3 and 4, with a singlet (proton) being observed at position 2. The chemical shift position at number 1 was due to the protons attached to the amine ($-\text{NH}_2$) group (S. Liu et al, 2012).

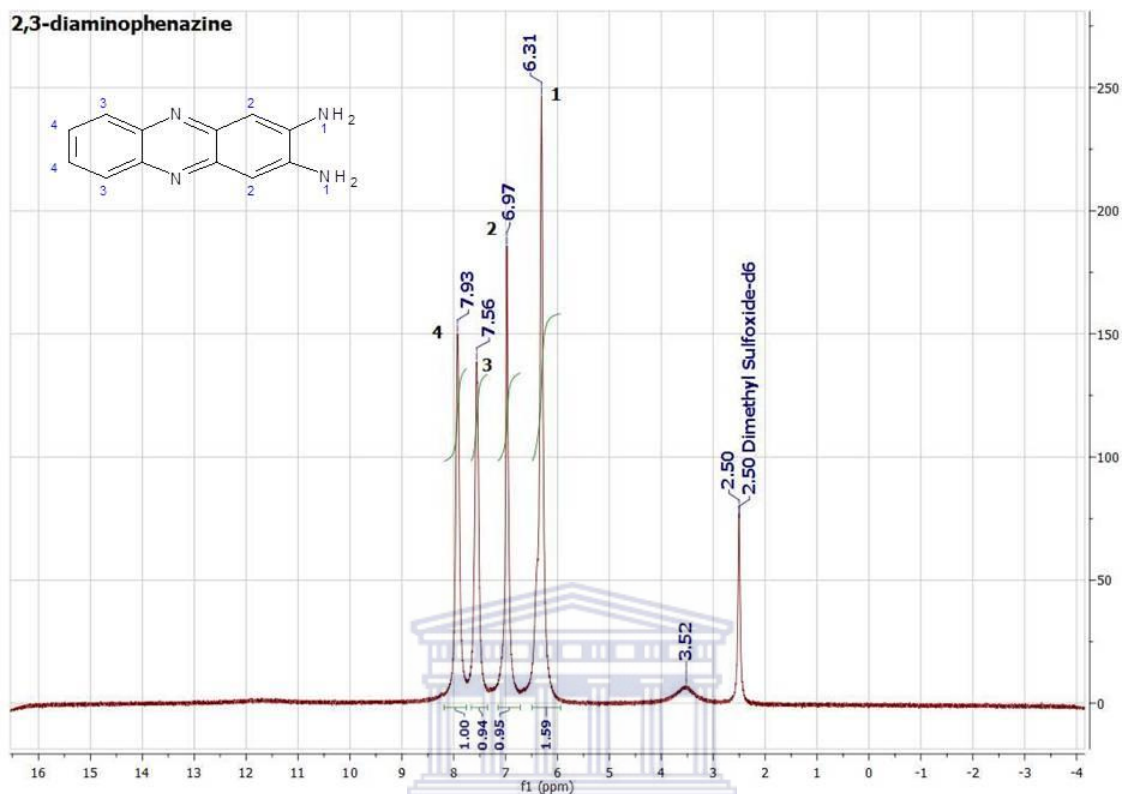


Figure 21. 300 MHz ¹H NMR spectrum of 2,3-diaminophenazine in DMSO-d₆

Furthermore the electrochemical behaviour of the material was studied by dissolving DAP in aqueous solvent and then performing cyclic voltammetry. According to K. Thomas et al, 2001, DAP was sensitive to reaction conditions such as light and oxygen. The cyclic voltammogram below represents DAP dissolved in 0.1 M HCl in the absence of both light and oxygen (figure 21). A reversible redox couple was present with a reduction (E_{pc}) peak positioned at -330 mV and a oxidation (E_{pa}) peak present at -263 mV.

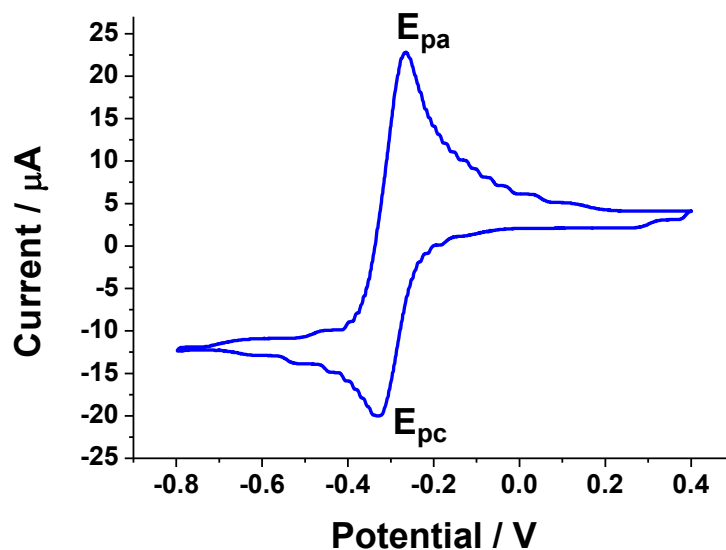


Figure 22. Cyclic voltammogram of 2,3-diaminophenazine in 0.1 M HCl.

Data obtained from UV/Vis, FTIR and ^1H NMR was in good agreement with published characteristic data, verifying the integrity of the chemicals used to synthesis of the monomer.

4.2.2 Pyrrole-2-carboxaldehyde

FTIR analysis of the solid chemical pyrrole-2-carboxaldehyde displayed a vibrational band at 3145 cm^{-1} which was due to the N-H stretching which was evident of secondary amines (figure 23). The IR bands present at 3078 cm^{-1} and 2978 cm^{-1} were due to the C-H stretching band, the former representing the aromatic C-H band and the latter was assigned to the aldehyde C-H band. The intense band present at 1627 cm^{-1} was due to the C=O aldehyde stretching. The band present at 1441 cm^{-1} was assigned to C=C stretching, with the aromatic amine present (C-N) at 1317 cm^{-1} (B. Stuart, 2004).

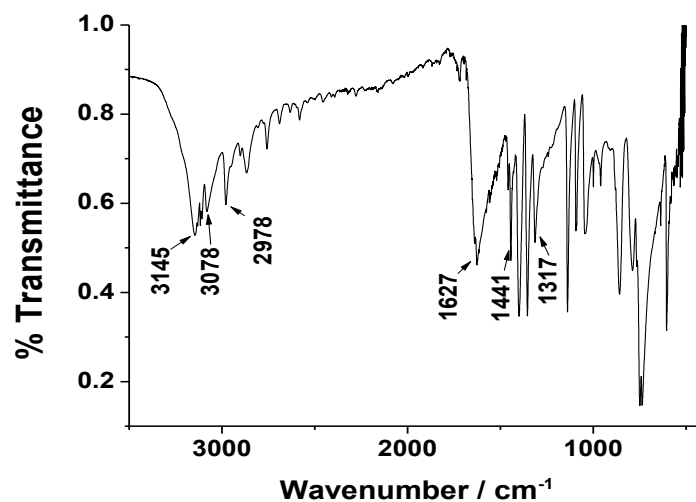


Figure 23. FTIR spectrum of pyrrole-2-carboxaldehyde.

¹H NMR displayed two doublets (protons positioned at 2 and 4) and one triplet (proton at position 3) in the aromatic region (figure 24). The proton (position 5) which was coupled to the aldehyde was the most intense band and was observed further downfield due to lower shielding effect compared to other aromatic protons. The remaining peak was assigned to the N-H proton. The data obtained below was compared to material safety data sheets (MSDS) and NMR documents obtained from Sigma-Aldrich and was found to be in good agreement.

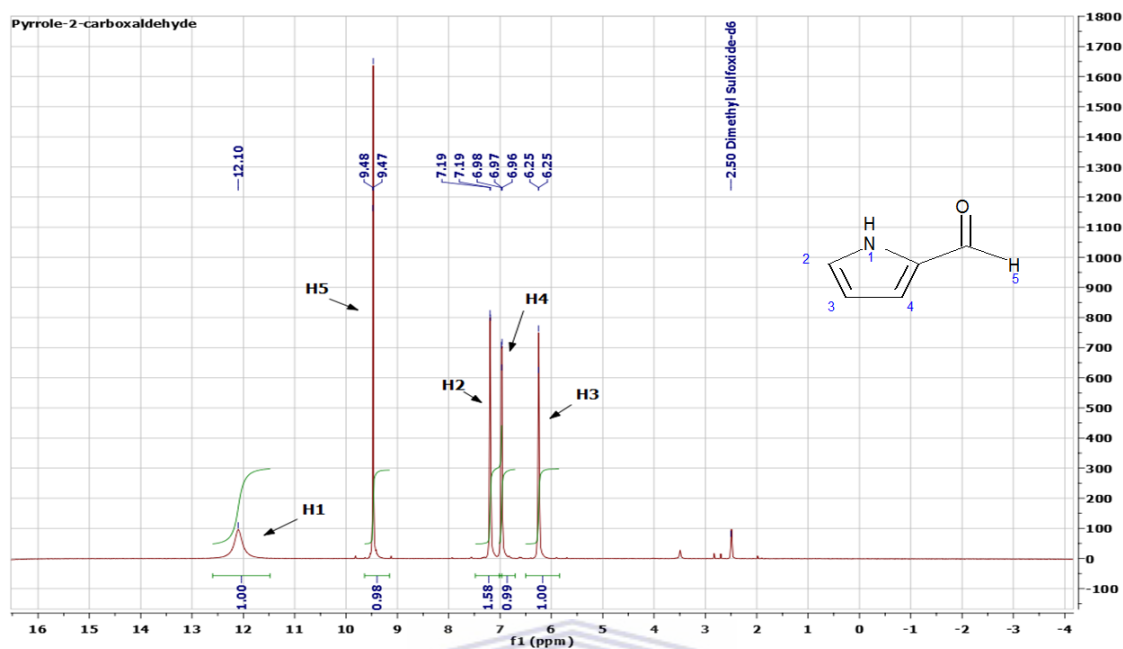


Figure 24. 300 MHz ¹H NMR spectrum of pyrrole-2-carboxaldehyde in DMSO-d₆

The electrochemical behaviour of pyrrole-2-carboxaldehyde displayed a reversible couple (figure 25). The reduction peak (E_{pc}) was present at -600 mV and the oxidation (E_{pa}) was present at 3.4 mV vs Ag/AgCl.

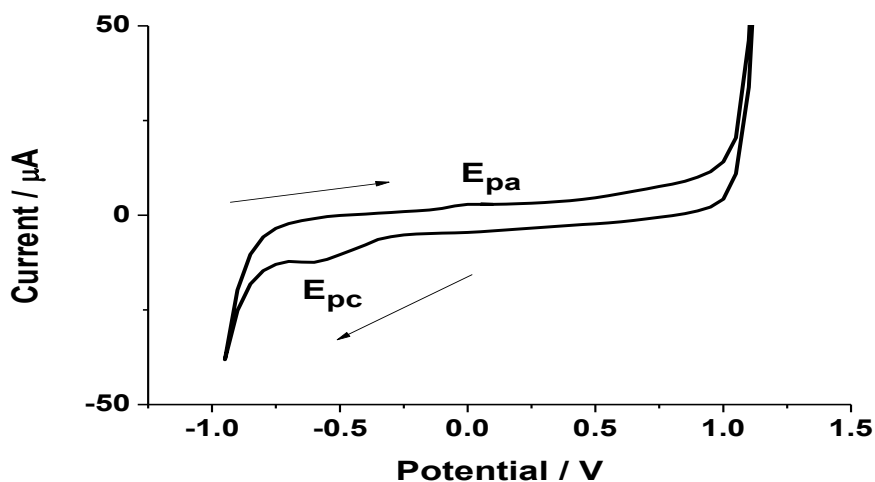
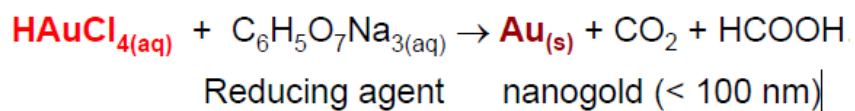


Figure 25. Cyclic voltammetry of pyrrole-2-carboxaldehyde in 0.1 M HCl.

4.3 Gold (Au) Nanoparticles

Au nanoparticles were synthesized by the reduction of the chloride salt with sodium citrate (K. Grabar et al, 1995). Gold a very stable and non-toxic material which was commonly used in dentistry, is inert in air and is not affected by common reagents, it is also a good conductor of both heat and electricity.



Scheme.7. Chemical reaction for Au Nanoparticle synthesis.

Upon completion of the synthesis a deep red colloidal suspension of gold was obtained. UV/Vis absorption of Au nanoparticles (figure 26), showed an absorption band at 526 nm which was also confirmed by V. Amendola et al, 2010. According to A. Gopalan et al, 2009 the band present at 526 nm corresponds to that of surface plasma resonance.

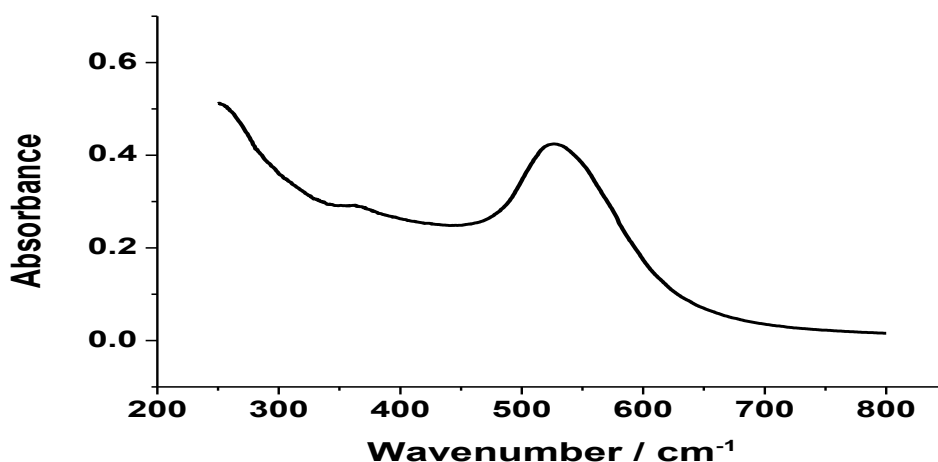


Figure 26. UV/Vis of Au Nanoparticles

4.4 Characterization of PDP material

FTIR analysis was performed on the material to confirm that the required monomer material was obtained. The vibrational band present at 3702 cm^{-1} was related to the N-H stretching. The two bands present at 1574 cm^{-1} and 1469 cm^{-1} , with the latter assigned to the C=N stretching and the former assigned to the C=C stretching (figure 27).

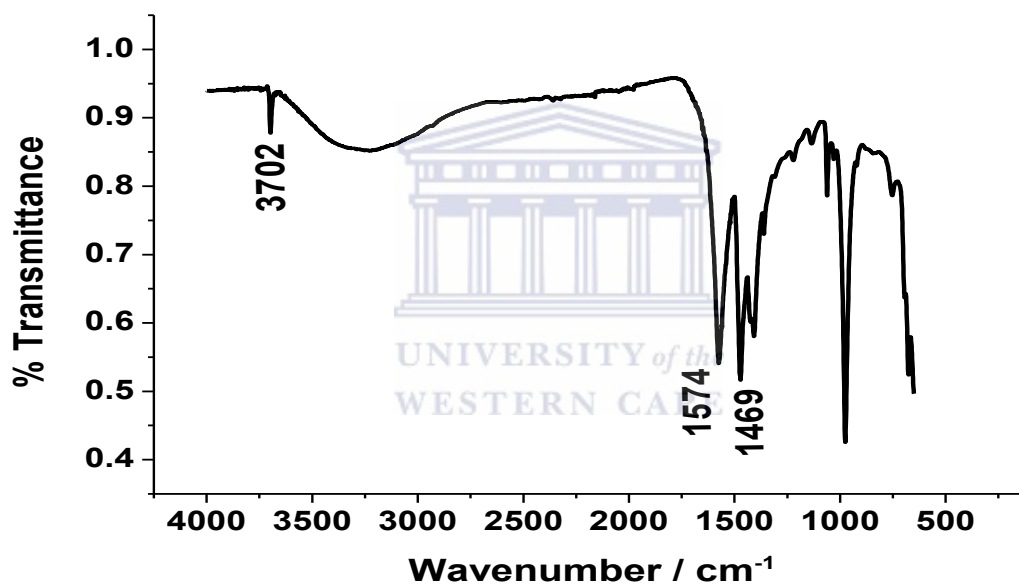


Figure 27. FTIR data of synthesized monomer, Phenazine-2,3-diimino(pyrrole-2-yl) PDP.

Table 7. Peak assignment for starting materials and monomer material.

Peak Assignment	Wavenumber / cm^{-1}
2,3-diaminophenazine	
NH ₂	3429 and 3167
C=N	1641
C=C	1487
C-N	1222 (aliphatic amine)
Pyrrole-2-carboxaldehyde	
N-H	3145
C-H	3078 (aromatic) and 2978 (aldehyde)
C=O	1627 (aldehyde)
C=C	1441
C-N	1317 (aromatic amine)
Phenazine-2,3-diimino(pyrrole-2-yl) PDP	
N-H	3702
C=N	1574
C=C	1469

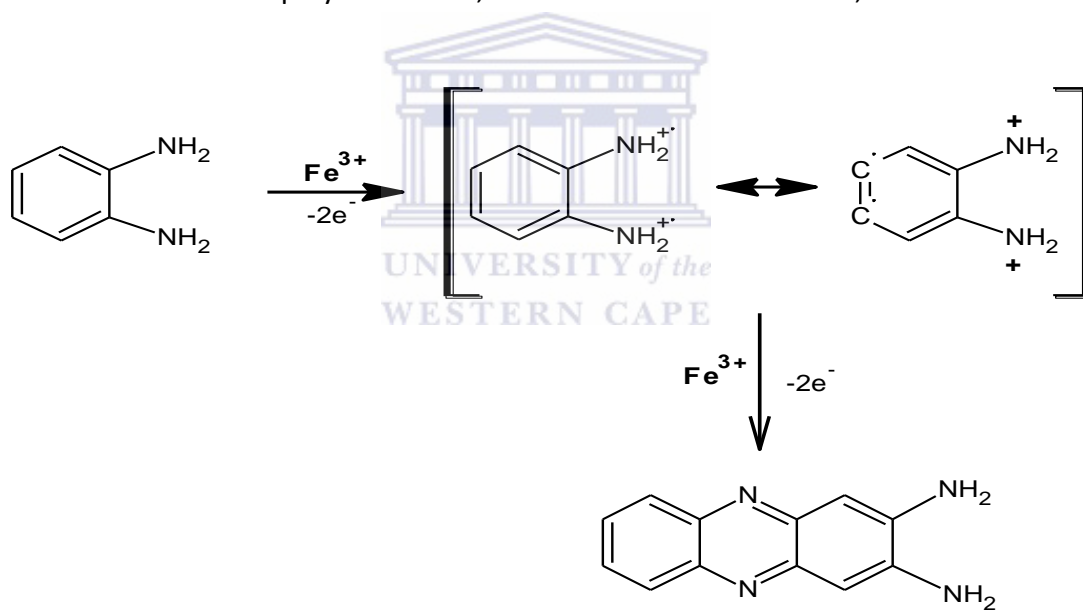
The data obtained from the FTIR spectra of both starting materials and the monomer material provided evidence that the linkage between the two starting materials occurred at the cleavage of the aldehyde group. This is supported by the disappearance of the C=O stretching band in the FTIR spectra of the monomer material (Table 7). Characterization of the monomer material provided support for the reaction mechanism provided, indicating that the desired monomer material was obtained (scheme 4, page number 37)

CHAPTER 5

PPDP POLYMERIZATION AND CHARACTERIZATION

5.1 Chemical Polymerization

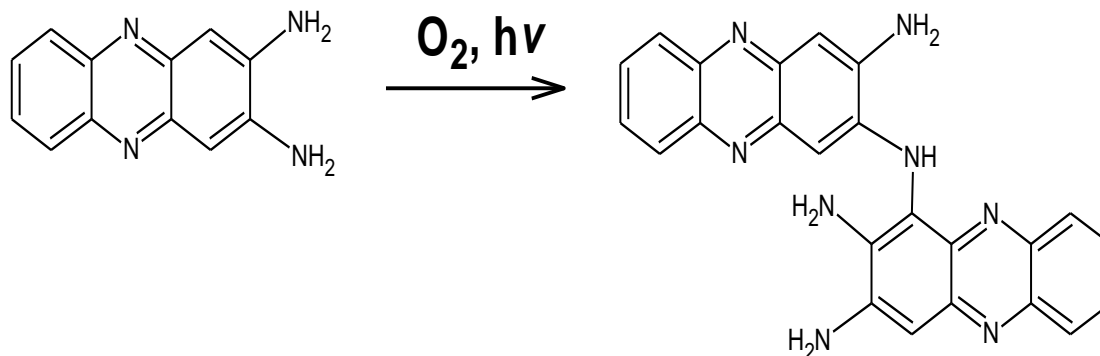
Polymerization of the monomer was achieved by the using FeCl_3 as oxidant with stirring for 24 hours which allowed for complete polymerization to occur. If oxidizing strengths and temperatures are too high, the rate of polymerization becomes too fast resulting in aggregated, low conductivity materials. There are a few possibilities for material formation as a result of polymerization, which should be considered;



Scheme.8. Mechanism 1 for possible polymerization method (D. He et al, 2007).

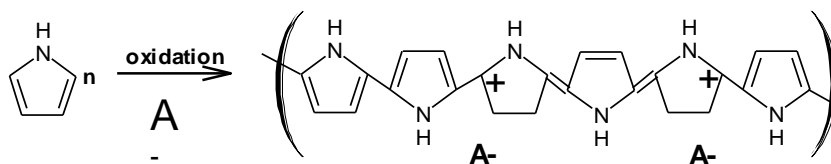
Oxidative polymerization to form 2,3-diaminophenazine which is rich in π -bonding and proton donor and acceptor sites. Upon investigation it was discovered that this possible method could not be plausible since the binding sites indicated would not be present

during polymerization (scheme 8). The amine bonding sites were lost during coupling of phenazine and pyrrole starting materials to form the monomer.



Scehem.9. Mechanism 2 for possible polymerization method (K. Thomas et al, 2001).

2,3-diaminophenazine being light sensitive needs to be appropriately stored; to avoid exposure to light and oxygen. If exposed to these conditions; the colour as well as the structure will change. Our synthesized monomer no longer displayed free amine groups which formed the basis of coupling during the second polymerization mechanism (scheme 9). Hence the suggested product is also not feasible.



Scheme.10. Mechanism 3 for possible polymerization method (T. Vernitskaya et al, 1997)

The possibility of the monomer coupling via polymerization of the pyrrole functionality was deemed the most feasible mechanism for formation of the zig-zag polymer (scheme 10). FTIR and 1H NMR characterization confirmed the presence of the secondary amine

(NH) on the pyrrole ring, which could be activated to polymerize and couple to at least another monomer unit. The rigid geometry of the synthesized monomer material precluded cyclisation. Therefore the proposed link between two monomer units could involve at least a two unit (possibly more) polypyrrole chain linking the phenazine hinge molecule into a zig-zag polymer configuration (figure 28).

The polymerization of pyrrole by chemical and electrochemical polymerization was produced under ambient conditions. Yield and conductivity of PPDP was affected by the solvent used, oxidant used, mixing ratios, temperatures and polymerization time. Shorter times and lower temperatures led to materials with greater conductivities. The yield obtained for the polymer after polymerization was found to be 45 %.

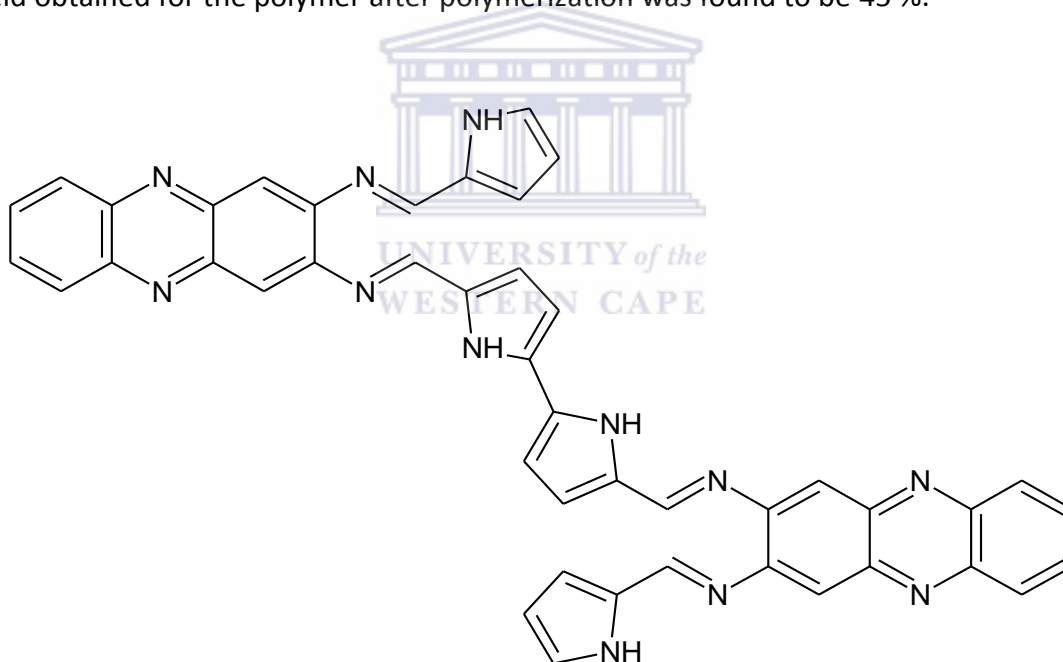


Figure 28. Zig-zag polymer material, poly(Phenazine-2,3-diimino(pyrrole-2-yl)) PPDP.

5.2 Electrochemical Polymerization

Electrochemical polymerization of the monomer material led to the same product formation as the chemically synthesized material; however there are a few advantages over the chemical process. The product produced during polymerization is an electroactive thin film on the surface of the electrode and has higher conductivities. The purity of the material on the surface of the electrode is near 100 %, which provided the possibility of mass and film thickness control. The properties of the material could be controlled during polymerization by controlling the electrochemistry condition. The polymerization conditions used were at a scan rate of 50 mV/s and between a potential window of -400 mV to +700 mV.

5.3 Polymer Characterization

5.3.1 Electrochemical Behaviour of polymer material system

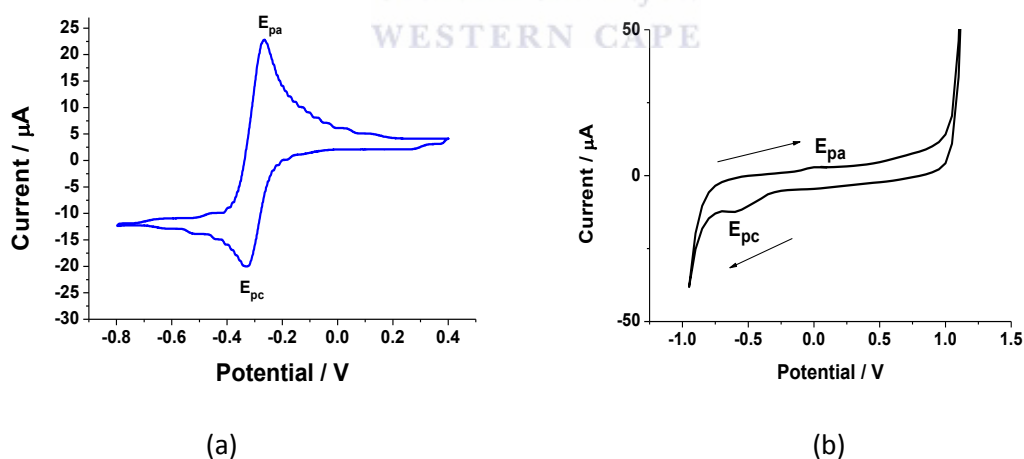


Figure 29. CV of 2,3-diaminophenazine (a) and pyrrole-2-carboxaldehyde (b).

Cyclic voltammetry of individual starting materials, monomer and the polymer was performed in order to ascertain the redox chemistry for the progression of the

polymerization mechanism. The monomer was chemically synthesized to produce electrochemically synthesized polymer. The Au nanoparticle modified polymer was produced from a starting solution containing a mixture of monomer and Au nanoparticles.

The electrochemistry of the starting materials could be clearly distinguished from monomer and polymers. 2,3-diaminophenazine displayed prominent redox peaks at -263 mV and -330 mV, while the pyrrole-2-carboxaldehyde displayed a reversible redox couple at -614 mV and 3.4 mV (figure 29). The modified and unmodified polymer displayed very similar redox electrochemistry. (figure 30).

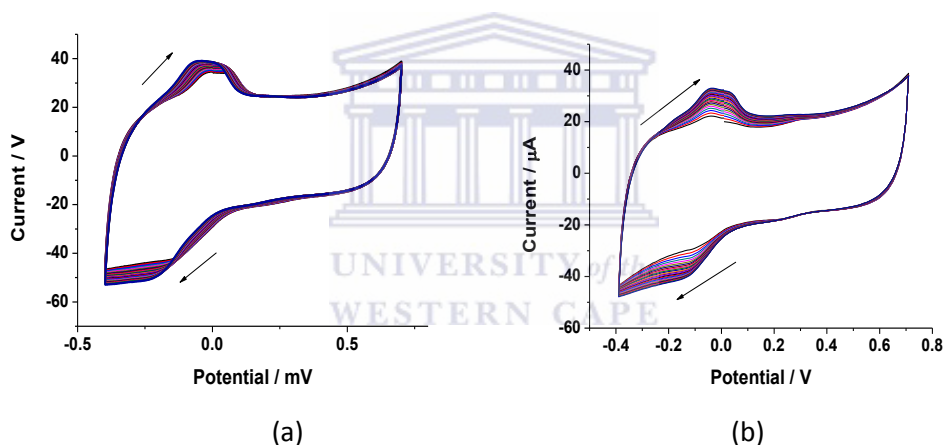
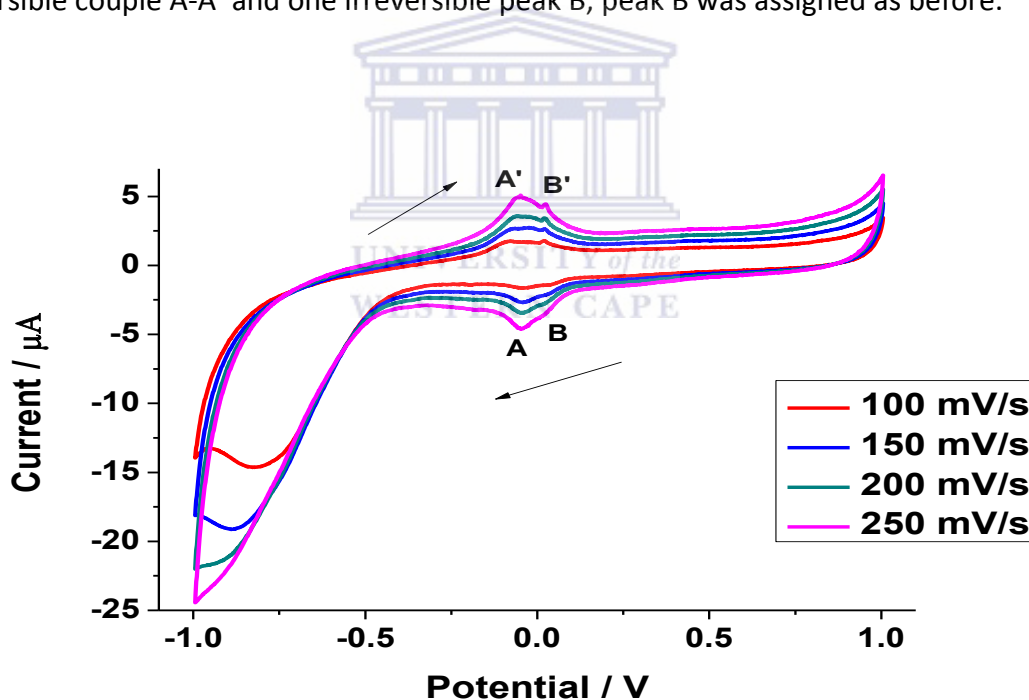


Figure 30. Electropolymerization to form the polymer PPDP (a) and PPDP-Au (b).

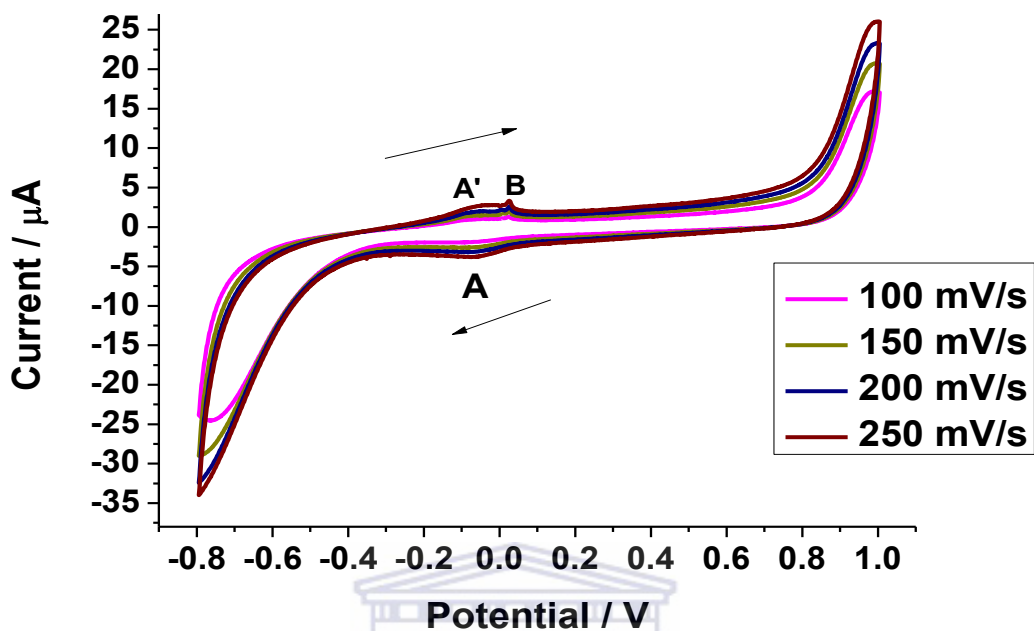
The upper potential limit during polymerization was controlled to avoid over oxidizing and degradation at high potentials, while greater negative potentials led to hydrogen evolution. The electrochemical behaviour of the material (increase in peak current) indicated that a conducting polymer was formed. The electrochemical signature clearly indicated that the new material produced at the electrode surface was not due to the polymerization of the starting materials. The cyclic voltammogram in figure 31(a)

displayed 2 fully reversible redox couples A-A' and B-B'. The polymerization solution was not homogeneous since it contained insoluble monomer, which created the possibility for entrapment of insoluble monomer material during the polymerization. The A-A' redox couple displayed an anodic peak at -50.7 mV and a cathodic peak at -107.4 mV. The B-B' redox couple displayed behaviour of the unreacted material. Extraction of the pure polymer and its subsequent electrochemical investigation will be presented later (chapter 6).

The electrochemical behavior of 2,3-diaminophenazine displayed a reversible couple which was associated with the redox couple A-A'. The figure 31(b) displayed one reversible couple A-A' and one irreversible peak B, peak B was assigned as before.



(a)



(b)

Figure 31. Characterization of PPDP (a) and PPDP-Au (b) in 0.1 M HCl solution at scan rates ranging between 100 – 250 mV/s.

Table 8. Current values obtained from the above cyclic voltammogram for both PPDP and PPDP-Au (figure 33).

PPDP			
Scan Rate (mV/s)	$i_{pa} / \mu A$ (A)	$i_{pc} / \mu A$ (A')	i_{pa}/i_{pc} (A-A')
100	1.6698	1.6411	1.02
150	2.7321	2.7799	0.98
200	3.4880	3.5359	0.99
250	4.6267	4.9426	0.94
PPDP-Au			
Scan Rate	$i_{pa} / \mu A$ (A)	$i_{pc} / \mu A$ (A')	i_{pa}/i_{pc} (A-A')
100	2.0789	0.9145	2.27
150	2.6815	1.5170	1.77
200	3.1286	1.9641	1.59
250	3.9449	2.7222	1.50

The current ratios of I_{pa}/I_{pc} for the PPDP system ranged from 1.02 (100 mV/s) to 0.94 (250 mV/s) for the A-A' redox couple which indicated a one electron system. The modified PPDP-Au system displayed one redox couple A-A' with an I_{pa}/I_{pc} ratio which ranged from 2.27 (100 mV/s) to 1.50 (250 mV/s) which indicated a two electron process. The peak separation (table 9) of PPDP and PPDP-Au for redox couples A-A' respectively displayed properties of a fully reversible system. The change in peak separations with scan rates indicated that the system is diffusion controlled with electron movement taking place across the polymer backbone (chain).

Table 9. Peak separations obtained from the PPDP and PPDP-Au system

PPDP			
Scan Rate (mV/s)	E_{pa} (A) / mV	E_{pa} (A') / mV	ΔE_p(A-A') / mV
100	-41.1	-92.9	51.8
150	-41.1	-76.6	35.5
200	-41.1	-57.4	16.3
250	-52.1	-52.1	0
PPDP-Au			
100	-67.5	-81.0	13.5
150	-67.5	-67.5	0
200	-66.2	-64.8	1.4
250	-66.2	-51.3	14.9

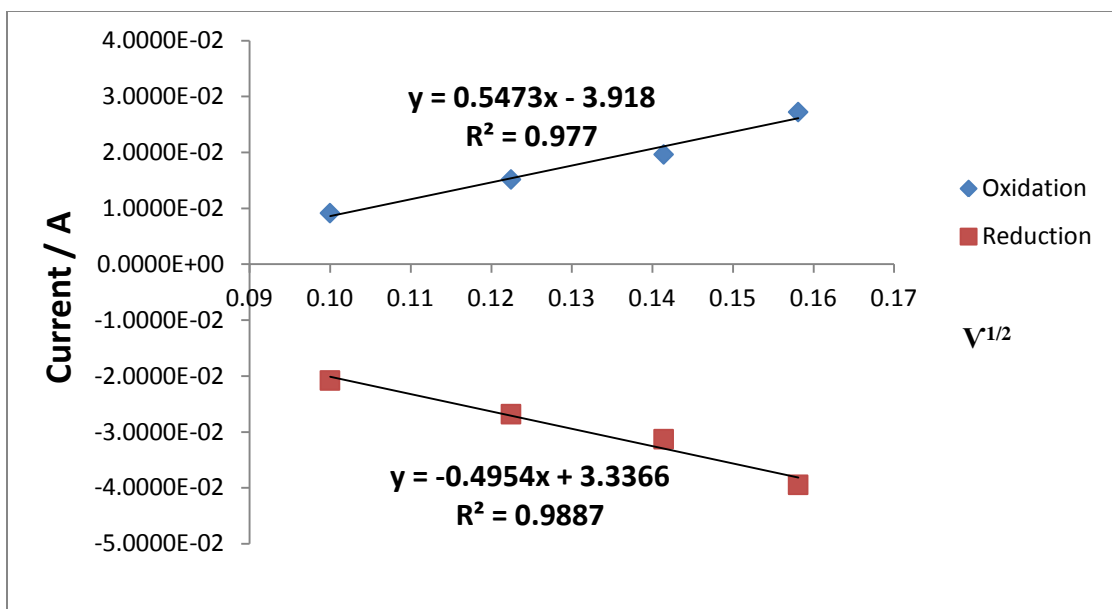


Figure 32. Randles-Sevcik for PPDP, plot of current vs square root of scan rate.

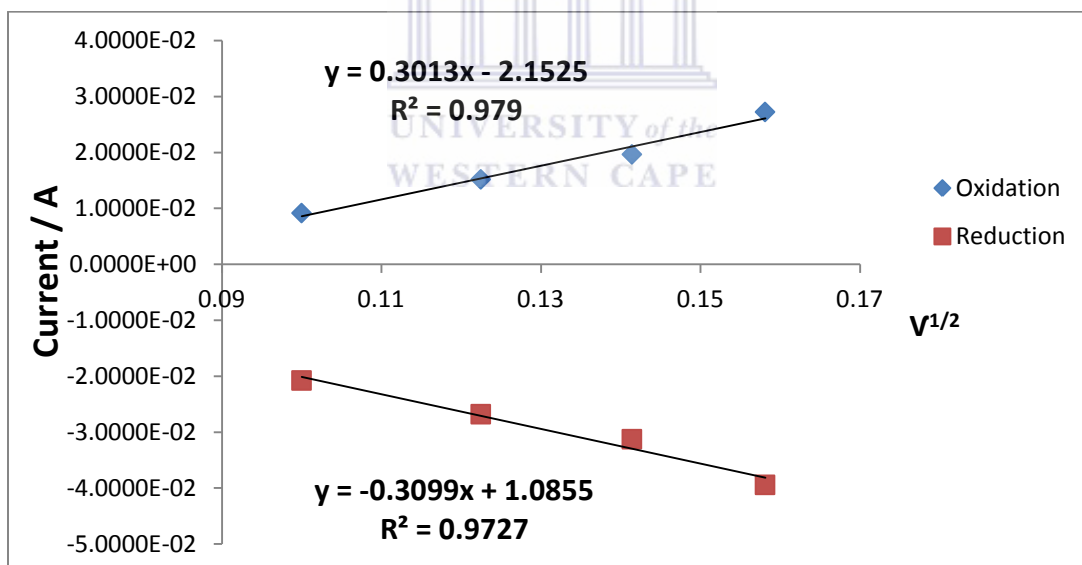


Figure 33. Randles-Sevcik for PPDP-Au, plot of current vs square root of scan rate.

The Randles-Sevcik plots for figures 31(a) and 31(b) were used in the calculation for the diffusion coefficient values of both systems. Upon determination that the systems were diffusion controlled, the diffusion coefficient values were determined using equation 7 (A. Bard et al, 2001);

$$i_p = (2.687 \times 10^5) n^{3/2} \nu^{1/2} D_0^{1/2} C A \quad \text{eqn. 7}$$

Where;

D_0 = Diffusion Coefficient in cm^2/s

i_p = peak current

n = no. of electrons involved

C = concentration of solution in mol/cm^3

A = area of the electrode in cm^2

ν = scan rate



Table 10. Diffusion coefficient values of PPDP and PPDP-Au systems.

	PPDP		PPDP-AU	
	A-A'		A-A'	
	Oxidation	Reduction	Oxidation	Reduction
Diffusion Coefficient ($\text{cm} \cdot \text{s}^{-1}$)	1.0287×10^{-2}	8.4289×10^{-3}	3.1179×10^{-3}	3.2984×10^{-3}

The standard reduction potential for Au reduction, according to D. Ebbing et al, 2002 was found to be +1.50 volts. However the signature electrochemistry for Au was not evident in the modified polymer. The surface concentration of the polymer was determined using the Brown Anson equation by plotting peak currents vs. scan rates (100 – 250 mV/s), as follows;

$$I_p = n^2 F^2 \Gamma_{\text{PPDP-PVSA}}^* (A \nu / 4RT) \quad \text{eqn. 8}$$

Where;

F = Faradaic constant (96485 C/mol)

A = Electrode surface area (0.071 cm²)

R = Molar gas constant (8.314 J.K⁻¹.mol⁻¹)

T = Temperature (298 K)

n = no. of electrons

Γ^* = surface concentration

I_p = peak current

ν = scan rate

The surface concentration values determined were dependent on the scan rate (table 11). The values ranged between 2.5036 x 10⁻⁷ mol.cm⁻² at 100 mV/s to 2.7749 x 10⁻⁷ mol.cm⁻² at 250 mV/s for PPDP and 3.1170 x 10⁻⁷ mol.cm⁻² at 100 mV/s to 2.3659 x 10⁻⁷ mol.cm⁻² at 250 mV/s for PPDP-Au.

Table 11. Surface concentration of PPDP and PPDP-Au systems of the redox couple A-A' over various scan rates.

Surface Concentration		
PPDP		
Scan Rate (mV/s)	Oxidation / mol/cm ²	Reduction / mol/cm ²
100	2.5036 x 10 ⁻⁷	2.4606 x 10 ⁻⁷
150	2.7293 x 10 ⁻⁷	2.7787 x 10 ⁻⁷
250	1.4938 x 10 ⁻⁷	2.6508 x 10 ⁻⁷
250	2.7749 x 10 ⁻⁷	2.9643 x 10 ⁻⁷
PPDP-Au		
100	3.1170 x 10 ⁻⁷	1.3712 x 10 ⁻⁷
150	2.6804 x 10 ⁻⁷	1.5164 x 10 ⁻⁷
200	2.3455 x 10 ⁻⁷	1.4725 x 10 ⁻⁷
250	2.3659 x 10 ⁻⁷	1.6326 x 10 ⁻⁷

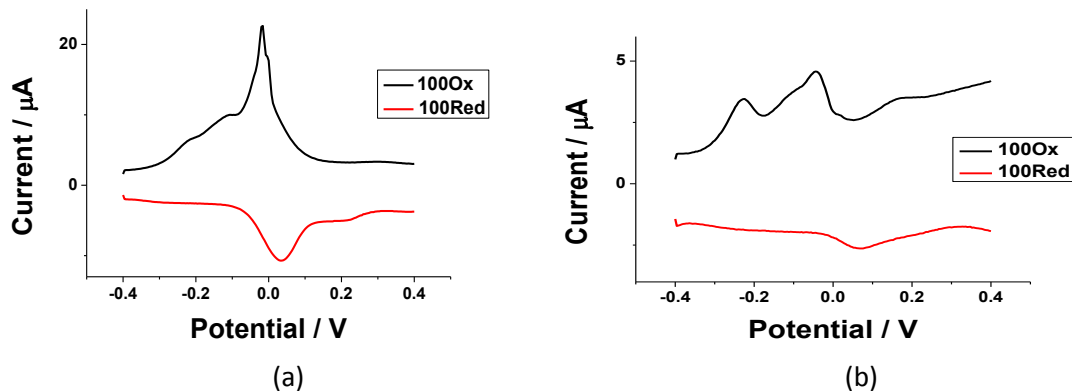


Figure 34. OSWV of PPDP (a) and PPDP-Au (b) both in 0.1 M HCl solution.

Formal potentials ($E^{0'}$) were calculated using the OSWV's in figure 34(a) and 34(b) and were found to be 26.95 mV for PPDP and 13.4 mV for PPDP-AU vs. Ag/AgCl.

Diffusion coefficient values obtained for the reversible redox couples of PPDP and PPDP-Au indicated that the deviation from reversibility did not involve permanent electronic changes in the polypyrrole film (A. Bard et al, 2001).

5.3.2 Electrochemical Impedance Spectroscopy

Data collected was in the potential range between -500 mV to 500 mV for the PPDP/PVSA system and between -400 mV to 400 mV for the modified PPDP-Au/PVSA system, potential steps were performed in 100 mV increments. The potential range was determined by using the redox window of the respective cyclic voltammograms, this was used for the assessment of formal potential values determined from square wave.

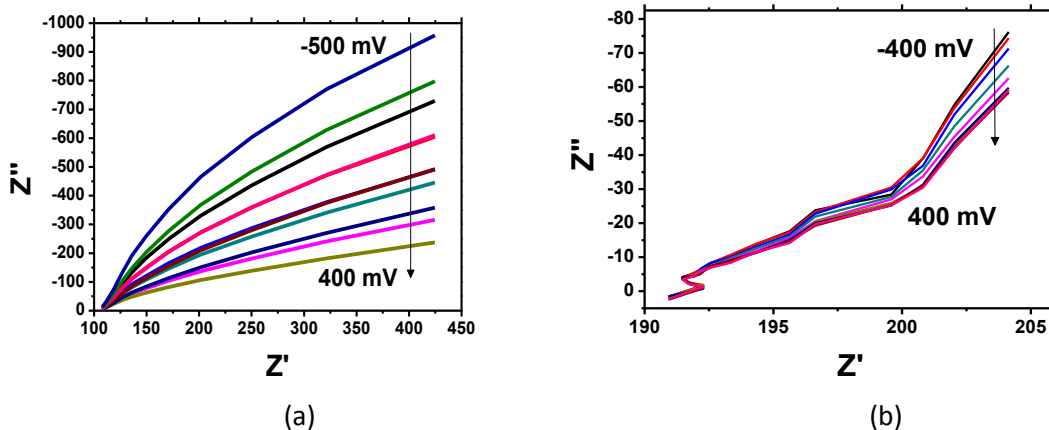


Figure 35. EIS spectra of PPDP (a) with +100 mV potential steps starting from -500 mV to 400 mV (vs Ag/AgCl) and PPDP-Au (b) with +100 mV potential steps starting from -400 mV to 400 mV (vs Ag/AgCl).

According to A. Eckermann et al, 2010, the Nyquist plot displayed linear spectra that never approached the Z_{RE} (real impedance) axis, but instead both systems increasingly approached large Z_{IM} (imaginary impedance) values, figure 35(a) and 35(b). The Randles circuit is one of the simplest models for electron transfer for a redox species attached to a monolayer. The circuit can determine individual elements by measuring impedance over a wide variety of frequencies.

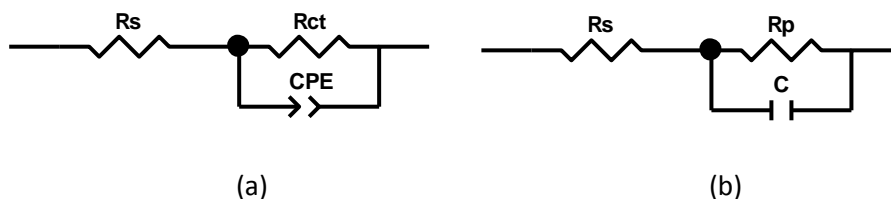
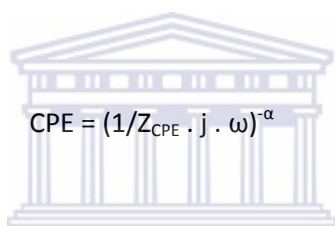


Figure 36. Randles equivalent circuit of PPDP (a) and PPDP-Au (b).

Quantification of the EIS results was achieved by electrical equivalent circuit modelling based on typical Randles circuits. The circuit for PPDP (figure 36(a)) included a solution resistance between the working and reference electrode. The constant phase element (CPE) exponent was found to be $\alpha = 0.85$ which was the representation of capacitor behaviour (double layer capacitance). The deviation from unity was due to inhomogeneity at the interface. The charge transfer resistance (R_{ct}) resulted from a single kinetically controlled electrochemical reaction. The Au modified PPDP (figure 36(b)) was modelled as before but the interfacial capacitance was modelled as a pure capacitor in the equivalent circuit fitting. The capacitance for the impedance data was obtained using the following equation (J. Jorcin et al, 2006, J. Chang et al, 2007 and R. Ahmed et al, 2012);



$$CPE = (1/Z_{CPE} \cdot j \cdot \omega)^{-\alpha}$$

eqn. 9

Where;

α = fractional exponent (values between 0 to 1)

j = imaginary number ($= \sqrt{-1}$)

ω = angular frequency ($\omega = 2\pi f$)

Z_{CPE} = Real Impedance

CPE = Capacitance

Both systems displayed linear behaviour throughout the impedance spectra (table 12). Incorporation of the Au nanoparticles into the polymer matrix was seen to reduce the charge transfer resistance from 4589.45 to 314.76 Ω , which confirmed that the objective in terms of improving conductivity was successfully demonstrated for the electropolymerized PPDP polymer.

Table 12. Impedance data obtained from PPDP and PPDP-Au.

IMPEDANCE DATA		
Circuit Elements	PPDP	PPDP-Au
Solution Resistance (R_s) / Ω	106.44	192.60
Constant Phase Element (CPE) / F	0.85	n/a
Capacitance / F	3.46×10^{-6}	7.14×10^{-6}
Charge Transfer Resistance (R_{ct}) / Ω	4589.45	314.76



5.4 Electrical conductivity of Polymer

Various methods for conductivity (σ) measurements were performed on the PPDP polymer material, but could not be repeated for the Au-PPDP polymer. The research was conducted as a partnership between University of the Western Cape (South Africa) and the University of Cergy Pontoise (Paris, France) funded by French Embassy (RSA) bursary and support from the European Scientific network artificial muscle (ESNAM,FP7 framework). The synthesis and characterization of the polymer materials are the initial investigations towards developing a suitable material for actuation applications.

The conductivity measurements were conducted at University of Cergy Pontoise and included 4-probe measurement, cyclic voltammetry and electrochemical impedance. The polymer was compressed into a pellet (thick film) as instruments had special cells for conductivity measurements. All four probes of the Universal Probe combined with the RM3000 Test Unit were in contact with the pellet surface, the measurement was performed and the data obtained exceeded the maximum limit of the instrument. The measurement range of the instrument is from 10^{-3} to $10^8 \Omega$. The conductivity value was too low for the instrument to measure. Usually conducting polymers have high conductivities of up to magnitudes of ~ 500 S/cm in the doped state (C. Chen et al, 2011). The 4-probed instruments produces more accurate results compared to the 2-probed instrument due to the fact that the 4-probe has two reference probes on either side of the pellet (S. Ma et al, 2007).

Table 13. Conductivity measurements using the 4-probed instrument

PPDP (S/m)	PPy (S/m)	PPy/COOH (S/m)*
Min. 10^{-3}	10^2	10^{-2}

- J. Lee et al, 2006.

Conductivity of the polymer under investigation PPDP (max – limit of the instrument indicating low conductivity) was significantly lower than that of Polypyrrole (PPy – 10^2). The modified PPy pellet PPy/COOH has higher conductivity 10^{-2} (in the range of a semiconductor, 10^2 to 10^{-6} S/m) than that of PPDP even after some conductivity has been lost. The loss of conductivity can be accounted for by the disruption of the π -electron configuration due to harsh oxidation conditions (J. Lee et al, 2006).

Physical properties of the polymer pellet were found to be; thickness (l) = 0.15 mm = 0.015 cm and Surface (s) = 1.25 cm². Conductivity by means of I/V curves performed by using a Biologic Potentiostat. The pellet was sandwiched between two electrodes and by means of Cyclic Voltammetry (CV), the plot of Current (I) vs. Potential (V) was recorded. The CV curve was performed at a low scan rate of 20 mV/s between a potential window of -1V and +1V, with the limit of the instrument almost reached. Resulting from this CV, the slope of the I/V curve gave the resistance of the pellet, which was found to be 285 M Ω . The conductivity was found to be 4.21×10^{-11} S/cm, which was determined by using the following equation;

$$\sigma = 1/R \times l/s \quad \text{eqn. 10}$$

where;

σ = conductivity

R = resistance

l = thickness

s = surface

An electrochemical impedance experiment (0.01Hz to 100 kHz) was setup in order to determine the conductivity of the thick film. Upon determination of real and imaginary parts (Z' and Z'') of impedance, the resistance was determined and was found to be 350

kΩ (determined at the highest frequency). The equation above was used for the determination of the conductivity value of the polymer, the conductivity using this calculation was found to be 3.43×10^{-8} S/cm.

An alternative calculation was used for the Dielectric Interface which was used to confirm the conductivity result obtained (A. Hasim et al, 2012), the conductivity using the equation below was found to be 4.43×10^{-10} S/cm;

$$\sigma_{AC} = 2\pi \times f \times C/d \times \tan \delta \quad \text{eqn.11}$$

with;

$$\epsilon_r = C/d/\epsilon_0 A \quad \text{and} \quad \epsilon_r \epsilon_0 = C/d/A$$

Where;

f = frequency

d = thickness

C = capacitance

A = area of the cell

$\tan \delta = \epsilon_i/\epsilon_r$ with; ϵ_i = imaginary permittivity; ϵ_r = real permittivity;

ϵ_0 = absolute dielectric constant



Determination of the thick film conductivities by analysis of all three techniques revealed that relative to polypyrrole and 2,3-diaminophenazine, the conductivity of PPDP is relatively low. Nanobelts which are identified in the form of 2,3-diaminophenazine assemblies display a direct current (DC) conductivity of 1.38×10^{-6} S/cm (D. He et al, 2007). Polypyrrole which is an insulator by nature, has the ability to display good electrical conductor ability (oxidized derivatives of polypyrrole), with

conductivity ranges between 10^{-3} to 10 S/cm. Dopant solutions as well as temperature conditions both affect the rate of polymerization and the relative conductivity of the polymer material (U. Ramelow et al, 2001). Due to these factors the conductivity of polypyrrole is temperature dependent which displayed transitions from a semi-conducting material to that of a metallic material, this resulted from the increase in temperature (V. Shaktawat et al, 2008). Upon completion of all the conductivity tests, it was discovered that the PPDP material has a very low conductivity or loses its initial conductivity. The conductivity of polymer materials can be slightly improved by two or three magnitudes by the addition of a second dopant usually in the form of an inert solution including; DMSO, DMF and THF (C. Chen et al, 2011). Incorporation of Gold (Au) Nanoparticles leads to a significant increase in electrical conductivities of polymer materials (K. Choi et al, 2012).



5.5 FTIR of Polymer

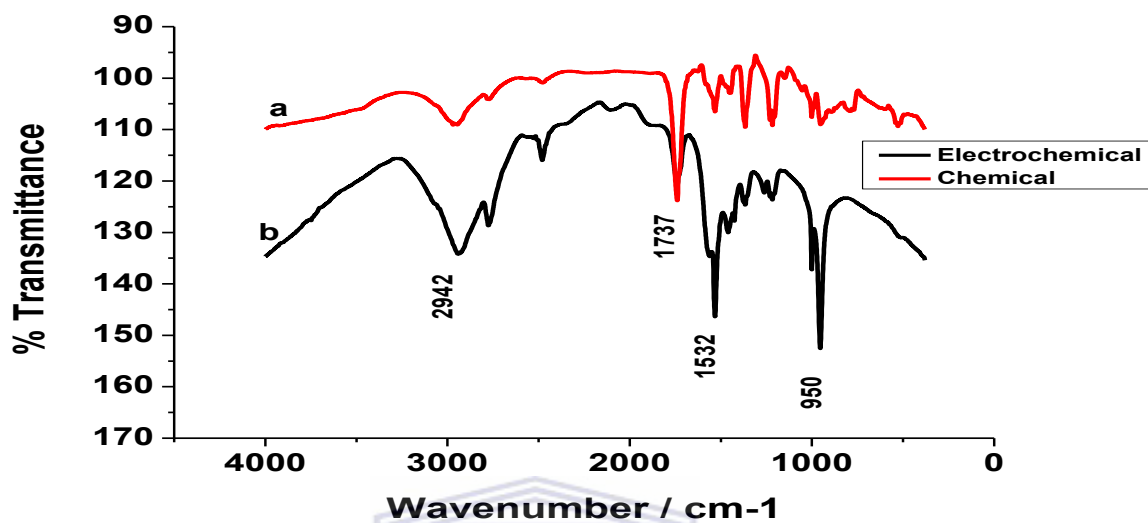


Figure 37. FTIR of chemically (a) and electrochemically (b) polymerized polymer material.

Figure 37 displayed the FTIR of the polymer material with the electrochemically polymerized material (curve b) displaying more intense bands than the chemically synthesized material (curve a). The electrochemically synthesized material was prepared by polymerizing onto the surface of a glassy carbon electrode (GCE). The purity of the polymer at the electrode surface is in direct relation as to how intense the bands are. Both polymerization methods yielded the same material when investigated by FTIR. Vibrational frequency bands are present at 2942 cm⁻¹, 2769 cm⁻¹, 2472 cm⁻¹, 1737 cm⁻¹, 1532 cm⁻¹ and 950 cm⁻¹ respectively, data displayed in table 14.

Table 14. FTIR of PPDP

Peak Assignment	Wavenumber / cm-1
poly(Phenazine-2,3-diimino(pyrrole-2-yl)) PPDP	
C-H	2942 (aromatic)
C=N	1737
C=C	1532
=C-H	950

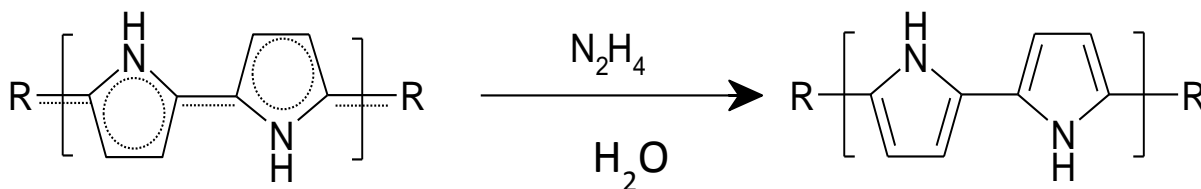
5.6 Solubility

Polymer solubility testing was performed using various organic solvents including; DMSO, THF, DCB, Chloroform, DMF, Methanol, Ethanol, Acetone and various strong acids. Analysis performed revealed that the polymer material was either insoluble or partially soluble in these common organic solvents even by ultrasonic treatment (I. Kukoyama et al, 2002). The insolubility is in direct relation to the stiffness of the polymer backbone which creates problems for large scale applications (S. Taj et al, 1992, J. Yoo et al, 2009). Solubility testing improvements have been achieved by S. Taj et al, 1992 with the incorporation of polar functional groups or long flexible alkyl chains in the polymer backbone; to prepare water or organic soluble polymers.

5.7 Spectral properties (absorption – emission)

After the initial characterization (FTIR, electrical conductivity and solubility testing) the polymer material was dedoped using Hydrazine (35 % wt solution in water), as the polymer material was in the oxidized state. This was done by mixing 10 mL of Hydrazine with 30 mL of H₂O and approximately 100 mg PPDP. The solution was then filtered to obtain the dedoped polymer, which was then dried at 70 °C under vacuum. Hydrazine is

a reducing agent which was used for the removal of the counter-ion and the charge on the backbone.



Scheme 11. Dedoping of PPDP.

UV/Vis analysis was performed by dissolving the polymer in THF (concentration of 1 mg/ml). The UV/Vis spectra displayed peaks in the visible region (421 nm) and in the IR region (272 nm), from this data the energy gap was determined from the onset of the π - π^* transition peak. The UV/Vis spectra in figure 38(a) displayed the monomer material with a peak present in the visible region at 414 nm (curve a), 2,3-diaminophenazine (curve b) displayed bands at 260 nm and 440 nm respectively (P. Zhou et al, 2011 and J. Kui et al, 1998). The polymer material in figure 38(b) displayed bands at 272 nm (related to π - π transitions) and 417 nm (related n- π transitions).

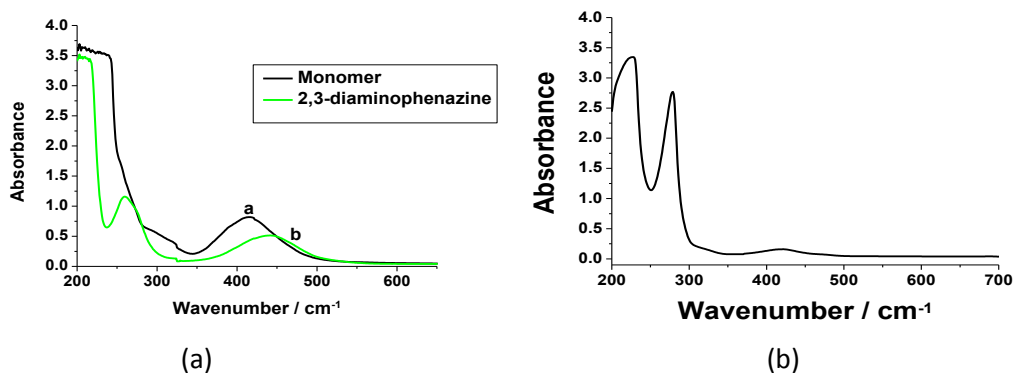


Figure 38. UV/Vis of 2,3-diaminophenazine (a), monomer material (a) and polymer (b)

UV/Vis spectrum of PPDP dissolved in THF represented in figure 38(b), figure 38(a) displayed the UV/Vis of PDP (curve a) dissolved in equimolar ratio of DMF:0.1 M HCl solution and 2,3-diaminophenazine (curve b) was dissolved in DMF:0.1 M HCl solution. According A. Nan et al, 2010, the conducting polymer polypyrrole displayed a UV/Vis band present at 480nm and even in a colloidal solution of Ag/PPy the band is present at 417nm.

$$E_g = 1240/\lambda_{\text{onset}}$$

eqn.12

The λ onset of the PPDP material was found to be 501 nm, with the resulting band gap (E_g) being 2.48 eV, this was compared to the band gap of polypyrrole studied by V. Shaktawat et al, 2008. V. Shaktawat et al, 2008, studied the band gaps of polypyrrole which was doped with different acids, band gaps were found to be 2.38 (Cl^-), 2.39 (SO_4^{2-}) and 2.33 (DBS^-) eV respectively. Determination of the band gap led to the determination of the type of material present. According to M. Hoffman et al band gaps < 3eV represented materials with semiconductor behavior where larger band gaps (> 4eV) are evident of insulator materials.

The onset wavelength of PPDP was used in the determination of the photoluminescence of the material. Figure 39 displayed a photoluminescent band at 502 nm which according to K. Shinde et al, 2013, was evident of a green photoluminescence. Photoluminescent studies of polypyrrole have revealed that photoluminescence displayed a band at 395 nm according to S. Ashokan et al, 2005, and 540 nm for both chemically and electrochemically synthesized polypyrrole.

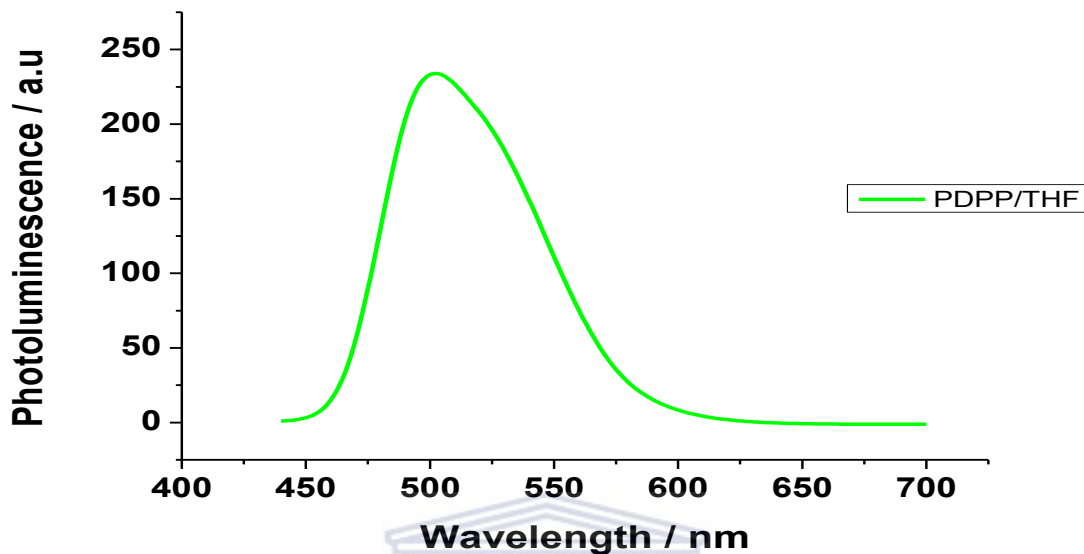


Figure 39. Photoluminescence of PPDP (polymer material) dissolved in THF.

5.8 Thermal Analysis

Thermogravimetric analysis of figure 40 (curve a - chemically synthesized polypyrrole) displayed initial segment weight loss below 100 °C which can either be attributed to desorption of water or solvent. The second segment weight loss was caused by the remaining oxidation agent as well as the carbonization and main-chain scission of polypyrrole (H. Chiu et al, 2011). According to T. Sandu et al, 2012, functionalized polypyrrole was more stable than pure polypyrrole which was due to the high stability of methylene-ammonium salt. Polypyrrole displayed the highest weight loss compared to curve a and curve b. The initial weight loss of curve c was associated with 2,3-diaminophenazine, resulted from 20 % weight loss of $-NH_2$ groups (approximately 300 °C). Higher temperatures displayed a weight loss which may be due to the oxidative decomposition in air. The material displayed high stability up to approximately 300 °C

(D. He et al, 2007). PPDP (curve b) displayed an initial weight loss of 10 % which may be due to water or solvent loss below 100 °C. Higher temperature values revealed further weight loss which could be attributed to the main-chain scission of PPDP, the polymer material displayed high thermal stability as the material had not reached 100 % weight loss degradation. The high thermal stability may be attributed to the linkage during polymerization resulting in the maximum thermal degradation not being reached.

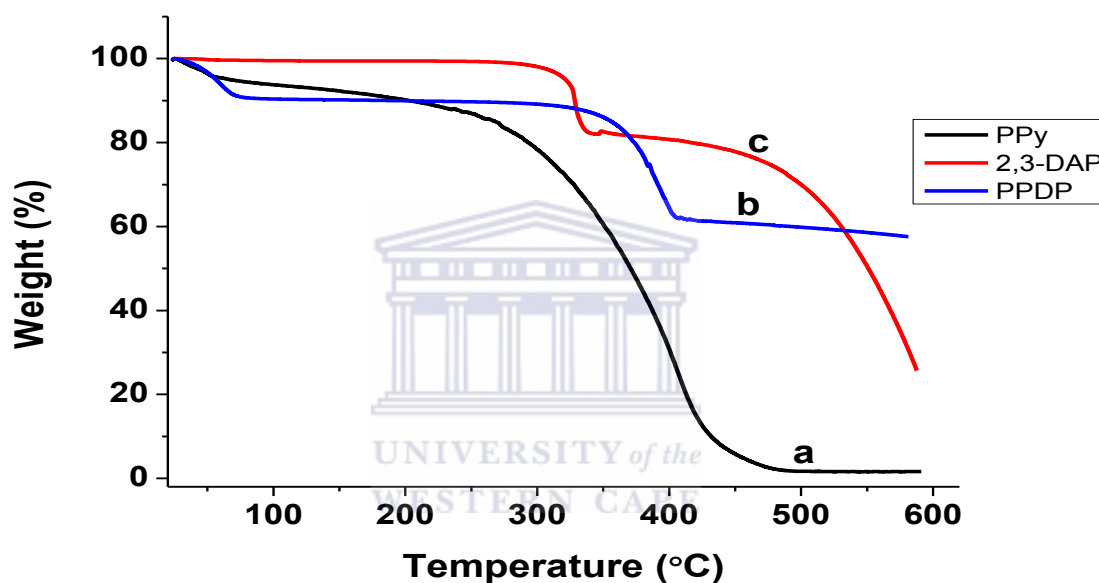


Figure 40. TGA analysis of the 2,3-diaminophenazine, Polypyrrole and PPDP over a temperature ramp of 20 to 60 °C.

The reaction to form polyaniline (PANI)/DBS complex displayed high thermal stability which was attributed to the crosslinkage during this reaction, maximum degradation of the complex was not reached due to this thermal stability (V. Schmidt et al, 2004). K. Castagno et al, 2011, studied the thermal behavior of the complex PPy/SDBS (sodium dodecylbenzene sulfonate) which revealed that the complex had not reached the maximum degradation as 35% residue remained after analysis.

DSC of conducting polymer complexes can display various thermal behaviour, with the complex of PPy/SDBS (sodium dodecylbenzene sulfonate) displayed no endothermic melting transitions (K. Castagno et al, 2011). PANI/lignosulfonic acid complex however displayed DSC properties different to that of the PPy complex, with the transitions ranging from 130 to 180 °C and enthalpy values between 10 to 30 J/g (E. Hrehorova et al, 2011).

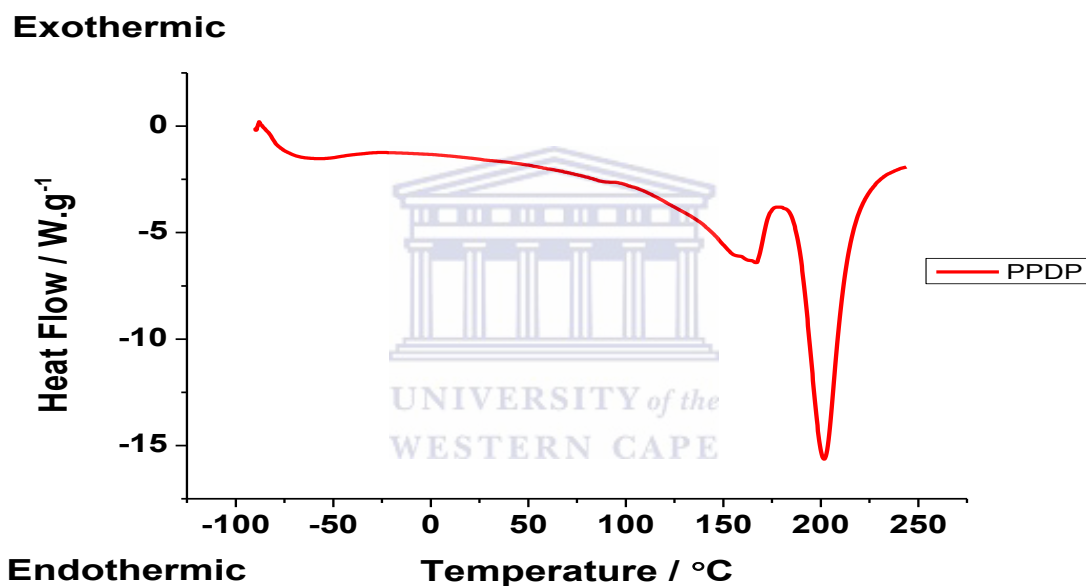


Figure 41. DSC analysis of PPDP, which displayed two endothermic transitions.

A. Cirpan et al, 2003, studied the thermal behaviour of poly(p-phenylene vinylene) and determined that there was 3 transitions present in the material. The initial transition was due to the solvent removal from the polymer, the second transition was related to the elimination reaction. The third transition was associated with the degradation of the polymer. Figure 41 displayed two endothermic transitions in the polymer material, with the first transition present at 160 °C which represents the solvent removal from the polymer. The second transition at 201.9 °C may be associated with the degradation

of the polymer material. Thermal analysis of the material revealed that the polymer material was thermally stable at higher temperatures, proved by thermogravimetric analysis. DSC measured the amount of heat absorbed or released by the polymer material during temperature transitions.

5.9 Surface Morphology

Surface morphology was performed in order to differentiate between materials

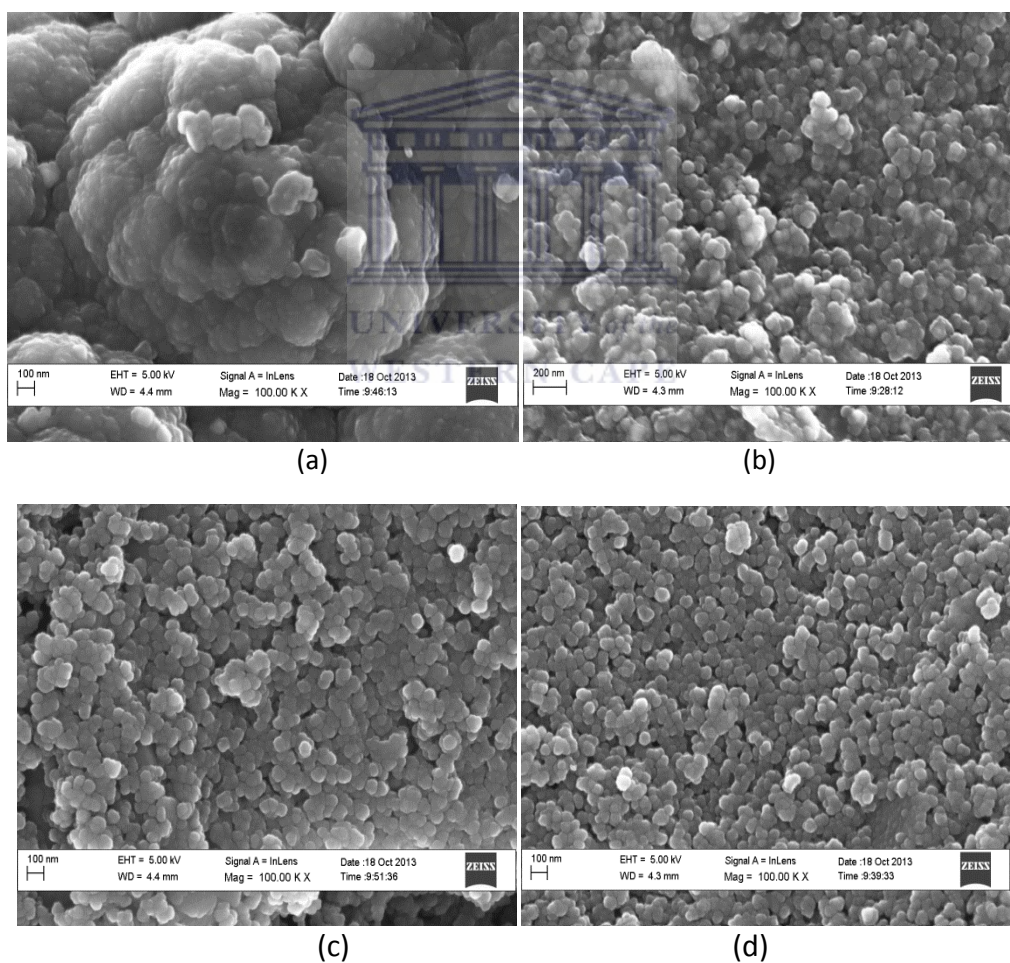


Figure 42. SEM of Polypyrrole (a), Au nanoparticles (b), PPDP (c) and PPDP-Au modified system (d).

Figure 42(a) displayed cauliflower shaped cluster of polypyrrole electropolymerized onto the surface of a carbon screen print electrode in the presence of LiClO_4 dopant solution. Gold nanoparticles displayed spherical shaped particles present which were prepared and then drop coated onto the surface of a screen print carbon electrode. The Au nanoparticles displayed in figure 43 showed spherical shapes with sizes ranging from 69.78 to 87.40 nm.

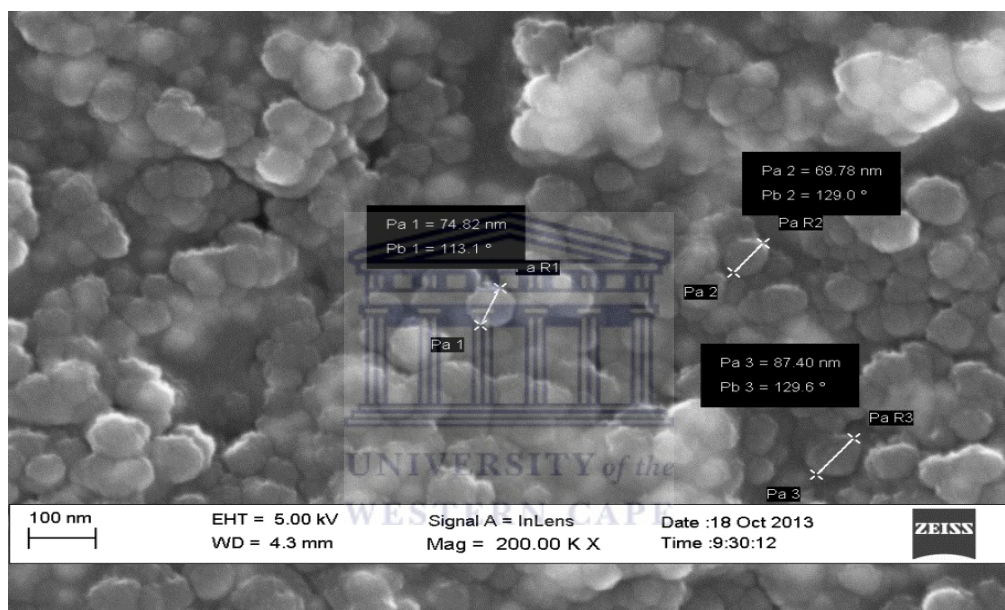


Figure 43. Spherically shaped Au nanoparticles

The representation in figure 42(c) displayed spherical shaped particles which are due to the electrochemically synthesized polymer material. The polymer system was modified with Au nanoparticles (PPDP-Au) displayed similar shaped sphere particles to the unmodified polymer system (figure 42(d)).

Based on the evidence provided, the novel monomer material was successfully synthesized and characterized in terms of spectroscopy, electrochemistry and morphology. FTIR analysis of the monomer material was used to confirm that

crosslinking occurred between starting materials, with the functional groups present in the material being the main focus. Crosslinking of starting materials led to the formation and design of the zig-zag molecule, formed by chemical and electrochemical polymerization. Extensive evaluation of this zig-zag molecule was performed to determine if actuation possibilities could be met. The zig-zag molecule was electrochemically synthesized as a thin film and studied by cyclic voltammetry which revealed the redox behaviours, diffusion rates, formal potentials and peak separations of the material. Electrochemical impedance spectroscopy of the thin film displayed a high charge transfer resistance value, 4589.455 Ω which was evident of low conductivity values. Improvement of the conductivity of the thin film, was made possible by the incorporation of gold nanoparticles, the resulting charge transfer value obtained was found to be 314.7556 Ω (evident of an increase in conductivity by reduction in resistance). Chemical preparation of the polymer material was used to study the optical behaviour of the material, band gap values determined from UV/Vis were found to be 2.48 eV (indicative of semi-conductive behaviour). Various methods used for measurements of conductivity values for thick films, confirmed the values obtained from thin films. The values obtained for these thick films ranged between $\sim 10^{-8}$ to $\sim 10^{-11}$ S/m. Thermal behaviour of the material displayed properties of high thermal stability (polymer did not degrade at high temperatures).

CHAPTER 6

Verification of the Monomer Composition

This chapter presents a comparison between unfiltered solution of monomer (yellow solution with black precipitate) and the filtered solution (yellow in colour with no precipitate) in terms of Polymerization, purity by Cyclic Voltammetry, Square Wave Voltammetry, UV/Vis Spectroscopy and FTIR will be discussed.

Electropolymerization of the monomer was performed as in the previous chapter, further investigation into the solution revealed that some precipitate remained. This led to further investigation into the polymerization, the solution was filtered and the polymerization of monomer was then performed again. The polymerization solution used was from previous experiments which displayed different cyclic voltammograms to that of a freshly prepared solution.

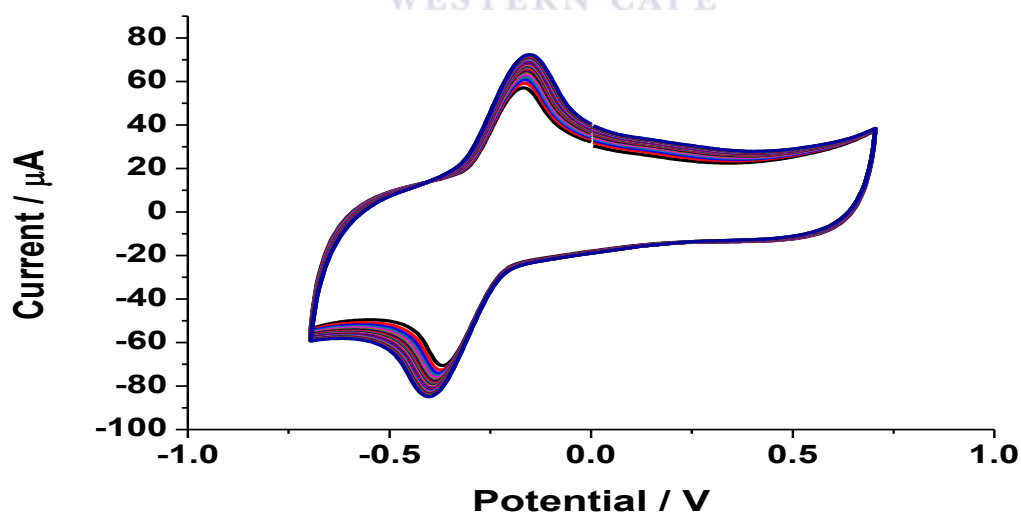


Figure 44. Polymerization of the monomer of unfiltered and filtered solutions displayed the same voltammogram

Determination of the polymerization cyclic voltammograms was not conclusive enough for comparison. Their respective electrochemical behaviour was studied in 0.1 M HCl for the determination of redox behaviour. The cyclic voltammogram in figure 45 displayed the comparison between the filtered and unfiltered solutions with a potential range between ± 1.5 V at a scan rate of 150 mV/s.

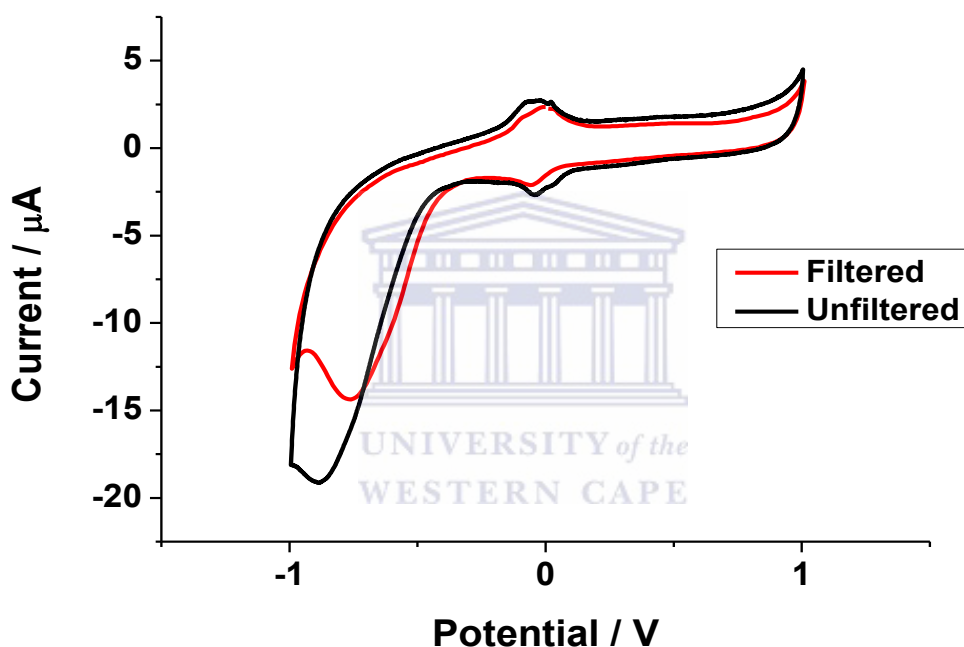


Figure 45. Comparison of filtered and unfiltered solutions of PPDP.

Square wave analysis was also performed on the solution and the resulting formal potentials were calculated in figure 46. The formal potential was calculated and was found to be 10.27 mV (filtered), 1.15 mV (unfiltered). The filtered solution displayed a fully reversible redox couple of high purity, the unfiltered sample displayed an oxidation peak which was split into three peaks. This could be the result of the unreacted material absorbing to the surface of the electrode before the thin polymer film.

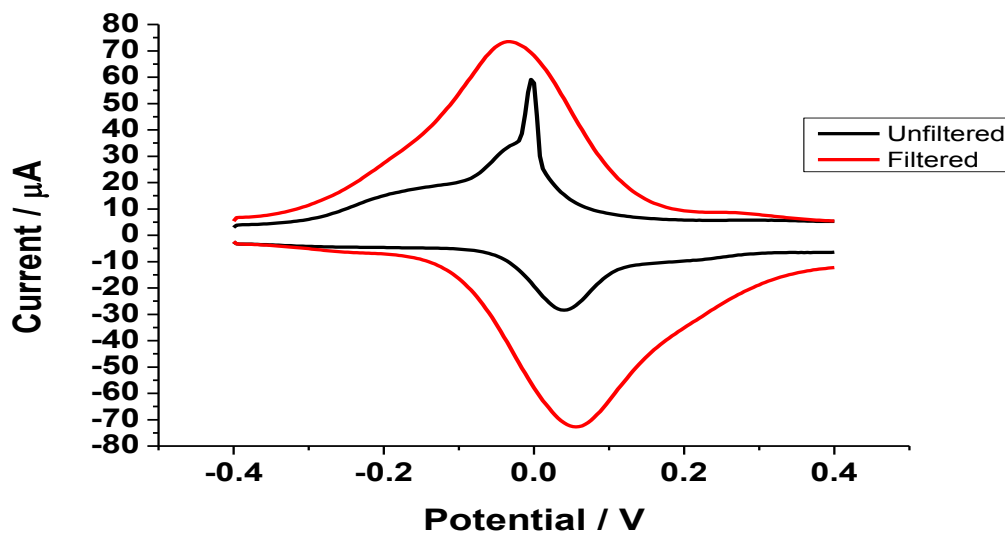


Figure 46. SWV of filtered and unfiltered PPDP at 200 mV/s.

Data obtained from the electrochemical behaviour can be used for comparison but further experimental data will be needed. The optical properties of the filtered solution and the polymer were studied in terms of UV/Vis analysis and later FTIR. The UV analysis of the filtered yellow solution displayed an absorption band present at 415 nm and the polymer bands present at 272 nm and 417 nm (figure 47(b)). The assignment of the bands present in figure 47(a) was already assigned and characterized (chapter 5.7, page 91).

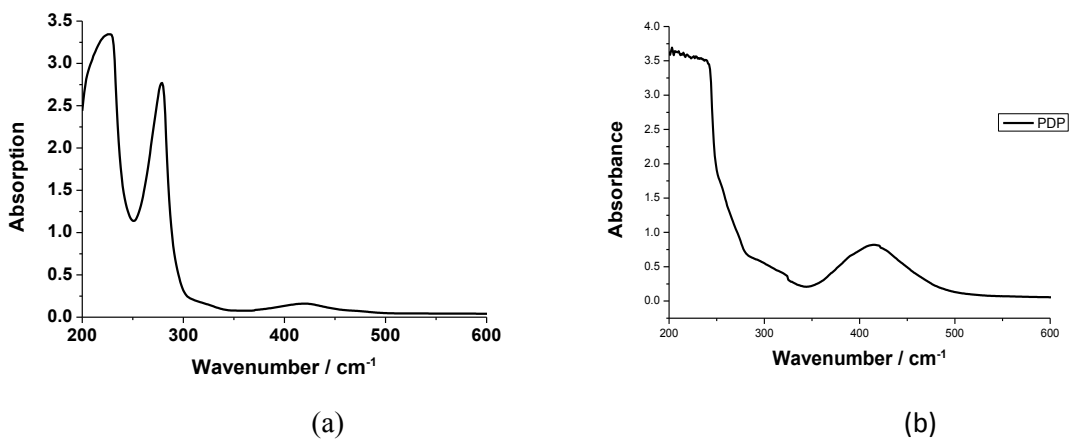


Figure 47. UV/Vis analysis of PPDP dissolved in THF (a), filtered yellow monomer solution (b) dissolved in a ratio of 1:1 of DMF and HCl.

The FTIR analysis of the filtered solution was performed and compared to the monomer material. The filtered solution represented in figure 48 displayed bands present at 3383 cm^{-1} , 2952 cm^{-1} , 1649 cm^{-1} and 1390 cm^{-1} respectively.

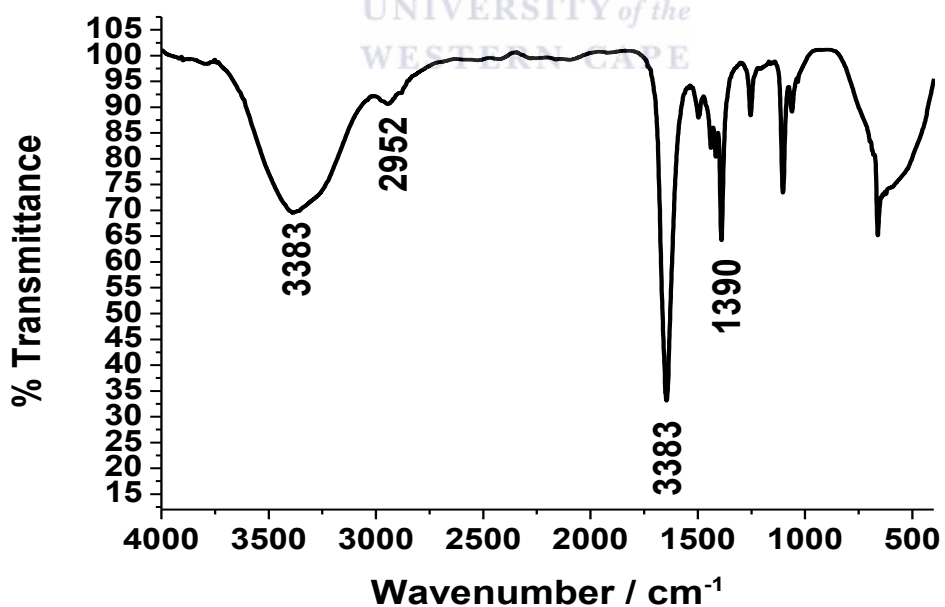


Figure 48. FTIR analysis of the filtered solution

Table 15. Filtered solution compared to the monomer material.

Peak Assignment	Wavenumber / cm^{-1}
Phenazine-2,3-diimino(pyrrole-2-yl) PDP (Monomer)	
N-H	3702
C=N	1574
C-C	1469 (aromatic)
Filtered Solution (Monomer)	
N-H	3383
C-H	2952 (aromatic)
C=N	1649
C-C	1390 (aromatic)

The remaining unknown precipitate of the filtered solution was studied in terms on FTIR and the respective spectrum is displayed below in figure 49. This was done in order to determine what the unknown precipitate was. The precipitate was compared to the starting materials as well as the monomer. The FTIR spectrum displayed stretching bands present at 3400 cm^{-1} , 1615 cm^{-1} , 1425 cm^{-1} and 1192 cm^{-1} .

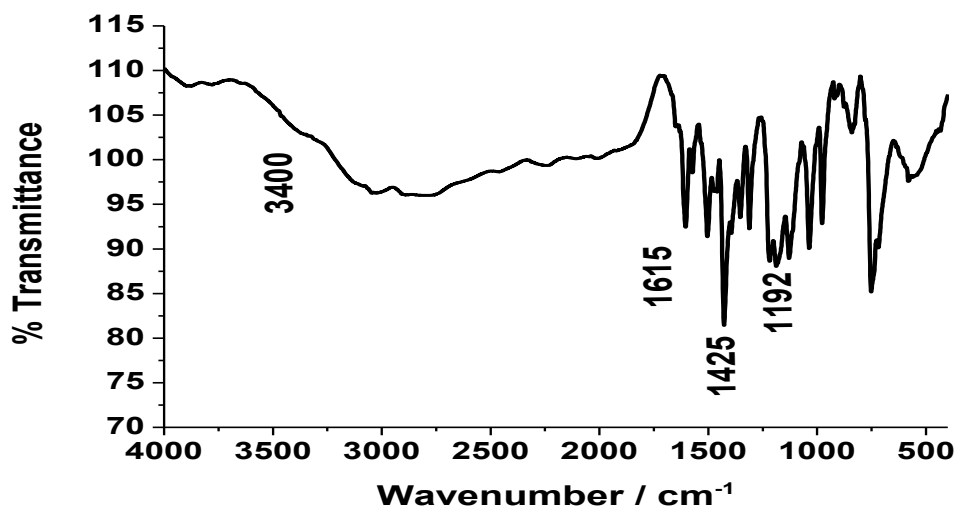


Figure 49. FTIR of unknown precipitate remaining after filtration.

Upon determination of the FTIR data it was revealed that the precipitate displayed similar stretching bands to that of 2,3-diaminophenazine, displayed in table 16.

Table 16. Comparison of Unknown Precipitate with starting materials.

Peak Assignment	Wavenumber / cm^{-1}
2,3-diaminophenazine	
N-H	3429, 3301 and 3167
C=N	1641
C=C	1487
C-N	1222 (aliphatic amine)
Pyrrole-2-carboxaldehyde	
N-H	3145
C-H	3078 (aromatic) and 2978 (aldehyde)
C=O	1627 (aldehyde)
C=C	1441
C-N	1317 (aromatic amine)
Unknown Precipitate	
N-H	3400
C=N	1615
C=C	1425
C-N	1192 (aliphatic amine)

Comparison of the unknown precipitate with the starting materials revealed that the unknown precipitate had similarities to that of the both starting materials. The stretching band that was used for the determination of the unknown precipitate was that of the aliphatic amine group present in 2,3-diaminophenazine.

According to the experimental data obtained, it can be convincingly concluded that the yellow filtered solution is a pure form of the synthesized monomer material in solution. The solubility testing of the material in these common organic solvents could then be used as the synthesized product.

CHAPTER 7

Conclusion and Future work

7.1 Conclusion

Actuation of polymer systems has been widely studied due to its ability to behave in the manner in which our muscles move. In this work different actuation mechanisms were presented including pneumatic muscle actuators, piezoelectric actuators and electroactive polymer actuators. Properties of these actuators revealed that the most favourable properties were that of electroactive polymers actuators.

Further investigation into these actuators were necessary to fully understand the materials used in these actuators. Two categories of electroactive polymers include; electronic and ionic electroactive polymers were explored with the main desired advantages for actuation favouring the ionic group. Conducting polymers (ionic electroactive polymers) were used as the materials in the actuators due to the ability of these materials to expand and contract upon electrical stimulus. In this work the zig-zag molecular design conducting polymer was extensively explored. Modification by crosslinking of polypyrrole to affect a zig-zag polymer structure was performed. Crosslinking of a pyrrole derivative with diaminophenazine led to the formation of this desired zig-zag molecule. The monomer proposed in this work is completely novel and has not been used in actuation evaluation before. Important parameters for efficient actuation in electroactive polymers are conductivity and solubility testing.

The evidence provided revealed that the novel monomer material was successfully synthesized and characterized in terms of spectroscopy, electrochemistry and morphology. Determination of the functional groups present in the monomer material

revealed that the desired crosslinking had been successfully obtained. According to the reaction mechanism in the formation of imines by the reduction of amine, the disappearance of the carbonyl group in the monomer material was observed. The desired zig-zag molecule was obtained by chemical and electrochemical polymerization. Desired actuation capabilities of the polymer material led to extensive evaluation of this zig-zag molecule. Electrochemical synthesis was used in the formation of a thin film which was studied by cyclic voltammetry; which revealed the redox behaviours, diffusion rates, peak separation and formal potentials of the material.

Electrochemical impedance spectroscopy of the thin film displayed high charge transfer resistance value, 4589.455 Ω which was related to that of low conductivity values. Improvement of the conductivity value of the thin film was made possible by the incorporation of gold nanoparticles, the resulting charge transfer resistance value obtained was found to be 314.7556 Ω (evident of an increase in conductivity by reduction in resistance). Chemical preparation of the polymer material was used to study the optical behaviour of the material, band gap values determined from UV/Vis were found to be 2.48 eV (indicative of semi-conductive behaviour). Methods used for measurements of conductivity values for thick films, confirmed the values obtained from thin films. The values obtained for the thick films ranged between $\sim 10^{-8}$ to $\sim 10^{-11}$ S/m. Thermogravimetric analysis behaviour of the material displayed properties of high thermal stability (polymer did not degrade at high temperatures), with DSC analysis revealing that there was no evidence of glassy transition peaks. During the polymerization process the electrochemistry revealed an undesired reversible couple which led to the investigation of the unreacted material present in the solution. Investigation into the unreacted material displayed functional groups in the FTIR analysis which were similar to that of 2,3-diaminophenazine. This led to the determination of the unreacted material absorbing to the surface of the electrode

before the thin film was formed. Filtration of the polymerization solution produced a yellow solution which was then used for polymerization and characterization to study the behaviour of this filtered solution. Cyclic voltammetry of the filtered solution was compared to that of the unfiltered polymerization (original solution for polymerization) and it was discovered that the filtered solution was a purer form of the monomer in solution. The purity is evident in chapter 6 with square wave voltammetry revealing a single reversible redox couple for the filtered solution whereas the unfiltered solution displayed three peaks in the oxidation process. Successful synthesis and characterization of the desired novel monomer and polymer material provided in this work will lead to future work.

7.2 Future Work

As a direct result of the improvements in conductivity results will play an important role for the incorporation of the polymer material into interpenetrating polymer networks actuators. The evaluation of this polymer material in dye sensitized solar cells as well as the use of doped polypyrrole nanocomposites in the design of highly sensitive gas phase sensors.

The major limitations in fully concluding and testing the actuation potential of the polymer materials prepared include conductivity testing of Au-PPDP pellet and band gap determination of the polymer after incorporation of the Au nanoparticles. These tests rely on the preparation of the Au-PPDP polymer by chemical synthesis to produce sufficient material for pellet preparation. However it was clear from chemical synthesis of the PPDP that the synthesis method would have to be revised in order to improve yield and purity of the chemically synthesized product. In future work we will evaluate

the use of milder oxidizing agents such as ammonium persulfate and tosylate salts to provide milder oxidation conditions.

We have also demonstrated that a pure form of the chemically synthesized PPDP polymer may be extracted using primary alcohols such as ethanol and methanol. The polymer present in the extracted solution was confirmed by redox electrochemistry (CV) and spectroscopy (FTIR). However further work is required to produce the purified PPDP and Au-PPDP either by extraction and recrystallization or by improved chemical synthesis conditions.

The characterization by TGA, DSC, ¹H-NMR, fluorescence and four probe conductivity which was done at University Cery Pontoise (France) facilitated a clear understanding of actuator design requirements and the acquisition of the necessary analytical skills. The characterization for future work may now be attempted at University of the Western Cape, though continued collaboration and locally available instrumental resources and will be pursued during PhD registration.

The requirement for solubility analysis of the polymer relates directly to the preparation of the polymer in bilayer actuator format and has successfully been resolved through extraction of the pure polymer into alcohol solution. The polymer extract was confirmed to contain pure polymer PPDP and could in principle be drop coated onto a non-conducting flexible substrate for the production of a bilayer actuator system for testing the actuation potential of the PPDP and Au-PPDP materials synthesized. The bilayer format and interpenetrating network design of actuators will be pursued in future research.

REFERENCES

1. V. Amendol, M.Meneghetti, Laser ablation synthesis in solution and size manipulation of noble metal nanoparticles, **Physical Chemistry Chemical Physics**; 11 (2009), 3805–3821.
2. P.A. Anquetil, Hsiao-hua Yu, John D. Madden, Peter G. Madden, Timothy M. Swager, Ian W. Hunter. Recent Advances in Thiophene-based Molecular Actuators. **The international society for optical engineering**; 5051, Smart Structures and Materials 2003: Electroactive Polymer Actuators and Devices (EAPAD), 42, 2003.
3. R. Ansari. Polypyrrole conducting electroactive polymers; Synthesis and stability studies. **E-Journal of Chemistry** ; Volume 3, Issue 4, Pages 186-201, 2006.
4. S. Asokan, Karl M Krueger, Ammar Alkhalaf, Alessandra R Carreon, Zuzana Mu, Vicki L Colvin, Nikos V Mantzaris, Michael S Wong. The use of heat transfer fluids in the synthesis of high-quality CdSe quantum dots, core/shell quantum dots, and quantum rods. **Nanotechnology**; 16 (2005) 2000–2011.
5. Y. Bar-Cohen, Electroactive polymers (EAP) actuators as artificial muscles, reality, potential, and challenges, 2nd edition, **SPIE PRESS**, 2004.
6. A.J. Bard and L.R. Faulkner, Electrochemical methods, fundamentals and applications, 2nd edition, chapter 6, pg. 226-243, John Wiley & Sons, 2001.
7. V. Bhardwaj, Gargi Harit, Sokindra Kumar. Interpenetrating Polymer Network (IPN): Novel Approach in Drug Delivery. **International Journal of Drug Development & Research**; Volume 4 (2012), Issue 3.
8. E. Biddiss and Tom Chau. Dielectric elastomers as actuators for upper limb prosthetics: Challenges and opportunities. **Medical Engineering and Physics**; 30(4):403-18, 2008.
9. D. Braga, Fabrizia Grepioni, Kumar Biradha, V.R. Pedreddi, Gautum R. Desiraju. Hydrogen Bonding in Organometallic Crystals. 2. C-H.cntdot. .cntdot. .cntdot.O

- Hydrogen Bonds in Bridged and Terminal First-Row Metal Carbonyls. **Journal of the American Chemical Society**; 1995, 117(11), pp. 3156-3166.
10. D. Brandell, Heiki Kasemägi, Johann Citérin, Frédéric Vidal, Claude Chevrot, Alvo Aabloo. Molecular dynamics studies of interpenetrating polymer networks for actuation devices. **The international society for optical engineering**; 6927, Electroactive Polymer Actuators and Devices (EAPAD), 2008.
 11. K.R.L. Castagno, Viviane Dalmoro, Denise S. Azambuja. Characterization and corrosion of polypyrrole/sodium dodecylbenzene sulfonate electropolymerized on aluminium alloy 1100. **Journal of Polymer Research**; 17(5), pp. 647, 2011.
 12. L. Ceseracciu, Maurizio Biso, Alberto Ansaldo, Don N. Futaba, Kenji Hat, Alberto C. Barone, Davide Ricci. Mechanics and actuation properties of bucky gel-based electroactive polymers. **Sensors and Actuators B**; 156 (2011) 949–953.
 13. J. Chang, Jungil Park, Youngmi Kim Pak, James Jungho Pak. Fitting improvement using a new electrical circuit model for the electrode-electrolyte interface. Neural Engineering, CNE '07. 3rd **Institute of Electrical and Electronics Engineers**; Conference, 572 – 574, 2007.
 14. V. Chechik, Richard M. Crooks. Monolayers of Thiol-terminated dendrimers on the surface of planar and colloid gold. **Langmuir**; 15 (1999), pp. 6364-6369.
 15. G. Chen, Stephen Bouzan, Yuming Zhao. Synthesis and properties of TTFV-hinged molecular tweezers. **Tetrahedron Letters**; 51 (2010) 6552–6556.
 16. C. Chen, John C. LaRue, Richard D. Nelson, Lawrence Kulinsky and Marc J. Madou, Electrical conductivity of polymer blends of poly(3,4-ethylenedioxythiophene): poly(styrenesulfonate): N-Methyl-2-pyrrolidinone and polyvinyl alcohol. **Journal of Applied Polymer Science**; Volume 125 (2011), Issue 4, 3134–3141.
 17. H. Chiu, Tzong-Yiing Chiang, Chi-Yung Chang, Ming-Tai Kuo, Carbon black/polypyrrole/nitrile rubber conducting composites: synergistic properties and

- compounding conductivity effect. **European Polymer Federation**; 11(1), pp.412–427, 2011.
18. K. Choi, Choongho Yu, Highly doped carbon nanotubes with gold nanoparticles and their influence on electrical conductivity and thermopower of nanocomposites, PLoS ONE vol. 7, issue 9, p. e44977, 2012.
 19. Cirpan, Zuhul Kucukyavuz, Savas Kucukyavuz. Synthesis, characterization and electrical conductivities of poly(p-phenylene vinylene). **Turkish Journal of Chemistry**; 27 (2003), pp.135-143.
 20. S.K.N. Dhoble, S.J, Swart, H.C, Park, K. Phosphate Phosphors for solid state lighting. **Springer Series in Materials Science**; 174, 2013.
 21. D.D. Ebbing, S.D. Gammon, General chemistry, 7th edition, chapter 20, pg.839-882, Hughton Mifflin Company, 2002.
 22. A.L. Eckermann, Daniel J. Feld, Justine A. Shaw, and Thomas J. Meade. Electrochemistry of redox-active self-assembled monolayers. **Coordination Chemistry Reviews**; 254 (2010) 1769–1802.
 23. J. Guo, Sze Keat Chee, Takeshi Yano, Tashiro Higuchi, Micro-vibration stage using piezo actuators, **Sensors and Actuators A**; 194 (2013) 119– 127, 2013.
 24. S. Garcia, Edward Kunitz and Kim Sampson. Piezoelectric effect and its applications, <http://ice.chem.wisc.edu/~ice/materials/piezo.html>, 1-13, 1998.
 25. Gopalan, D. Ragupathy, H.T. Kim, K.M. Manesh, K.P. Lee, Pd (core)-Au (shell) nanoparticles catalyzed conversion of NAPh to NAD⁺ by UV-vis spectroscopy—a kinetic analysis, **Spectrochimica Acta, Part A: Molecular and Biomolecular Spectroscopy**; 74(3), pp. 678-84, 2009.
 26. G. Gordon, Wallace, Geoffrey M. Spinks, Leon A.P. Kane-Maguire, Peter R. Teasdale, Conduction electroactive polymers, intelligent polymer systems, 3rd edition, chapter 2, **CRC Press**, 2009.

27. G. Han, Gaoquan Shi. High-response tri-layer electrochemical actuators based on conducting polymer films. **Electroanalytical Chemistry**; Volume 569, No. 2, pp. 169-174, 2004.
28. A.N. Hashim, Alimuddin A, Shalendra Kumar, SagarE.Shirsath, E.M.Mohammed, Hanshik Chung , Ravi Kumar. Studies on the activation energy from the ac conductivity measurements of rubber ferrite composites containing manganese zinc ferrite. **Physica B**; 407 (2012), 4097-4103, 2012.
29. D. He, Yu Wu, Bo-Qing Xu. Formation of 2,3-diaminophenazines and their self-assembly into nanobelts in aqueous medium. **European polymer journal**; 43, 3703-3709, 2007.
30. Hilderbrandt, O. Sawodny, R. Newman, A. Hartmann. A cascaded tracking control concept for pneumatic muscle actuators. **Institute of Automation and Systems Engineering**; American Control Conference, 2005.
31. E. Hrehorova, Laura k. Wood, Jan Pekarovic, Alexandra Pekarovicova, Paul D. Fleming, Valery Bliznyuk. The properties of conducting polymers and substrate for printed electronics. **Baltimore, MD**; pp. 197-202, 2005.
32. E.W.H. Jager, Elisabeth Smela, Olle Inganas. Microfabricating conjugated polymer actuators. **Science Volume**; 290, 1540-1545, 2001.
33. E.W.H. Jager, N. Masurkar, N.F. Nworah, B. Gaihre, G. Alici, G.M. Spinks. Individually controlled conducting polymer tri-layer microactuators. **Euroensors XXVII**; 542-545, 2013.
34. J. Jorcin, Mark E. Orazem, Nadene Pebere, Bernard Tribollet. CPE analysis by local electrochemical impedance spectroscopy. **Electrochimica Acta**; volume 5 (8-9), pp. 1473-1479, 2006.
35. M. Karpelson, Guo Yeou Wei, Robert. J. Wood. Driving high voltage piezoelectric actuators in microrobotic applications. **Sensors and Actuators A**; 176 (2012) 78–89, 2012.

36. Khaldi, Cédric Plesse, Caroline Soyer, Eric Cattan, Frédéric Vidal, Claude Chevrot, Dominique Teyssie. Draft: Dry etching process based on conducting interpenetrating polymer network actuator for a flapping fly micro robot, **International Mechanical Engineering Congress and Exposition**; 11-17, 2011.
37. K.J. Kim and Satoshi Tadokoro. Electroactive Polymers for Robotic Applications Artificial Muscles and Sensors, **Springer-Verlag London Limited**, 2007, pg 3 - 7.
38. J. Kui, Sun Gang and Zhang Shusheng. Enzyme-catalyzed reaction of OPD-H₂O₂-HRP voltammetric enzyme-linked immunoassay system. **Science in China Series B: Chemistry**; Volume 41, Issue 4, pp 345-352, 1998.
39. J. Lee, Fransico Serna, Jonathan Nickels and Christine E. Schmidt. Carboxylic acid-functionalized conductive polypyrrole as a bioactive platform for cell adhesion. **Biomacromolecules**; 6(2006), 1692-1695.
40. D. Li, Qiang He, Junbai Li. Smart core/shell nanocomposites: Intelligent polymers modified gold nanoparticles. **Advances in Colloid and Interface Science**; 149 (2009), pp. 28-38.
41. I.K. Li, Xin Zhang, Yanhang Zhang, Inelastic deformation of bilayer microcantilevers with nanoscale coating. **Sensors and Actuators A**; 168 (2011) 1–9, 2011.
42. S. Liou, Xiaoyun Qin, Jingqi Tian, Lei Wang, Xuping Sun. Photochemical preparation of fluorescent 2,3-diaminophenazine nanoparticles for sensitive and selective detection of Hg(II) ions. **Sensors and Actuators B**; 171– 172 (2012) 886– 890.
43. Y. Lui, Ling-Min Yu, Say Chye Joachim Loo, Richard G. Blair, Qichun Zhang. Co-assembly of Zn(SPh)₂ and organic linkers into helical and zig-zag polymer chains. **Journal of solid state chemistry** 191 ; 283-286, 2012.
44. S. Ma and Hirokazu Tanaka. Measuring conductivity of proton conductive membrane in the direction of thickness, part II: using the 4-probe method in the direction of thickness. Espec Technology Report No. 23(2007); http://www.espec.co.jp/english/tech-info/tech_info/pdf/07_01/contents1.pdf.

45. J.D.W. Madden, Vandesteeg, N.A, Anquetil, P.A, Madden, P.G.A, Takshi, A, Pytel, R.Z, Lafontaine, S.R, Wieringa, P.A, Hunter, I.W, Artificial muscle technology: physical principles and naval prospects. **Institute of Electrical and Electronics Engineers**; Oceanic Engineering, (Volume 29, Issue 3), 706 – 728, 2004.
46. K. Maksymiuk. Chemical reactivity of polypyrrole and its relevance to polypyrrole based electrochemical sensors. **Electroanalysis**; Volume 18, Issue 16, pages 1537–1551, 2006.
47. S. Meghdadi, Mehdi Amirnas , Kurt Mereiter, Hajar Molaee, Ahmad Amiri. Synthesis, structure and electrochemistry of Co(III) complexes with an unsymmetrical Schiff base ligand derived from 2-aminobenzylamine and pyrrole-2-carboxaldehyde. **Polyhedron**; 30(10):1651-1656, 2011.
48. Mukoyama, Koichi Aoki, jingyuan Chen, Electrochemical dissolution of polythiophene films, **Journal of Electroanalytical Chemistry**; 531(2), pp. 133-139(7), 2002.
49. Nan, Izabell Craciunescu and Rodica Turcu (2012). Conducting Polypyrrole Shell as a Promising Covering for Magnetic Nanoparticles, Dr. Artur Motheo (Ed.), ISBN: InTech, Available from: <http://www.intechopen.com///conducting-polypyrrole-shell-as-a-promising-covering-for-magnetic-nanoparticles>.
50. C.H. Nguyen, Gursel Alici, Gordon G. Wallace. Modelling trilayer conjugated polymer actuators for their sensorless position control. **Sensors and Actuators A**; 185 (2012) 82– 91.
51. Y. Nishioka, Polypyrrole soft actuators, <http://www.intechopen.com/books/electropolymerization/polypyrrole-soft-actuators>, 2011.
52. R. Palakodeti, Kessler, M.R. Influence of frequency and prestrain on the mechanical efficiency of dielectric electroactive polymer actuators. **Materials Letters**; 60, 3437–3440, 2006.

53. P. Phuengphai, Sujitra Youngme, Narongsak Chaichit, Jan Reedijk. New 3D supramolecular networks built from 1D and 2D frameworks via π - π and H-bonding interactions: Topology and catalytic properties. **Inorganica chimica acta** 403; 35-42, 2013.
54. C. Plesse, Caroline Soyer, David Troadec, Frédéric Vidal, Eric Cattanm. Micro-beam actuator based on conducting interpenetrating polymer networks: from patterning process to actuation in open air. **16th International conference on solid-state Sensors, Actuators and Microsystems Conference (TRANSDUCERS)**; 462-465, 2011.
55. U.S. Ramelow, J.H. Ma and R. Darbeau. Electrical conductivities of polypyrrole reacted with dopant solutions. **Material Research Innovations**; Volume 5, Issue 1, pp 40-49, 2001.
56. Rasha, Ahmed, R.A. Farghali, A.M. Fekry. Study for the stability and corrosion inhibition of electrophoretic deposited chitosan on mild steel alloy in acidic medium. **International Journal of Electrochemical Science**; 7 (2012) 7270 – 7282.
57. T. Sandu, Andrei Sarbu, Floriana Constatin, Cătălin Ilie Spataru, Raluca Augusta Gabor, Raluca Şomoghi and Horia Iovu. Characterization of functionalized polypyrrole. **Revue Roumaine de Chimie**; 57(3), pp. 177-185, 2012.
58. V. Schmidt, S.C. Domenech, M.S. Soldi, E.A. Pinheiro, V. Soldi. Thermal stability of PANI/ethylene propylene diene rubber blends prepared by solvent casting. **Polymer Degradation and Stability**; 83(3), pp. 519-527, 2004.
59. V. Shaktawat, Neeraj Jain, Manasvi Dixit, N.S. Saxena, Kananbala Sharma and T.P. Sharma. Temperature dependence of conductivity of polypyrrole doped with sulphuric acid. **Indian Journal of Pure & Applied Physics**; 427-430, 2008.
60. V. Shaktawat, K. Sharma, N.S. Saxena. Structural and electrical characterization of protonic acid doped polypyrrole. **Journal of Ovonic Research**; 6(6), p. 239 – 245, 2010.

61. B.K. Singha, Anant Prakasha, Hemant K. Rajour, Narendar Bhojaks, Devjani Adhikari. Spectroscopic characterization and biological activity of Zn(II), Cd(II), Sn(II) and Pb(II) complexes with Schiff base derived from pyrrole-2-carboxaldehyde and 2-amino phenol. **Spectrochimica Acta Part A: Molecular and Biomolecular Spectroscopy**; 76, 376-383, 2010.
62. B. Stuart, *Infrared Spectroscopy: Fundamentals and applications*, John Wiley and Sons, chapter 4, pp.71-88, 2004.
63. B.H. Stuart, *Infrared Spectroscopy: Fundamentals and Applications*, 2004.
64. K.C. Grabar, R. Freeman, T. Michael, B. Hommer, and Michael J. Natan. Preparation and characterization of Au colloidal monolayers. **Analytical Chemistry**; 67 (1995), 735-743.
65. D. Sutar, D.K. Aswal, S.K. Gupta, J.V. Yakhmi. Electrochemical actuator from conductive electroactive polymer polypyrrole deposited on gold. **Indian journal of pure and applied physics**; Vol 45, April 2007, pp.354-357.
66. S. Sylvestre, S. Sebastian, K. Oudayakumar, T. Jayavarthanam, N. Sundaraganesan. Experimental (FTIR, FT-Raman and UV-Vis) spectra and theoretical DFT investigations of 2,3-diaminophenazine, **Spectrochimica Acta Part A: Molecular and Biomolecular Spectroscopy**: 401-12, 2012.
67. S. Taj, M.F. Ahmed, S. Sankarapapa Vinsam. Poly(para-aminophenol) a new soluble, electroactive conducting polymer. **Journal of Electroanalytical Chemistry**; Volume 338(1-2), Pages 347-352, 1992.
68. Y. Tan and Khashayar Ghandi. Kinetics and mechanism of pyrrole chemical polymerization, **Synthetic Metals**; 175, 183- 191, 2013. B. Tondu, P. Lopez. Modelling and control of McKibben artificial muscle robot actuators, **Institute of Electrical and Electronics Engineers**; Control Systems, (Volume:20, Issue: 2), 15 - 38, 2000.

69. P.J. Tarcha, Victor P. Chu and Dave Whittern. 2,3-diaminophenazine is the product from the horseradish peroxidase-catalyzed oxidation of o-phenylenediamine. **Analytical Biochemistry**; 165(1):230-3, 1987.
70. N. Terasawa and Kentaro Yamato. Comparison of electrochemical and electromechanical properties of a high performance carbon black polymer actuator and a single-walled carbon nanotube polymer actuator. **Sensor and Actuators B**; 176 (2013), 1103-1109.
71. K.A. Thomas and William B. Euler. An electrochemical spectroscopic and theoretical study of poly(2,3-diaminophenazine). **Journal of electroanalytical chemistry**; 501, 235-240, 2001.
72. T.V. Vernitskaya, O.N. Efimov. Polypyrrole: a conducting polymer; its synthesis, properties and applications, **Russian Chemical Reviews**; 66(5) 443-457,1997.
73. A.Y. Vibhute, S.S.Mokle, Y.S. Nalwar, Y.B.Vibhute and Vasant M. Gurav. An Efficient and Operationally Simple Synthesis of Some New Schiff Bases Using Grinding Technique. **Bulletin of the Catalysis Society of India**; 8, 164-168, 2009.
74. S. Miglani, Monika Mishra and Pooja Chawla. The rapid synthesis of schiff-bases without solvent under microwave irradiation and their antimicrobial activity. **Der Pharma Chemica**; 4(6):2265-2269, 2012.
75. T. Vo-Minh, Tegoeh Tjahjowidodo, Herman Ramon, and Hendrik Van Brussel. A new approach to modelling hysteresis in a pneumatic artificial muscle using the maxwell-slip model. **Institute of Electrical and Electronics Engineers, Transaction**; (Volume 16, Issue 1), 177 – 186, 2010.
76. Y. Wang, Rubner, M. F. An investigation of the conductivity stability of acid-doped polyanilines. **Synthetic Metals**; 47 (1992), 255.
77. K.C. Wickramatunge, Thananchai Leephakpreeda. Study on mechanical behaviours of pneumatic artificial muscle. **International Journal of Engineering Science**; 48 (2010) 188–198.

78. H. Xu, Chong Wang, Chunlei Wang, Jim Zoval, Marc Madou. Polymer actuator valves toward controlled drug delivery application, **Biosensors and Bioelectronics**; 21, 2094–2099, 2006.
79. Y. Xuan, Xu Guo, Yushuang Cui, Changsheng Yuan, Haixiong Ge, Bo Cui, Yanfeng Chen. Crack-free controlled wrinkling of bilayer film with a gradient interface. **Soft Matter**, 8 (2012), 9603-9609.
80. J.E. Yoo, Kwang Seok Lee, Andres Garcia, Jacob Tarver, Enrique D. Gomez, Kimberly Baldwin, Yangming Sun, Thuc-Quyen Nguyena and Yeuh-Lin Loo. Directly patternable, highly conducting polymers for broad applications in organic electronics. **Proceedings of the National Academy of Sciences**; 107(13), pp. 5712-5717, 2010.
81. P. Yurkanis Bruice, Organic Chemistry Prentice Hall, 4th edition, Prentice Hall, chapter 18, pp. 747-752, 2004.
82. U.L. Zainudeen, M.A. Careem, S. Skaarup. PEDOT and PPy conducting polymer bilayer and trilayer actuators. **Sensors and Actuators B**; 134 (2008) 467–470.
83. P. Zhou, Hao Liu, Shicheng Chen, Lucian Lucia, Haiyu Zhan and Shiyu Fu. 2,3-Diaminophenazine. **Molbank**; 2011(3), 1-5.
84. TiNi Aerospace, Inc., Frangibolt Product Introduction,
<http://www.tiniaerospace.com/html/Frangibolt/FrangiboltFamily.html>. 26.7.2001.